Aus der Klinik für Gastroenterologie, Infektiologie und Rheumatologie
der Medizinischen Fakultät Charité – Universitätsmedizin Berlin

DISSERTATION

Inhibition der PI3K/AKT/mTOR-Signaltransduktion: innovative Therapieoptionen für neuroendokrine Tumore auf Basis eines tieferen Verständnisses intrazellulärer Prozesse in NEN

zur Erlangung des akademischen Grades
Doctor rerum medicinalium (Dr. rer. medic.)

vorgelegt der Medizinischen Fakultät
Charité – Universitätsmedizin Berlin

von

Helma Freitag

aus Celle

Datum der Promotion: 16.06.2018

INHALT

EINLEITENDE ANMERKUNG

Teilergebnisse der vorliegenden Arbeit wurden in den folgenden Aufsätzen vorab publiziert:

1. Freitag et al., Inhibition of mTOR's Catalytic Site by PKI-587 Is a Promising Therapeutic Option for Gastroenteropancreatic Neuroendocrine Tumor Disease, Neuroendocrinology, 2016 (1)
2. Nölting et al., The selective PI3Kα inhibitor BYL719 as a novel therapeutic option for neuroendocrine tumors: Results from multiple cell line models, Plos One, 2017 (2)
3. Briest et al., FOXM1: A novel drug target in gastroenteropancreatic neuroendocrine tumors, Oncotarget, 2015 (3)

Die erste Publikation beschreibt mein Hauptforschungsprojekt, welches ich im Wesentlichen selbstständig geplant und durchgeführt habe. In den anderen beiden Projekten war ich eingebunden in die Planung und Durchführung der Experimente, die sich mit der Analyse von Zellviabilität und Zellzyklus beschäftigen.

ZUSAMMENFASSUNG

Die seltenen gastroenteropankreatischen Neoplasien (GEP-NENs) sind eine klinisch sehr heterogene Gruppe maligner Tumore, für die kaum wirksame Behandlungsmöglichkeiten vorhanden sind. Da der häufig in GEP-NEN überaktivierte PI3K/AKT/mTOR-Signalweg mit der Pathogenese assoziiert wird, wurden in dieser Arbeit der duale PI3K/mTOR-Inhibitor Gedatolisib, der selektive Inhibitor von PI3Kα Alpelisib und der FOXM1-Inhibitor Siomycin A, *in vitro* auf Wirksamkeit überprüft. Die Wirksamkeit dieser drei Verbindungen ist in den Zelllinien BON-1, KRJ-I und QGP-1 sowie der schlecht differenzierten, aggressiven Zelllinie LCC-18 und dem typischen Lungen-Karzinoid NCI-H727 dem mTOR-Inhibitor Everolimus, der für die Behandlung von neuroendokrinen Tumoren zugelassen ist, überlegen. Eine nähere Charakterisierung zeigte die Induktion von Zellzyklus-Arrest und Apoptose, jedoch kein zytotoxisches Potential. Da das Ansprechen auf Gedatolisib mit der Dephosphorylierung von 4E-BP1 korreliert, scheint die Wirkung auf molekularer Ebene über die durch 4E-BP1 stimulierte Protein-Translation vermittelt zu werden, die weiterhin mit einer Regulation der Genexpression über Rb/E2F verknüpft zu sein scheint.

Die verschiedenen Tumormodelle verhalten sich recht unterschiedlich, vor allem die schlecht differenzierten LCC-18 Zellen zeigten ein charakteristisch abweichendes Ergebnis.

Insgesamt stellen die drei Wirkstoffe aber vielversprechende Optionen dar, um zukünftig NENs besser behandeln zu können.

ABSTRACT

The rare gastroenteropancreatic neoplasms (GEP-NENs) are clinically very heterogeneous and malignant tumors lacking effective treatment options. Because of the frequently over-activated PI3K/mTOR pathway, which is connected to pathogenesis, the efficacy of the dual PI3K/mTOR inhibitor gedatolisib, the selective inhibitor of PI3Kα aplelisib, and the FOXM1 inhibitor siomycin A have been investigated *in vitro* and in this study. The efficacy of these three treatmens in the cell lines BON-1, KRJ-I and QGP-1 as well as the poorly differentiated, aggressive cell line LCC-18 and the typical lung carcinoid NCI-H727 is superior to mTOR inhibitor everolimus as an approved compound for treatment of NENs. Further characterization revealed induction of cell cycle arrest and apoptosis without showing cytotoxic potential. The correlation between response of cells after gedatolisib treatment and dephosphorylation of 4E-BP1 points to regulatory mechanisms via the cap-dependent protein translation, further, influencing gene expression via Rb/E2F.

The different tumor models, however, behave quite differently, especially the poorly differentiated LCC-18 cells showed a characteristic deviating result.

Overall the three active ingredients are promising options for future treatment of GEP-NENs.

1. EINFÜHRUNG

Gastroenteropankreatische neuroendokrine Neoplasien (GEP-NENs) zeigen klinisch ein sehr heterogenes Bild. Eine Untergruppe verhält sich durchaus aggressiv und proliferiert stark, die meisten dieser Tumore weisen aber ein charakteristisch langsames Wachstumsverhalten auf, wodurch sie schlecht bis überhaupt nicht auf klassische Chemotherapie ansprechen (4). GEP-NENs gehören zu den seltenen Erkrankungen, die Inzidenz ist jedoch ansteigend (5). Auch in der Lunge sind neuroendokrine Tumore selten, sie machen ca. 20-30% aller NENs aus (6).

Über den Pathomechanismus ist wenig bekannt, der häufig in NENs überaktivierte PI3K/AKT/mTOR-Signalweg (Phosphatidylinositol-4,5-bisphosphate 3-kinase/ Protein kinase B/ mechanistic target of rapamycin), der die Zellteilung steigert sowie Apoptose reduziert, wird aber mit der Pathogenese assoziiert (4, 7). Ursächliche Mutationen scheinen allerdings keine bedeutende Rolle zu spielen (4).

Bisher sind zwei medikamentöse Optionen aus dem Bereich der zielgerichteten (*targeted therapies*) Therapie für aggressive Untergruppen von pankreatischen NENs zugelassen: die beiden Wirkstoffe Everolimus (RAD001) und Sunitinib (8-10). Sunitinib ist ein Multikinase-Inhibitor, Everolimus dagegen ist ein mTOR-Inhibitor, der Raptor(regulatory-asociated protein of mTOR)-abhängig die Komplexbildung verhindert und so selektiv die Kinasefunktion des mTOR-Komplexes C1

(mTORC1) unterbindet (7). Beide Arzneistoffe führen zu einer Stabilisierung, der Erkrankung (11-13). Everolimus konnte diesen Effekt auch in Lungen-NEN zeigen, darüber hinaus gehende Remissionen sind dagegen aber selten (klinische Studie RADIANT 4 (14, 15)).

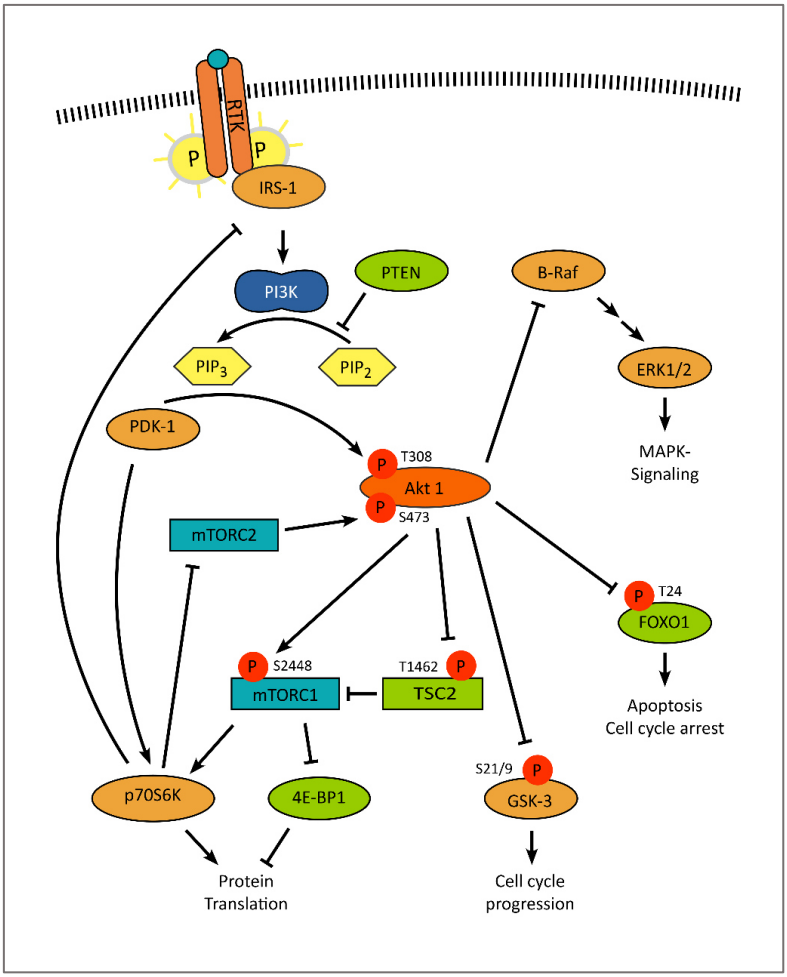

Abb. 1 Der PI3K/AKT/mTOR-Signalweg ist häufig in NENs überaktiviert. Extrazelluläre Signale werden von der RTK (Rezeptor-Tyrosinkinase) über IRS-1, PI3K und PDK1 (3-Phosphoinositid-abhängige Proteinkinase 1) zu AKT weitergeleitet. Für die Aktivierung von AKT ist zusätzlich die Phosphorylierung durch mTORC2 notwendig.
Die aktivierte Kinase AKT phosphoryliert ein breites Spektrum verschiedener Substrate, häufig werden ihre Zielstrukturen inhibiert. Insgesamt werden durch diesen Prozess Proteintranslation und Zellzyklusprogression stimuliert sowie apoptotische Prozesse inhibiert.
Verschiedene *Feedback Loops* (z.B. über mTORC1/p70S6K/ IRS-1) regulieren die AKT-Aktivität, außerdem bestehen verschiedene Verbindungen zu anderen Signalwegen (z.B. MAPK-Signalweg) (1).

mTOR wird als zentraler Schaltpunkt in der Signaltransduktion, unterhalb von AKT gelegen, angesehen (16). Diese Kinase bildet mit unterschiedlichen Bindungspartnern Komplexe, die verschiedene Aufgaben erfüllen und entsprechend unterschiedliche Zielstrukturen ansteuern (17). Das Protein Raptor ist maßgeblich beteiligt am Komplex mTORC1 mit den Zielstrukturen p70S6K (Ribosomal protein S6 kinase beta-1) und 4E-BP1 (Eukaryotic translation initiation factor 4E-binding protein 1), die wiederum die Proteintranslation regulieren (18). An mTOR-Komplex C2 (mTORC2) ist Raptor unbeteiligt, die Kinaseaktivität dieses Komplexes phosphoryliert AKT an S473 (siehe Abb.1).

Innerhalb des gesamten Signaltransduktionsnetzwerkes sind verschiedene, sich gegenseitig regulierende *Feedback Loops*

vorhanden, die als limitierende Faktoren für die Everolimus-Wirkung diskutiert werden. Darunter fallen die reflektorische Aktivierung von AKT durch mTORC2 über p70S6K, sowie die Aktivierung von PI3K über p70S6K und IRS-1 (Insulin receptor substrate 1). Beide Mechanismen haben zur Folge, dass die Hemmung des Signalweges durch verstärkte Aktivierung desselben wieder aufgehoben wird (19-22) (Abb.1).

Darüber hinaus gibt es Hinweise darauf, dass Everolimus und andere Rapamycin-Analoga, nur selektiv Phosphorylierungen an p70S6K verhindern, nicht jedoch an 4E-BP1. Man hat initiale Effekte auf beide Zielproteine beobachtet, aber auch eine rasche Rephosphorylierung von 4E-BP1, während die Dephosphorylierung von p70S6K bestehen blieb (23, 24). Beim Vergleich dieser beiden Zielstrukturen, wird p70S6K eher mit Tumorgenese assoziiert. 4E-BP1 hingegen wird als entscheidender Faktor für das Wachstum von Krebszellen angesehen (25) und mit Malignität und ungünstiger Prognose in Zusammenhang gebracht (26). Außerdem konnte gezeigt werden, dass durch mTOR-Inhibition durch die allosterische Blockade des katalytischen Zentrums der Kinase die Rephosphorylierung von 4E-BP1 verhindert werden kann (25).

Ein Ansatz, diese limitierenden Faktoren zu umgehen und so die Wirkung einer Therapie zu steigern, ist die Entwicklung von dualen PI3K/mTOR-Inhibitoren, die durch eine ATP-kompetitive Blockade des katalytischen Zentrums die Kinaseaktivität hemmen (27). Da die ATP-Bindetaschen der Kinasen PI3K und mTOR strukturell sehr ähnlich sind, findet eine Inhibition beider Kinasen statt. Die *Feedback*-Aktivierung über p70S6K/IRS-1/PI3K soll damit verhindert werden. Auch beschränkt sich die Wirkung nicht wie bei Everolimus auf den mTOR-Komplex C1, sondern hemmt ebenfalls die Kinaseaktivität von mTORC2, der die AKT-Phosphorylierung an S473 reguliert.

In vitro hat sich bereits ein dualer PI3K/mTOR-Inhibitor namens BEZ235 in pankreatischen NEN als wirksam erwiesen (28), klinische Studien mussten allerdings wegen Unverträglichkeit abgebrochen werden (29). Eine vielversprechende Alternative stellt die Verbindung Gedatolisib (PKI587) dar (30), deren Unverträglichkeitspotential in der Phase I Studie als kontrollierbar eingestuft wurde (31). Im Hauptforschungsprojekt dieser Arbeit wurde dieser Wirkstoff funktionell *in vitro* gegen Everolimus als Referenzstandard in verschiedenen GEP-NEN Tumormodellen verglichen und seine Auswirkungen auf das Signaltransduktionsnetzwerk (Protein- und Genexpressionsebene) untersucht.

Eine weitere Überlegung, um sowohl die limitierenden *Feedback Loops* zu umgehen, als auch eine gut verträgliche Substanz zu finden um NENs zu behandeln, sind selektive PI3Kα-Inhibitoren. Diese greifen *upstream* des durch mTOR-Inhibition aktivierten Mediators AKT an. Die 110α Untereinheit von PI3K ist die vorherrschende katalytische Einheit in neuroendokrinen pankreatischen ß-Zellen (32) und ist dort u.A. beteiligt an Angiogenese (33). Der Vertreter Alpelisib (BYL719 (34, 35)) hat

bereits in einer vorangegangenen *in vitro* Studie antiproliferative Effekte in GEP-NEN Zelllinien (BON-1 und QGP-1) gezeigt (28). Im zweiten Projekt dieser Arbeit, einer separaten *in vitro* Studie, wurde auch dieser Wirkstoff im Rahmen des deutschlandweiten Kooperationsprojektes GERMAN NET-Z sowohl funktionell als auch seine molekularen Auswirkungen auf die Signaltransduktion untersucht. Dabei wurden die Experimente zur Viabilität und zum Zellzyklus von mir betreut.

Das dritte Projekt dieser Arbeit beschäftigt sich ebenfalls mit einem Mediator, der mit der AKT-Signaltransduktion verknüpft ist. FOXM1 (Forkhead box protein M1) ist ein Transkriptionsfaktor, der *downstream* von AKT die Transkription von verschiedenen pro-proliferativen Genen wie z.B. Cyclin A, B und D1, cdc25B, c-myc, Aurora A und B oder survivin reguliert (3). Außerdem wird FOXM1 mit dem Differenzierungsgrad, mit einer VEGF-abhängigen Angiogenese-Stimulation und über MMP-2 und MMP-9 mit Tumormigration in Verbindung gebracht (3). Gegenspieler von FOXM1 sind p53 über RB/E2F (36) und FOXO3, die ebenfalls mit der AKT-Signaltransduktion verknüpft sind.

In dieser Studie wurde FOXM1 in Patientenmaterial detektiert und mit klinischen Daten korreliert, außerdem wurde FOXM1 *in vitro* am Zelllinienmodell als mögliche innovative Angriffsstruktur einer Pharmakotherapie evaluiert. Dazu wurde der FOXM1 Inhibitor Siomycin A verwendet und die funktionelle Wirksamkeit dieser Behandlung untersucht. Auch bei dieser Studie habe ich die Viabilitäts- und Zellzyklus-Assays betreut.

2. METHODIK

2.1 Zellkultur

Es wurden die pankreatischen neuroendokrinen Tumorzelllinien BON und QGP-1 verwendet, sowie die neuroendokrinen Tumorzelllinien KRJ-I aus dem Ileum, LCC-18 aus dem Kolon und NCI-H727 aus der Lunge (typisches Carcinoid). BON und KRJ-I Zellen wurden in DMEM/Ham's F12 (1:1) Medium (Biochrome GmbH) kultiviert, QGP-1 und NCI-H727 in RPMI Medium, LCC-18 in DMEM Medium (beide PAA Laboratories GmbH). Alle Medien enthielten 10% FBS Gold (PAA Laboratories GmbH, dieselbe Charge für die gesamte Studie), 1% Penicillin/Streptomycin (PAA) und stabiles Glutamin, RPMI und DMEM wurden außerdem 25mM HEPES-Puffer (Biochrome) zugesetzt.

Die Zellen wurden nach laborinternen Standards kultiviert (1), vor Beginn der Studie authentifiziert (DSMZ, Deutsche Sammlung von Mikroorganismen und Zellkulturen, Braunschweig) und regelmäßig verifiziert, sowie auf Mykoplasmen untersucht (1).

2.2 Wirkstoffe

Gedatolisib (PKI-587) wurde von Pfizer Inc. (Milwaukee, Wis., USA) zur Verfügung gestellt, Alpelisib (BYL719) von Novartis Parmaceuticals (Basel, Schweiz). Siomycin A wurde über Sigma Aldrich bezogen, Everolimus (RAD001) über Cell Signaling Tec. Inc.

2.3 Zell-Viabilität-Assay

Die Zellen wurden in 96-*well*-Platten ausgesät (je nach Zelllinie 7.000-20.000 Zellen/*well*), adhärierten über Nacht, es folgte die Inkubation (24h, 48h, 96h) mit verschiedenen Konzentrationen (in präliminären Experimenten ermittelt) von Gedatolisib, Everolimus, Alpelisib und Siomycin A gegen Kontrolle (DMSO). Fünf technische Replikate pro Experiment, jedes Experiment wurde in drei biologischen Replikaten durchgeführt. Das Cell Proliferation Reagent WST-1 (Roche Diagnostics GmbH) wurde gemäß Herstellerangaben angewendet, die Messung erfolgte kolorimetrisch (Tecan Sunrise,Tecan Trading AG) (1). Berechnung der Dosis-Wirkungs-Kurve (GraphPad PRISM 6 Software) und Ermittlung der *Efficacy* (maximale Wirksamkeit, unteres Plateau der Kurve) der relativen IC_{50} (c bei halb-maximalem Effekt (37)) und der Konzentrationen c_{mid} (IC_{20}, ca. 80% des maximalen Effekts) und c_{max} (möglichst geringe Konzentration bei maximalem Effekt) (1-3).

2.4 Multiplex-Assay Zellviabilität, Zytotoxizität und Apoptose

Die Zellen (BON-1, KRJ-I, LCC-18, QGP-1) wurden in 96-*well*-Platten ausgesät (je nach Zelllinie 7.000-20.000 Zellen/*well*), adhärierten über Nacht und wurden in drei technischen Replikaten mit Gedatolisib und Everolimus inkubiert (12h und 36h, IC_{50} und c_{max}, DMSO als Kontrolle). Das Apotox-Glo Triplex Assay Kit (Promega) wurde gemäß Herstellerprotokoll angewendet, die Messung der Viabilität und Zytotoxizität (verschiedene Wellenlängen) erfolgte fluorimetrisch (Tecan Infinite M200), die anschließende Messung der Caspase 3/7- Aktivität luminometrisch (Bertold Centro LB 960). Jedes Experiment wurde in drei biologischen Replikaten durchgeführt (1).

2.5 Zellzyklus-Analyse und Bestimmung des Mitotischen Index

Die Zellen wurden in 3,5cm-Schalen ausgesät (je nach Zelllinie 125.000-500.000/*dish*), adhärierten über Nacht und wurden in jeweils vier biologischen Replikaten mit verschiedenen Konzentrationen von Gedatolisib, Everolimus, Alpelisib und Siomycin A inkubiert (48h und 96h, DMSO als Kontrolle). Die geernteten Zellen wurden nach Standardprotokoll fixiert, gefärbt (DNA-Gehalt: Propidiumjodid, Invitrogen, mitotische Zellen: phospho(Ser10)-Histon-H3-Primärantikörper

1:1.600 und Alexa Fluor 488 Sekundärantikörper 1:500, Cell Signaling) und unverzüglich durchflusszytometrisch analysiert (BD FACSCalibur mit CellQuest Pro Software, die Auswertung erfolgte mit FlowJo 8.7 Software) (1-3).

2.6 Bestimmung des mitochondrialen Membranpotentials (frühe Apoptose)

Die Zellen (BON-1, KRJ-I, LCC-18, QGP-1) wurden in 3,5cm Schalen ausgesät (375.000/*dish*), adhärierten über Nacht, und wurden in je vier biologischen Replikate mit Gedatolisib und Everolimus inkubiert (16h, IC_{50} und $c_{max,}$ DMSO als Kontrolle). Die geernteten Proben wurden mit JC-1 Reagenz (5µM; AAT Bioquest) bei 37 °C für 30 Minuten gefärbt, CCCP (carbonyl-cyananid m-chlorophenyl hydrazon, 50µM; Abcam Biochemicals) wurde als Positivkontrolle verwendet. Die Messung der Fluoreszenzsignale erfolgte durchflusszytometrisch (BD FACSCalibur mit CellQuest Pro Software, Auswertung mit FlowJo 8.7 Software) (1).

2.7 Western Blot Analyse

Die Zellen (BON-1, KRJ-I, LCC-18, QGP-1) wurde in Zellkulturflaschen (T25 oder T75, je vier biologische Replikate) kultiviert und mit Gedatolisib und Everolimus inkubiert (24h, c_{mid}, DMSO als Kontrolle). Die Durchführung von Ernte, Lyse, Bestimmung des Proteingehalts, SDS-PAGE, Western Blot und Antikörper-Inkubation wurde nach etabliertem Standardprotokoll ausgeführt (1, 3) (20µg Protein/Bahn, PVDF-Membran, Block in 5%Milch/TBS-T für 60 Minuten, HRP-Sekundärantikörper/ECL Prime Western Blotting Reagenz). Für die Detektion wurde ein Fujifilm LAS 4000 Lumineszenz-Image Analyzer verwendet, für die densitometrische Auswertung die Fujifilm MultiGauge Software (Version 3, Normalisierung auf Coomassie-Färbung des Gesamtproteins (38), Mittelwert der 4 Replikate)(1, 3).

2.8 Genexpressionsanalyse mit dem nCounter® System (NanoString® Technology)

Die Zellen (KRJ-I, LCC-18 und QGP-1) wurden in 6cm Schalen ($1{,}5 – 4 \times 10^6$ Zellen/*dish*) ausgesät, adhärierten über Nacht und wurden in je zwei biologischen Replikaten mit Gedatolosib und Everolimus (60h, c_{mid}, DMSO als Kontrolle) inkubiert. Die RNA wurde mit einem RNeasy Mini Kit (Qiagen) gemäß Herstellerprotokoll extrahiert und mit einem NanoDrop 2000c Spektrophotometer (Thermo Fisher Scientific) quantifiziert. Je 60ng RNA wurden pro Probe eingesetzt, die Probenvorbereitung und Messung erfolgte gemäß Anweisungen des Herstellers mit dem PanCancer Pathway Panel Kit, der nCounter® PrepStation 5s und dem nCounter® Digital Analyzer 5s (NanoString®).

Die Datensätze wurden durch die zugehörige nSolver® 2.5 Software mit dem PanCancer Pathway Modul mittels Hauptkomponentenanalyse ausgewertet. Die daraus resultierenden *log fold changes* relevant regulierter Gene (Änderung der mRNA-Menge im Vergleich zur Kontrolle; *Cut-off* >1,5 und <0,5; p<0,05) wurden zu *Pathway Scores* summiert.

2.9 Statistische Methoden

Die statistische Auswertung erfolgte mit Microsoft Excel und GraphPad Prism 6 Analysis Software (San Diego, California, USA). Alle Datensätze wurden mit dem Kolmogorov-Smirnov Test (mit Dallal-Wilkinson-Lilliefors p Wert, geeignet für Datensätze unter 20 Punkten), auf Normalverteilung überprüft. Ausreißer wurden mittels Grubbs‘ Test (alpha = 0,05) identifiziert.
Zur Ermittlung der Dosis-Wirkungs-Kurve wurde die Methode der kleinsten Quadrate mit variabler Neigung verwendet; das Bestimmtheitsmaß wurde mit R^2 und der Summe der Abweichungsquadrate berechnet. Für die Analyse signifikanter Unterschiede zwischen zwei oder mehr Datensätzen, wurde ANOVA mit oder ohne wiederholter Messung (abhängig vom Experiment) verwendet. Als p-Wert wurde 0,05 zugrunde gelegt.

3. ERGEBNISSE

3.1 Reduktion der Zellviabilität in neuroendokrinen Tumorzellen (WST-1 Assay)

Sowohl Gedatolisib als auch Everolimus bewirken eine zeit- und dosisabhängige Reduktion der Zellviabilität. Gedatolisib ist dabei mit einer Reduktion auf 39-6% im Vergleich zur Kontrolle dem Referenzstandard Everolimus (Reduktion auf 53-48%) überlegen. Der PI3Kα Inhibitor Alpelisib reduzierte die Viabilität auf 21-9% (Abb. 2, KRJ-I, LCC-18 und NCI-H727 nicht gezeigt), der FOXM1 Inhibitor Siomycin A zeigte maximale Effekte von Reduktionen auf 15-0% (Daten nicht gezeigt).

3.2 Bestimmung von IC_{50}, c_{mid} und c_{max}

Tabelle 1 zeigt die Zusammenfassung der ermittelten Konzentrationen für die relative IC_{50}, c_{mid} und c_{max}.

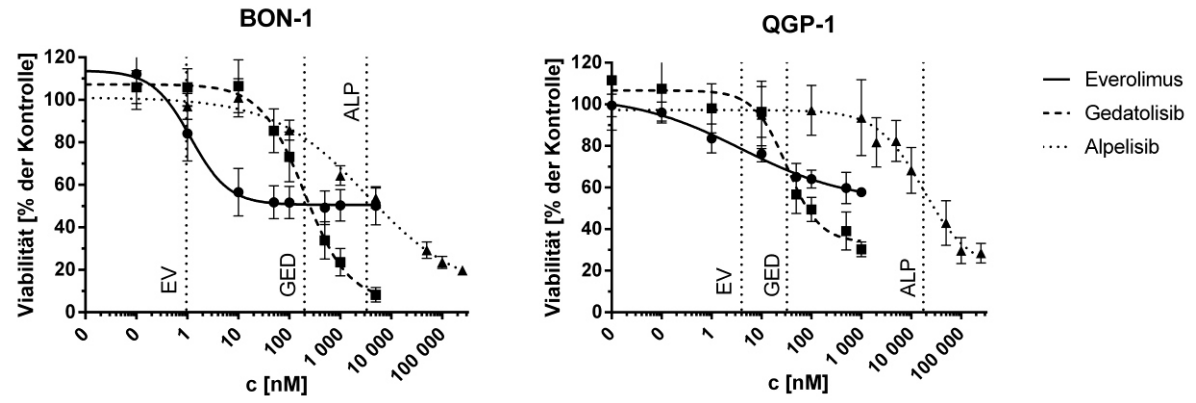

Abbildung 2 Viabilität und IC_{50} Dosis-Wirkungs-Kurven (*nonlinear curve fit*) verschiedener Inhibitoren der PI3K/AKT/mTOR-Signaltransduktion. Die Tumorzelllinien wurden 96h lang inkubiert, anschließend wurde die Zellviabilität (WST-1 Assay, Roche) ermittelt. Senkrechte Linien: IC_{50}. Unteres Plateau: maximale Effektivität

		BON-1	KRJ-1	LCC-18	QGP-1	NCI-H727
Everolimus	IC_{50}	1nM	2,5nM	2,5nM	2,5nM	
	c_{mid}	100nM	100nM	100nM	100nM	
	c_{max}	500nM	500nM	500nM	500nM	
Gedatolisib	IC_{50}	250nM	25nM	250nM	50nM	
	c_{mid}	1.000nM	500nM	1.000nM	500nM	
	c_{max}	10.000nM	1.000nM	10.000nM	1.000nM	
Alpelisib	IC_{50}	3.290nM			17.570nM	5.480nM
	c_{mid}	100.000nM			100.000nM	100.000nM
Siomycin A	IC_{50}	1.000nM	1.000nM	1.000nM	2.000nM	
	c_{max}	3.500nM	3.500nM	3.500nM	3.500nM	

Tabelle 1 IC_{50}, c_{mid} und c_{max} verschiedener Inhibitoren der PI3K/AKT/mTOR-Signaltransduktion in NEN-Zelllinien.

3.3 Gedatolisib induziert Apoptose in GEP-NEN (JC-1, Durchflusszytometrie)

Eine Änderung des Membranpotentials von Mitochondrien ($\Delta\psi_m$) zeigt frühe apoptotische Prozesse an. Nach Behandlung mit hohen Konzentrationen (c_{max}) Gedatolisib wurde in den Zelllinien BON-1 und LCC-18 ein signifikanter Anstieg der apoptotischen Zellen festgestellt. Auch bei KRJ-I Zellen konnte eine erhöhte aber nicht signifikante Apoptoseaktivität (p=0,09) detektiert werden (Abb. 3).

3.4 Simultanbestimmung von Viabilität, Apoptose und Zytotoxizität (Apotox-Glo Assay)

Viabilität: Die hier ermittelten Daten entsprachen im Wesentlichen den Daten der WST-1-Versuche und bestätigten diese (Daten nicht gezeigt).

Apoptose: Die Detektion der Caspase 3/7 Aktivität nach 36 Stunden Behandlung der Zellen mit hohen Konzentrationen (c_{max}) Gedatolisib zeigte einen signifikanten Anstieg apoptotischer Prozesse in BON-1, KRJ-I und LCC-18 Zellen. Everolimus dagegen löste nur in KRJ-I Zellen Apoptose aus. Diese Daten bestätigen die Ergebnisse aus dem durchflusszytometrischen JC-1 Assay (Abb. 3).

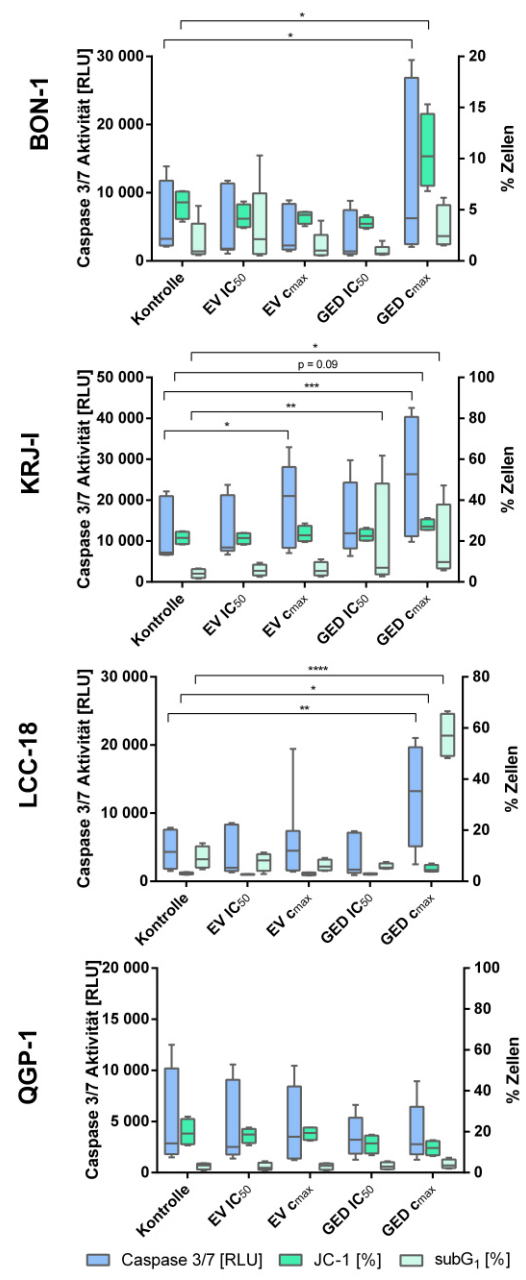

Abbildung 3 Wirkstoffinduzierte Apoptoseinduktion Die Tumorzelllinien wurden mit Everolimus oder Gedatolisib inkubiert, Messung der Apoptose mittels verschiedener Verfahren: Caspase 3/7 Aktivität, mitochondriales Membranpotential (JC-1) und Quantifizierung von *apoptotic bodies* ($subG_1$-peak). *: $p \leq 0.05$, **: $p \leq 0.01$, ***: $p \leq 0.001$, ****: $p \leq 0.0001$

Zytotoxizität: Nach 12 Stunden Behandlung konnte weder für Gedatolisib noch für Everolimus eine Änderung der detektierten *dead-cell-protease* im Vergleich zur Kontrolle nachgewiesen werden.

3.5 Verlangsamung des Zellzyklus und G_0/G_1-Arrest

Sowohl für Gedatolisib als auch für Everolimus wurde ein zeit- und dosisabhängiger Zellzyklus-Arrest in der G_0/G_1-Phase festgestellt, wohingegen die Anzahl der Zellen in der S, G_2 und M Phase verringert ist. Gedatolisib rief diesen Effekt deutlich stärker hervor, signifikant in BON-1 und QGP-1 Zellen (Abb. 4).

Zusätzlich konnte nach Gedatolisib-Behandlung das Auftreten von $subG_1$-peaks in den beiden intestinalen Zelllinien KRJ-I und LCC-18 beobachtet werden. Die hier detektierten *apoptotic bodies* zeigen eine weitgehend abgeschlossene Apoptose an (Abb. 3).

Auch die Behandlung mit der IC_{50} von Alpelisib führte zu einem G_0/G_1-Arrest in BON-1, QGP-1 und NCI-H727 (Abb. 4, NCI-H727 nicht gezeigt). In höheren Dosis traten zusätzlich $subG_1$-Peaks auf (Daten nicht gezeigt).

Da FOXM1 Gene des G_2/M-Übertritts reguliert (39), verursachte Siomycin A entsprechend eine signifikante Reduktion des mitotischen Index. Zusätzlich dazu wurden anhand deutlicher $subG_1$-peaks auch hier apoptotische Prozesse detektiert (Daten nicht gezeigt).

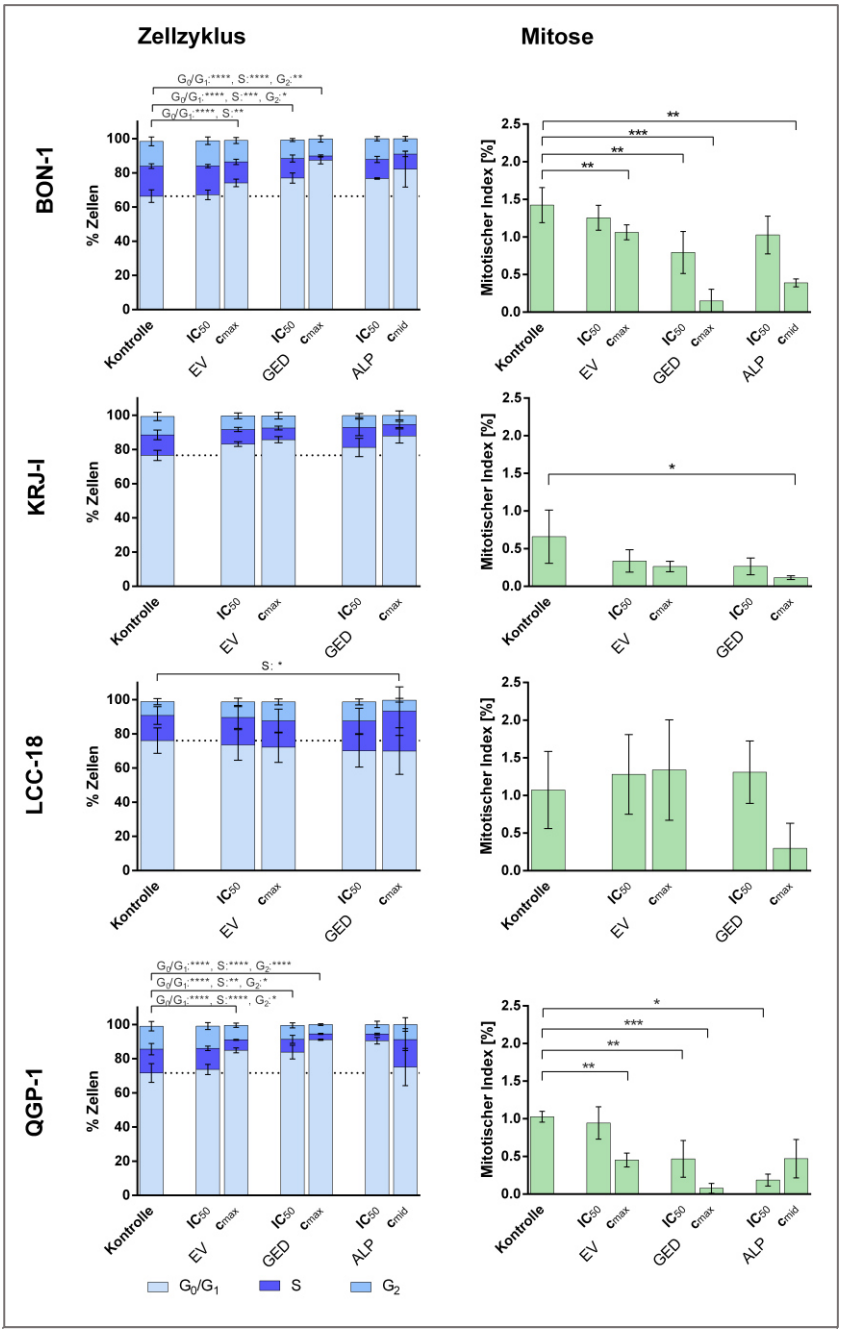

Abbildung 4 Wirkstoffinduzierte Restriktion des Zellzyklus Die Tumorzelllinien wurden mit Everolimus, Gedatolisib oder Alpelisib (nur BON-1 und QGP-1) inkubiert. Durchflusszytometrische Messung des DNA-Gehalts (Propidiumjodid) zur Unterscheidung der Zellzyklus-Phasen G_0/G_1, S und G_2. Detektion der mitotischen Zellen mittels spezifischem phospho-Histon H3(Ser10)-Antikörper. *: $p \leq 0.05$, **: $p \leq 0.01$, ***: $p \leq 0.001$, ****: $p \leq 0.0001$

3.6 Western Blot Analyse

Die detaillierten Ergebnisse sind in Tabelle 2 aufgeführt, sie stellen jeweils die Veränderung im Vergleich zur Kontrolle dar. Beispielhafte Banden eines der je vier Replikate sind in Freitag et al. (1) dargestellt. Insgesamt wurden vier verschiedene Fragestellungen bearbeitet.

Nachweis des Wirkprinzips: Es wurden verschiedene *downstream targets* von PI3K und mTOR und deren Phosphorylierung untersucht. Während sich die Effekte der beiden Wirkstoffe Gedatolisib und Everolimus im Vergleich zur Kontrolle bei p70S6K/pp70S6K (T389) und AKT/pAKT (S473 und T308) nicht wesentlich voneinander unterscheiden, gab es dagegen einen klaren Effekt von Gedatolisib auf die Phosphorylierung von 4E-BP1.

Feedback-Aktivierung von AKT: Es wurden verschiedene direkte Zielproteine von AKT und deren Phosphorylierung untersucht, um die Kinaseaktivität zu beurteilen. Everolimus hatte nur leichte Effekte auf die Zielstrukturen, die in keinem Fall Signifikanzniveau erreichten. Der duale Inhibitor Gedatolisib rief

		BON-1		KRJ-I		LCC-18		QGP-1	
		Everolimus	Gedatolisib	Everolimus	Gedatolisib	Everolimus	Gedatolisib	Everolimus	Gedatolisib
Wirk-Prinzip	p4E-BP1 (S65)	-	---*	--*	---*	+	-	--	---*
	4E-BP1	0	---*	-	-	+	0	0	--
	pp70S6K (T389)	---*	---	---*	---*	---*	0	---*	---*
	p70S6K	0	+	0	0	0	0	0	0
	pAkt (S473)	-	-	---*	---	0	0	0	0
	pAkt (T308)	0	0	0	0	0	0	0	0
	panAkt	+++*	++	0	0	0	0	+	0
Akt Aktivität	pmTOR (S2448)	0	0	0	++	0	0	-	0
	mTOR	+	++	0	-	0	0	0	0
	pTSC2 (T1462)	0	0	0	+	0	0	0	0
	TSC2	0	0	0	0	+	-	0	---*
	pFOXO1 (T24)	0	+++*	0	+	0	++	0	0
	FOXO1	0	+++*	0	0	0	0	+	+
	pGSK-3α (S21)	0	0	+	++	0	0	+	+++*
	pGSK-3β (S9)	0	0	+	++	0	0	+	+++*
	GSK-3β	0	0	0	0	0	0	0	0
Zellzyklus	pRb (S780)	0	+	---	--	0	0	---*	---*
	Rb	-	--	---*	---*	---	---	--	---
MAPK Signaling	pERK1/2 (T202/204)	++	+++*	+	++	0	+	0	+++*
	ERK 1/2	+	0	-	0	-	--	0	0

Tabelle 2 Zusammenfassung der Western Blot Daten. Die Tumorzelllinien wurden 24h mit Gedatolisib oder Everolimus inkubiert. Dargestellt ist die Änderung der Bandenintensität (Mittelwert aus vier biologischen Replikaten) im Vergleich zur unbehandelten Kontrolle (blau: schwächere Banden, rot: stärkere Banden, 0: kein Unterschied, *: signifikante Änderung)

eine stärkere Reaktion hervor (signifikanter Anstieg von FOXO1/pFOXO1 in BON-1 Zellen und von pGSK3 in QGP-1 Zellen), die aber je nach Zelllinie sehr unterschiedlich ausfällt.

Zellzyklusproteine: Alle Zelllinien zeigten nach Behandlung eine klare Reduktion von Rb, die beiden langsamer wachsenden Zelllinien KRJ-I und QGP-1 auch von pRb, es gab allerdings keinen Unterschied zwischen Everolimus und Gedatolisib.

MAPK Signalweg Aktivität: In allen Zelllinien wurden nach Gedatolisib-Behandlung stärkere pERK1/2 Banden detektiert als nach Everolimus-Behandlung.

3.7 Genexpressionsanalyse

Insgesamt wurden die mRNA-Level von 730 verschiedenen Genen aus 13 anerkannten Krebs-assoziierten Signalwegen (KEGG System) untersucht. Der *log fold change* relevant regulierter Gene wurde für jeden Signalweg zu einem *Pathway-Score* summiert, Tabelle 3 enthält alle ermittelten

	KRJ-I				LCC-18				QGP-1			
	Everolimus		Gedatolisib		Everolimus		Gedatolisib		Everolimus		Gedatolisib	
Signalweg	Score	Gene	Score	Gene	Score	Gene	Score	Gene	Score	Gene	Score	Gene
Apoptose			2.73	2			3.90	1	1.28	2	6.70	7
Zellzyklus	7.07	3	2.91	3					17.01	12	71.01	26
ChromMod	3.61	2	2.79	1					0.66	2	8.99	6
DNARepair			2.47	2	0.82	1	0.88	1	10.60	8	52.31	16
Hedgehog									5.01	2	6.65	2
MAPK	13.21	7	16.99	9	9.38	3	0.83	1	12.37	10	28.55	19
Notch	1.91	3	2.92	2	1.96	1	0.89	1	4.55	2	6.64	4
PI3K	11.83	8	23.68	10	5.32	2	3.37	2	10.69	9	41.06	23
RAS	4.03	2	10.99	6	8.27	3	2.78	3	8.58	5	27.95	16
STAT	14.59	5	26.53	9	1.44	1	3.26	3	2.45	3	16.66	11
TGFB			1.03	1					1.98	2	7.40	3
TXmisReg	6.89	2	9.26	4	1.44	1	2.20	2	8.87	7	26.93	10
Wnt	3.03	1	3.99	3	4.37	1			8.37	5	11.64	6
total	66.16	30	103.57	33	33.00	9	14.21	14	91.15	54	305.79	111

Tabelle 3 *Pathway-Scores* der Genexpressionsanalyse (730 Gene des PanCancer Pathway Panel, NanoString®). Die Tumorzelllinien wurden mit Gedatolisib oder Everolimus inkubiert. Die *log fold changes* (im Vergleich zur unbehandelten Kontrolle) von relevant regulierten Genen wurden zu *Pathway-Scores* summiert. Gene, die in verschiedenen Signalwegen eine Rolle spielen, wurden in jedem berücksichtigt. Die Höhe des *Scores* gibt das Ausmaß der wirkstoffinduzierten Genregulation an, die Spalte „Gene“ zeigt, wie viele Gene des Signalweges relevant reguliert werden.

Scores. Insgesamt regulieren QGP-1 Zellen durch die Behandlung ihre Genexpression am stärksten, LCC-18 Zellen am schwächsten. In allen Zelllinien werden durch Gedatolisib mehr Gene und diese stärker in ihrer Expression verändert als durch Everolimus.

Außerdem sind in Abbildung 5 die Expressionsänderung nach Behandlung einzelner Gene dargestellt. *EIF4EBP1* (Protein 4E-BP1) und *E2F1* (Protein E2F1) werden in KRJ-I und QGP-1 Zellen durch die Behandlung herunter reguliert, nicht jedoch in LCC-18 Zellen. In keiner der Zelllinien konnte eine Änderung der *RB1*-Expression beobachtet werden. Verschiedene Gene, die während der G_0/G_1 Phase eine Rolle spielen, sind in QGP-1 Zellen nach Behandlung stark verändert exprimiert (Abb. 5).

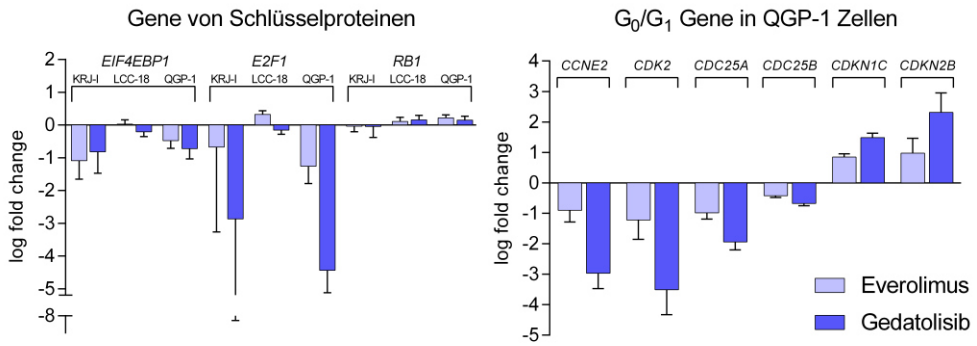

Abbildung 5 Änderung der Genexpression Wirkstoffinduzierte Änderung der Genexpression (*log fold changes*) einzelner Gene in NEN Tumorzelllinien nach Inkubation mit Gedatolisib oder Everolimus.

4. DISKUSSION

4.1 Gedatolisib ist Everolimus überlegen in Wachstumskontrolle und Apoptose-Induktion

Zwar sind von Gedatolisib höhere Konzentrationen als von Everolimus notwendig, um einen therapeutischen Effekt zu erzielen, jedoch senkt die duale Inhibition von PI3K und mTOR die Viabilität deutlich effektiver (siehe IC_{50} Tabelle 1 und Abb. 2). Die eingesetzten Dosen liegen dennoch im physiologischen und damit im klinisch einsetzbaren Bereich (12, 31). Auch der selektive PI3Kα Inhibitor Alpelisib und der FOXM1 Inhibitor Siomycin A senken die Viabilität in NENs stärker als Everolimus.

Der Gesamteffekt setzt sich zusammen aus einer Restriktion des Zellzyklus (G_0/G_1-Arrest) und der Induktion von Apoptose, die jeweils über das intrazelluläre Signaltransduktionsnetzwerk reguliert werden. Das funktionelle Ansprechen der verschiedenen Zelllinien und damit der unterschiedlichen Tumormodelle variiert dabei stark. Beispielsweise sprechen KRJ-I und QGP-1 Zellen generell schlechter auf die Behandlung an als BON-1 und LCC-18 Zellen. QGP-1 Zellen reagieren intensiv mit einer Restriktion des Zellzyklus im Gegensatz zu LCC-18, die hauptsächlich Apoptose induzieren. Um Tumormarker für NENs zu entwickeln und um für den individuellen Patienten die optimale Behandlung zu finden, ist es von Bedeutung, die zugrundeliegenden Prozesse besser zu verstehen.

4.2 4E-BP1 als entscheidender Faktor bezüglich Malignität und Ansprechen

In dieser Studie konnte 4E-BP1 als wichtiger Mediator der antitumoralen Aktivität des dualen Inhibitors Gedatolisib identifiziert werden. Durch die Inhibition von mTORC1 durch Everolimus wird die Phosphorylierung von 4E-BP1 nicht zuverlässig unterbunden (Tabelle 2). Auch Choo et al. berichteten bereits über eine solche Rapamycin-typische partielle Inhibition von mTORC1 (23). Durch die Inhibition des katalytischen Zentrums von mTOR durch Gedatolisib konnten dagegen deutliche Effekte auf diesen Mediator gezeigt werden (Tabelle 2). Diese Unterschiede zwischen den beiden Wirkstoffen korrelieren mit dem funktionellen Ansprechen der Zelllinien.

KRJ-I Zellen, die am besten differenziert sind und am langsamsten wachsen, zeigten den geringsten Unterschied zwischen den beiden Wirkstoffen was die Viabilität, die Induktion von Apoptose, die Restriktion des Zellzyklus sowie die Regulation der Genexpression angeht. Damit einhergehend wurden signifikant reduzierte p4E-BP1-Banden für beide Wirkstoffe detektiert. In dieser Zelllinie wurde auch die geringste basale *EIF4E-BP1* mRNA Expression detektiert.

Ein größerer Unterschied zwischen Gedatolisib und Everolimus bestand in allen Bereichen für die Zelllinien BON-1 und QGP-1, auch hier korrelierte das funktionelle Ansprechen mit der

Phosphorylierung von 4E-BP1. In diesen beiden Zelllinien sowie in NCI-H727 Zellen wurde auch eine Reduktion von p4E-BP1 durch den Einsatz des selektiven PI3Kα Inhibitors Alpelisib detektiert (40).
In den schlecht differenzierten LCC-18 Zellen dagegen wurde eine sechsfach höhere Menge *EIF4E-BP1* mRNA gefunden (Daten nicht gezeigt), was mit einer entsprechend höheren Malignität einhergeht. Diese aggressive Zelllinie zeigte im Vergleich zu den anderen Tumorzelllinien abweichende Ergebnisse, die scheinbar nicht mit p4E-BP1 in Verbindung stehen.

Da die Reduktion der Phosphorylierung an p70S6K, dem zweiten Zielprotein von mTORC1, für Gedatolisib und Everolimus ähnlich stark ausgeprägt ist, kann ausgeschlossen werden, dass der Mehrnutzen von Gedatolisib auf diesen Mediator zurückzuführen ist.

4.3 Wirkung von Gedatolisib unabhängig von mTORC2 Inhibition in GEP-NEN Zellen

In den Zelllinien BON-1 und KRJ-I konnte eine Reduktion von pAKT(S473) für Gedatolisib aber in gleichem Maße auch für Everolimus gezeigt werden. Obwohl mTORC2 generell als Rapalog-insensitiv gilt, nehmen wir eine Everolimus-induzierte Inhibition an, wie sie auch anderweitig bereits beschrieben wurde (41, 42). Da ebenso von stark erhöhten Konzentrationen berichtet wurde, um eine mTORC2 Inhibition zu erreichen, gehen wir davon aus, dass die von uns eingesetzte Dosierung in LCC-18 und QGP-1 Zellen zu niedrig war um einen Effekt auszulösen (43).

4.4 PI3K-Inhbition in GEP-NEN

Die Inhibition von PI3K, die im zellfreien Assay durch Gedatolisib erfolgreich belegt wurde (27), konnte in GEP-NENs nicht bestätigt werden. Weder Gedatolisib noch Everolimus bewirkten eine Veränderung von pAKT(T308). Die PI3K-unabhängige Wirksamkeit von Gedatolisib wurde in einer weiteren Studie ebenfalls beobachtet (44).
Durch den Einsatz des selektiven PI3Kα Inhibitors BYL719 in den Linien BON-1 und QGP-1 konnte dagegen die pAKT(T308) erfolgreich reduziert werden (Daten nicht gezeigt).

4.5 AKT Feedback Aktivierung und Escape-Mechanismus über ERK

Die für Everolimus beschriebene reflektorische Aktivierung von AKT durch *Feedback Loops* (19-22), konnte in dieser Studie nicht bestätigt werden, die Phosphorylierung verschiedener direkter AKT Zielproteine blieb nahezu unverändert. Dafür zeigte die Behandlung mit Gedatolisib bei einigen Targets eine verstärkte Phosphorylierung, allerdings mit deutlichen Unterschieden zwischen

den Zelllinien. Da AKT an S473 und T308 auch nicht stärker aktiviert scheint, sind Interaktionen weiterer Kinasen mit den AKT-Zielstrukturen eine mögliche Erklärung (45-48).
Escape-Mechanismen, die zu einer Aktivierung des MAPK/ERK Signalweges führen (44, 49), konnten dagegen für Gedatolisib eindeutig beobachtet werden, besonders ausgeprägt in den pankreatischen Zelllinien BON-1 und QGP-1. Alpelisib ruft keine reflektorische MAPK/ERK-Aktivierung hervor.

4.6 Zelllinienspezifisches Ansprechen

Das Ausmaß der wirkstoffinduzierten Regulation der Genexpression korreliert mit Restriktion des Zellzyklus und G_0/G_1-Arrest, beides ist in der Zelllinie QGP-1 am stärksten ausgeprägt. Im Einzelnen sind hier die Gene *CCNE2* (cyclin E2) und *CDK2* (CDK2), die für den Übertritt von der G_1 in die S-Phase notwendig sind, *down*-reguliert, genauso wie *CDC25A* und *B* (cdc25A/B), die CDK2 aktivieren. Gene für die inhibitorischen Proteine p57 (*CDKN1C*) und p15 (*CDKN2B*) dagegen sind *up*-reguliert (Abb. 5). Daran scheint der Transkriptionsfaktor E2F beteiligt zu sein, der die Expression von G_1/S-Übertritt-Genen aber auch von Rb und E2F selbst regelt (50) und ebenfalls *down*-reguliert ist. Die Reduktion von pRb auf Proteinebene spricht ebenfalls für eine verminderte Aktivität von E2F, die aber die Transkription von Rb interessanterweise nicht beeinflusst.
Die Zelllinie KRJ-I reagiert ähnlich wie QGP-1 Zellen bezüglich der Transkription von E2F und Rb, sowie der Phosphorylierung von Rb. Der Zellzyklus wird aber deutlich weniger stark einschränkt und es bestehen auch kaum Unterschiede in Zellzyklus-Restriktion und *Pathway Scores* zwischen den beiden Wirkstoffen. Vermutlich sind verschiedene Bedingungen und Prozesse wie zum Beispiel posttranslationale Modifikationen, andere interagierende Proteine oder epigenetische Regulation der Genexpression an den Unterschieden zwischen den Zelllinien beteiligt. Ein Zusammenhang mit der cap-abhängigen Proteintranslation über mTOR/4EB-P1/eIF4E die durch Gedatolisib inhibiert wird ist sehr wahrscheinlich.
LCC-18 Zellen zeigen kaum eine wirkstoffinduzierte Regulation der Genexpression und entsprechend ebenso keine Restriktion des Zellzyklus sowie keine Reduktion von p4E-BP1. Dafür werden durch die Behandlung mit Gedatolisib apoptotische Prozesse gestartet, die möglicherweise mit Autophagie-Prozessen in Zusammenhang stehen könnten, die durch eine mTORC1-Inhibition über ULK1/Atg13 vermittelt werden (51).

Mögliche Limitationen dieser Untersuchungen sind die verwendeten Zell-Linien, die bisher im Hinblick auf die Biologie von NET noch wenig charakterisiert sind.

5. LITERATUR

1. H. Freitag, F. Christen, F. Lewens, I. Grass, F. Briest, S. Iwaszkiewicz, B. Siegmund and P. Grabowski: Inhibition of mTORs Catalytic Site by PKI-587 is a Promising Therapeutic Option for Gastroenteropancreatic Neuroendocrine Tumor Disease. *Neuroendocrinology* (2016) doi:10.1159/000448843
2. S. Nolting, J. Rentsch, H. Freitag, K. Detjen, F. Briest, M. Mobs, V. Weissmann, B. Siegmund, C. J. Auernhammer, E. T. Aristizabal Prada, M. Lauseker, A. Grossman, S. Exner, C. Fischer, C. Grotzinger, J. Schrader and P. Grabowski: The selective PI3Kalpha inhibitor BYL719 as a novel therapeutic option for neuroendocrine tumors: Results from multiple cell line models. *PLoS One*, 12(8), e0182852 (2017) doi:10.1371/journal.pone.0182852
3. F. Briest, E. Berg, I. Grass, H. Freitag, D. Kaemmerer, F. Lewens, F. Christen, R. Arsenic, A. Altendorf-Hofmann, A. Kunze, J. Sanger, T. Knosel, B. Siegmund, M. Hummel and P. Grabowski: FOXM1: A novel drug target in gastroenteropancreatic neuroendocrine tumors. *Oncotarget*, 6(10), 8185-99 (2015)
4. F. Briest and P. Grabowski: PI3K-AKT-mTOR-signaling and beyond: the complex network in gastroenteropancreatic neuroendocrine neoplasms. *Theranostics*, 4(4), 336-65 (2014) doi:10.7150/thno.7851
5. I. M. Modlin, K. Oberg, D. C. Chung, R. T. Jensen, W. W. de Herder, R. V. Thakker, M. Caplin, G. Delle Fave, G. A. Kaltsas, E. P. Krenning, S. F. Moss, O. Nilsson, G. Rindi, R. Salazar, P. Ruszniewski and A. Sundin: Gastroenteropancreatic neuroendocrine tumours. *Lancet Oncol*, 9(1), 61-72 (2008) doi:10.1016/s1470-2045(07)70410-2
6. A. D. Herrera-Martinez, M. D. Gahete, R. Sanchez-Sanchez, R. O. Salas, R. Serrano-Blanch, A. Salvatierra, L. J. Hofland, R. M. Luque, M. A. Galvez-Moreno and J. P. Castano: The components of somatostatin and ghrelin systems are altered in neuroendocrine lung carcinoids and associated to clinical-histological features. *Lung Cancer*, 109, 128-136 (2017) doi:10.1016/j.lungcan.2017.05.006
7. P. J. Houghton: Everolimus. *Clin Cancer Res*, 16(5), 1368-72 (2010) doi:10.1158/1078-0432.ccr-09-1314
8. S. Faivre, C. Delbaldo, K. Vera, C. Robert, S. Lozahic, N. Lassau, C. Bello, S. Deprimo, N. Brega, G. Massimini, J. P. Armand, P. Scigalla and E. Raymond: Safety, pharmacokinetic, and antitumor activity of SU11248, a novel oral multitarget tyrosine kinase inhibitor, in patients with cancer. *J Clin Oncol*, 24(1), 25-35 (2006) doi:10.1200/jco.2005.02.2194
9. M. H. Kulke, H. J. Lenz, N. J. Meropol, J. Posey, D. P. Ryan, J. Picus, E. Bergsland, K. Stuart, L. Tye, X. Huang, J. Z. Li, C. M. Baum and C. S. Fuchs: Activity of sunitinib in patients with advanced neuroendocrine tumors. *J Clin Oncol*, 26(20), 3403-10 (2008) doi:10.1200/jco.2007.15.9020
10. E. Raymond, L. Dahan, J. L. Raoul, Y. J. Bang, I. Borbath, C. Lombard-Bohas, J. Valle, P. Metrakos, D. Smith, A. Vinik, J. S. Chen, D. Horsch, P. Hammel, B. Wiedenmann, E. Van Cutsem, S. Patyna, D. R. Lu, C. Blanckmeister, R. Chao and P. Ruszniewski: Sunitinib malate for the treatment of pancreatic neuroendocrine tumors. *N Engl J Med*, 364(6), 501-13 (2011) doi:10.1056/NEJMoa1003825
11. M. E. Pavel, J. D. Hainsworth, E. Baudin, M. Peeters, D. Horsch, R. E. Winkler, J. Klimovsky, D. Lebwohl, V. Jehl, E. M. Wolin, K. Oberg, E. Van Cutsem and J. C. Yao: Everolimus plus octreotide long-acting repeatable for the treatment of advanced neuroendocrine tumours associated with carcinoid syndrome (RADIANT-2): a randomised, placebo-controlled, phase 3 study. *Lancet*, 378(9808), 2005-12 (2011) doi:10.1016/s0140-6736(11)61742-x
12. J. C. Yao, C. Lombard-Bohas, E. Baudin, L. K. Kvols, P. Rougier, P. Ruszniewski, S. Hoosen, J. St Peter, T. Haas, D. Lebwohl, E. Van Cutsem, M. H. Kulke, T. J. Hobday, T. M. O'Dorisio, M. H. Shah, G. Cadiot, G. Luppi, J. A. Posey and B. Wiedenmann: Daily oral everolimus activity in patients with metastatic pancreatic neuroendocrine tumors after failure of cytotoxic chemotherapy: a phase II trial. *J Clin Oncol*, 28(1), 69-76 (2010) doi:10.1200/jco.2009.24.2669
13. J. C. Yao, M. H. Shah, T. Ito, C. L. Bohas, E. M. Wolin, E. Van Cutsem, T. J. Hobday, T. Okusaka, J. Capdevila, E. G. de Vries, P. Tomassetti, M. E. Pavel, S. Hoosen, T. Haas, J. Lincy, D. Lebwohl and K. Oberg: Everolimus for advanced pancreatic neuroendocrine tumors. *N Engl J Med*, 364(6), 514-23 (2011) doi:10.1056/NEJMoa1009290

14. J. C. Yao, N. Fazio, S. Singh, R. Buzzoni, C. Carnaghi, E. Wolin, J. Tomasek, M. Raderer, H. Lahner, M. Voi, L. B. Pacaud, N. Rouyrre, C. Sachs, J. W. Valle, G. D. Fave, E. Van Cutsem, M. Tesselaar, Y. Shimada, D. Y. Oh, J. Strosberg, M. H. Kulke and M. E. Pavel: Everolimus for the treatment of advanced, non-functional neuroendocrine tumours of the lung or gastrointestinal tract (RADIANT-4): a randomised, placebo-controlled, phase 3 study. *Lancet* (2015) doi:10.1016/s0140-6736(15)00817-x
15. FROM ECC 2015-neuroendocrine cancer: RADIANT-4 trial-NET improvement with everolimus? *Nat Rev Clin Oncol*, 12(12), 684 (2015) doi:10.1038/nrclinonc.2015.181
16. C. Porta, C. Paglino and A. Mosca: Targeting PI3K/Akt/mTOR Signaling in Cancer. *Front Oncol*, 4, 64 (2014) doi:10.3389/fonc.2014.00064
17. S. Wullschleger, R. Loewith and M. N. Hall: TOR signaling in growth and metabolism. *Cell*, 124(3), 471-84 (2006) doi:10.1016/j.cell.2006.01.016
18. M. Showkat, M. A. Beigh and K. I. Andrabi: mTOR Signaling in Protein Translation Regulation: Implications in Cancer Genesis and Therapeutic Interventions. *Mol Biol Int*, 2014, 686984 (2014) doi:10.1155/2014/686984
19. B. Svejda, M. Kidd, A. Kazberouk, B. Lawrence, R. Pfragner and I. M. Modlin: Limitations in small intestinal neuroendocrine tumor therapy by mTor kinase inhibition reflect growth factor-mediated PI3K feedback loop activation via ERK1/2 and AKT. *Cancer*, 117(18), 4141-54 (2011) doi:10.1002/cncr.26011
20. K. Zitzmann, J. Ruden, S. Brand, B. Goke, J. Lichtl, G. Spottl and C. J. Auernhammer: Compensatory activation of Akt in response to mTOR and Raf inhibitors - a rationale for dual-targeted therapy approaches in neuroendocrine tumor disease. *Cancer Lett*, 295(1), 100-9 (2010) doi:10.1016/j.canlet.2010.02.018
21. A. Ginion, J. Auquier, C. R. Benton, C. Mouton, J. L. Vanoverschelde, L. Hue, S. Horman, C. Beauloye and L. Bertrand: Inhibition of the mTOR/p70S6K pathway is not involved in the insulin-sensitizing effect of AMPK on cardiac glucose uptake. *Am J Physiol Heart Circ Physiol*, 301(2), H469-77 (2011) doi:10.1152/ajpheart.00986.2010
22. S. H. Kuo, C. H. Hsu, L. T. Chen, Y. S. Lu, C. H. Lin, P. Y. Yeh, H. J. Jeng, M. Gao, K. H. Yeh and A. L. Cheng: Lack of compensatory pAKT activation and eIF4E phosphorylation of lymphoma cells towards mTOR inhibitor, RAD001. *Eur J Cancer*, 47(8), 1244-57 (2011) doi:10.1016/j.ejca.2011.01.003
23. A. Y. Choo, S. O. Yoon, S. G. Kim, P. P. Roux and J. Blenis: Rapamycin differentially inhibits S6Ks and 4E-BP1 to mediate cell-type-specific repression of mRNA translation. *Proc Natl Acad Sci U S A*, 105(45), 17414-9 (2008) doi:10.1073/pnas.0809136105
24. H. M. S. Ismail: Downstream the mTOR: S6 Kinases between Divergence and Redundancy. *JBPR*, 1(2), 94-105 (2013)
25. A. C. Hsieh, M. Costa, O. Zollo, C. Davis, M. E. Feldman, J. R. Testa, O. Meyuhas, K. M. Shokat and D. Ruggero: Genetic dissection of the oncogenic mTOR pathway reveals druggable addiction to translational control via 4EBP-eIF4E. *Cancer Cell*, 17(3), 249-61 (2010) doi:10.1016/j.ccr.2010.01.021
26. G. Armengol, F. Rojo, J. Castellvi, C. Iglesias, M. Cuatrecasas, B. Pons, J. Baselga and S. Ramon y Cajal: 4E-binding protein 1: a key molecular "funnel factor" in human cancer with clinical implications. *Cancer Res*, 67(16), 7551-5 (2007) doi:10.1158/0008-5472.can-07-0881
27. A. M. Venkatesan, C. M. Dehnhardt, E. Delos Santos, Z. Chen, O. Dos Santos, S. Ayral-Kaloustian, G. Khafizova, N. Brooijmans, R. Mallon, I. Hollander, L. Feldberg, J. Lucas, K. Yu, J. Gibbons, R. T. Abraham, I. Chaudhary and T. S. Mansour: Bis(morpholino-1,3,5-triazine) derivatives: potent adenosine 5'-triphosphate competitive phosphatidylinositol-3-kinase/mammalian target of rapamycin inhibitors: discovery of compound 26 (PKI-587), a highly efficacious dual inhibitor. *J Med Chem*, 53(6), 2636-45 (2010) doi:10.1021/jm901830p
28. I. Passacantilli, G. Capurso, L. Archibugi, S. Calabretta, S. Caldarola, F. Loreni, G. Delle Fave and C. Sette: Combined therapy with RAD001 e BEZ235 overcomes resistance of PET immortalized cell lines to mTOR inhibition. *Oncotarget*, 5(14), 5381-91 (2014) doi:10.18632/oncotarget.2111
29. N. Fazio: Neuroendocrine tumors resistant to mammalian target of rapamycin inhibitors: A difficult conversion from biology to the clinic. *World J Clin Oncol*, 6(6), 194-7 (2015) doi:10.5306/wjco.v6.i6.194
30. R. Mallon, L. R. Feldberg, J. Lucas, I. Chaudhary, C. Dehnhardt, E. D. Santos, Z. Chen, O. dos Santos, S. Ayral-Kaloustian, A. Venkatesan and I. Hollander: Antitumor efficacy of PKI-587, a highly potent dual PI3K/mTOR kinase inhibitor. *Clin Cancer Res*, 17(10), 3193-203 (2011) doi:10.1158/1078-0432.ccr-10-1694

31. G. I. Shapiro, K. M. Bell-McGuinn, J. R. Molina, J. Bendell, J. Spicer, E. L. Kwak, S. S. Pandya, R. Millham, G. Borzillo, K. J. Pierce, L. Han, B. E. Houk, J. D. Gallo, M. Alsina, I. Brana and J. Tabernero: First-in-Human Study of PF-05212384 (PKI-587), a Small-Molecule, Intravenous, Dual Inhibitor of PI3K and mTOR in Patients with Advanced Cancer. *Clin Cancer Res*, 21(8), 1888-95 (2015) doi:10.1158/1078-0432.ccr-14-1306
32. J. Schrader, P. Niebel, A. Rossi, E. Archontidou-Aprin and D. Horsch: Differential signaling by regulatory subunits of phosphoinositide-3-kinase influences cell survival in INS-1E insulinoma cells. *Exp Clin Endocrinol Diabetes*, 123(2), 118-25 (2015) doi:10.1055/s-0034-1390461
33. M. Graupera, J. Guillermet-Guibert, L. C. Foukas, L. K. Phng, R. J. Cain, A. Salpekar, W. Pearce, S. Meek, J. Millan, P. R. Cutillas, A. J. Smith, A. J. Ridley, C. Ruhrberg, H. Gerhardt and B. Vanhaesebroeck: Angiogenesis selectively requires the p110alpha isoform of PI3K to control endothelial cell migration. *Nature*, 453(7195), 662-6 (2008) doi:10.1038/nature06892
34. C. Fritsch, A. Huang, C. Chatenay-Rivauday, C. Schnell, A. Reddy, M. Liu, A. Kauffmann, D. Guthy, D. Erdmann, A. De Pover, P. Furet, H. Gao, S. Ferretti, Y. Wang, J. Trappe, S. M. Brachmann, S. M. Maira, C. Wilson, M. Boehm, C. Garcia-Echeverria, P. Chene, M. Wiesmann, R. Cozens, J. Lehar, R. Schlegel, G. Caravatti, F. Hofmann and W. R. Sellers: Characterization of the novel and specific PI3Kalpha inhibitor NVP-BYL719 and development of the patient stratification strategy for clinical trials. *Mol Cancer Ther*, 13(5), 1117-29 (2014) doi:10.1158/1535-7163.mct-13-0865
35. P. Furet, V. Guagnano, R. A. Fairhurst, P. Imbach-Weese, I. Bruce, M. Knapp, C. Fritsch, F. Blasco, J. Blanz, R. Aichholz, J. Hamon, D. Fabbro and G. Caravatti: Discovery of NVP-BYL719 a potent and selective phosphatidylinositol-3 kinase alpha inhibitor selected for clinical evaluation. *Bioorg Med Chem Lett*, 23(13), 3741-8 (2013) doi:10.1016/j.bmcl.2013.05.007
36. J. Millour, N. de Olano, Y. Horimoto, L. J. Monteiro, J. K. Langer, R. Aligue, N. Hajji and E. W. Lam: ATM and p53 regulate FOXM1 expression via E2F in breast cancer epirubicin treatment and resistance. *Mol Cancer Ther*, 10(6), 1046-58 (2011) doi:10.1158/1535-7163.mct-11-0024
37. J. L. Sebaugh: Guidelines for accurate EC50/IC50 estimation. *Pharm Stat*, 10(2), 128-34 (2011) doi:10.1002/pst.426
38. G. M. Aldridge, D. M. Podrebarac, W. T. Greenough and I. J. Weiler: The use of total protein stains as loading controls: an alternative to high-abundance single-protein controls in semi-quantitative immunoblotting. *J Neurosci Methods*, 172(2), 250-4 (2008) doi:10.1016/j.jneumeth.2008.05.003
39. M. Fischer, P. Grossmann, M. Padi and J. A. DeCaprio: Integration of TP53, DREAM, MMB-FOXM1 and RB-E2F target gene analyses identifies cell cycle gene regulatory networks. *Nucleic Acids Res*, 44(13), 6070-86 (2016) doi:10.1093/nar/gkw523
40. S. Nölting, J. Rentsch, H. Freitag, K. Detjen, F. Briest, M. Möbs, V. Weissmann, B. Siegmund, C. Aurernhammer, E. Aristizabal Prada, M. Lauseker, A. Grossman, S. Exner, C. Fischer, C. Grötzinger, J. Schrader and P. Grabowski: The selective PI3Kα inhibitor BYL719 as a novel therapeutic option for neuroendocrine tumors: Results from multiple cell line models. *PLoS One*, accepted (2017)
41. D. D. Sarbassov, S. M. Ali, S. Sengupta, J. H. Sheen, P. P. Hsu, A. F. Bagley, A. L. Markhard and D. M. Sabatini: Prolonged rapamycin treatment inhibits mTORC2 assembly and Akt/PKB. *Mol Cell*, 22(2), 159-68 (2006) doi:10.1016/j.molcel.2006.03.029
42. D. D. Sarbassov, D. A. Guertin, S. M. Ali and D. M. Sabatini: Phosphorylation and regulation of Akt/PKB by the rictor-mTOR complex. *Science*, 307(5712), 1098-101 (2005) doi:10.1126/science.1106148
43. V. Serra, B. Markman, M. Scaltriti, P. J. Eichhorn, V. Valero, M. Guzman, M. L. Botero, E. Llonch, F. Atzori, S. Di Cosimo, M. Maira, C. Garcia-Echeverria, J. L. Parra, J. Arribas and J. Baselga: NVP-BEZ235, a dual PI3K/mTOR inhibitor, prevents PI3K signaling and inhibits the growth of cancer cells with activating PI3K mutations. *Cancer Res*, 68(19), 8022-30 (2008) doi:10.1158/0008-5472.CAN-08-1385
44. H. P. Soares, M. Ming, M. Mellon, S. H. Young, L. Han, J. Sinnet-Smith and E. Rozengurt: Dual PI3K/mTOR Inhibitors Induce Rapid Overactivation of the MEK/ERK Pathway in Human Pancreatic Cancer Cells through Suppression of mTORC2. *Mol Cancer Ther*, 14(4), 1014-23 (2015) doi:10.1158/1535-7163.mct-14-0669
45. K. M. Jacobs, S. R. Bhave, D. J. Ferraro, J. J. Jaboin, D. E. Hallahan and D. Thotala: GSK-3beta: A Bifunctional Role in Cell Death Pathways. *Int J Cell Biol*, 2012, 930710 (2012) doi:10.1155/2012/930710

46. A. Parrales, E. Lopez, I. Lee-Rivera and A. M. Lopez-Colome: ERK1/2-dependent activation of mTOR/mTORC1/p70S6K regulates thrombin-induced RPE cell proliferation. *Cell Signal*, 25(4), 829-38 (2013) doi:10.1016/j.cellsig.2012.12.023
47. S. Asada, H. Daitoku, H. Matsuzaki, T. Saito, T. Sudo, H. Mukai, S. Iwashita, K. Kako, T. Kishi, Y. Kasuya and A. Fukamizu: Mitogen-activated protein kinases, Erk and p38, phosphorylate and regulate Foxo1. *Cell Signal*, 19(3), 519-27 (2007) doi:10.1016/j.cellsig.2006.08.015
48. C. Sutherland, I. A. Leighton and P. Cohen: Inactivation of glycogen synthase kinase-3 beta by phosphorylation: new kinase connections in insulin and growth-factor signalling. *Biochem J*, 296 (Pt 1), 15-9 (1993)
49. R. Gedaly, P. Angulo, J. Hundley, M. F. Daily, C. Chen and B. M. Evers: PKI-587 and sorafenib targeting PI3K/AKT/mTOR and Ras/Raf/MAPK pathways synergistically inhibit HCC cell proliferation comparison PKI vs. PI-103. *J Surg Res*, 176(2), 542-8 (2012) doi:10.1016/j.jss.2011.10.045
50. S. Polager and D. Ginsberg: E2F - at the crossroads of life and death. *Trends Cell Biol*, 18(11), 528-35 (2008) doi:10.1016/j.tcb.2008.08.003
51. J. Zhang: Teaching the basics of autophagy and mitophagy to redox biologists--mechanisms and experimental approaches. *Redox Biol*, 4, 242-59 (2015) doi:10.1016/j.redox.2015.01.003

EIDESSTATTLICHE VERSICHERUNG

„Ich, Helma Freitag, versichere an Eides statt durch meine eigenhändige Unterschrift, dass ich die vorgelegte Dissertation mit dem Thema: **Inhibition der PI3K/AKT/mTOR-Signaltransduktion: innovative Therapieoptionen für neuroendokrine Tumore auf Basis eines tieferen Verständnisses intrazellulärer Prozesse in NEN** selbstständig und ohne nicht offengelegte Hilfe Dritter verfasst und keine anderen als die angegebenen Quellen und Hilfsmittel genutzt habe.
Alle Stellen, die wörtlich oder dem Sinne nach auf Publikationen oder Vorträgen anderer Autoren beruhen, sind als solche in korrekter Zitierung (siehe „Uniform Requirements for Manuscripts (URM)“ des ICMJE -*www.icmje.org*) kenntlich gemacht. Die Abschnitte zu Methodik (insbesondere praktische Arbeiten, Laborbestimmungen, statistische Aufarbeitung) und Resultaten (insbesondere Abbildungen, Graphiken und Tabellen) entsprechen den URM (s.o) und werden von mir verantwortet.
Meine Anteile an den ausgewählten Publikationen entsprechen denen, die in der untenstehenden gemeinsamen Erklärung mit der Betreuerin, angegeben sind. Sämtliche Publikationen, die aus dieser Dissertation hervorgegangen sind und bei denen ich Autor bin, entsprechen den URM (s.o) und werden von mir verantwortet.
Die Bedeutung dieser eidesstattlichen Versicherung und die strafrechtlichen Folgen einer unwahren eidesstattlichen Versicherung (§156,161 des Strafgesetzbuches) sind mir bekannt und bewusst.“

Datum _____ Unterschrift

ANTEILSERKLÄRUNG AN DEN ERFOLGTEN PUBLIKATIONEN

Helma Freitag hatte folgenden Anteil an den folgenden Publikationen:

Publikation 1: Helma Freitag, Irina Grass, Friederike Christen, Franziska Briest, Patricia Grabowski, Inhibition of mTOR's Catalytic Site by PKI-587 Is a Promising Therapeutic Option for Gastroenteropancreatic Neuroendocrine Tumor Disease, Neuroendocrinology, 2016

Beitrag im Einzelnen: Diese Publikation beschreibt mein Hauptprojekt. Ich habe es im Wesentlichen selbstständig geplant, sämtliche Methoden (bis auf WB) etabliert, die Experimente inklusive Zellkultur durchgeführt, ausgewertet und die Publikation verfasst. Das WB-Verfahren wurde von FB etabliert, FL, IG, FC und SI haben hin und wieder Teilarbeitsschritte wie z.B. WB-Detektionen übernommen oder halfen mir beim Pipettieren in der Probenaufarbeitung. FB und PG standen bei Fragen zur Projektplanung und Durchführung betreuend zur Seite.

Publikation 2: Svenja Nölting, Jakob Rentsch, Helma Freitag, Katharina Detjen, Franziska Briest, Markus Möbs, Victoria Weissmann, Britta Siegmund, Christoph J Auernhammer, Elke Tatjana Aristizabal Prada, Michael Lauseker, Ashley Grossmann, Samantha Exner, Christian Fischer, Carsten Grötzinger, Jörg Schrader, Patricia Grabowski, The selective PI3Kα inhibitor BYL719 as a novel therapeutic option for neuroendocrine tumors: Results from multiple cell line models, Plos One, 2017

Beitrag im Einzelnen: Authentifizierung und Verschickung der Zelllinien an alle Projektteilnehmer, Planung und Betreuung des Teilprojektes, das sich mit der Untersuchung der Zellviabilität und des Zellzyklus beschäftigt. Teilweise Mitwirkung am Manuskript und an der grafischen Darstellung der Ergebnisse.

Publikation 3: Franziska Briest, Erika Berg, Irina Grass, Helma Freitag, Daniel Kaemmerer, Florentine Lewens, Friederike Christen, Ruza Arsenic, Annelore Altendorf- Hofmann, Almut Kunze, Jörg Sänger, Thomas Knösel, Britta Siegmund, Michael Hummel, Patricia Grabowski, FOXM1: A novel drug target in gastroenteropancreatic neuroendocrine tumors, Oncotarget, 2015

Beitrag im Einzelnen: Etablierung von Methoden, Einarbeitung und Betreuung der durchführenden Personen (IG, FC und FL) sowie Hilfs- und Organisationsarbeiten bezüglich der Zellkultur und den Experimenten.

Unterschrift, Datum und Stempel des betreuenden Hochschullehrers/der betreuenden Hochschullehrerin

_____

PD Dr. Patricia Grabowski

Unterschrift des Doktoranden/der Doktorandin

_____

Helma Freitag

Original Paper

Neuro
endocrinology

Neuroendocrinology 2017;105:90–104
DOI: 10.1159/000448843

Received: March 9, 2016
Accepted after revision: August 2, 2016
Published online: August 12, 2016

Inhibition of mTOR's Catalytic Site by PKI-587 Is a Promising Therapeutic Option for Gastroenteropancreatic Neuroendocrine Tumor Disease

Helma Freitag[a] Friederike Christen[a, b] Florentine Lewens[a]
Irina Grass[a, c] Franziska Briest[a, c] Sara Iwaszkiewicz[a, b] Britta Siegmund[a]
Patricia Grabowski[a, d]

[a]Department of Gastroenterology, Infectious Diseases, Rheumatology CC13, Charité – Universitätsmedizin Berlin, [b]Institute of Biology, Humboldt-Universität Berlin, and [c]Department of Chemistry and Biochemistry, Freie Universität Berlin, Berlin, and [d]Department of Gastroenterology and Endocrinology, Zentralklinik Bad Berka GmbH, Bad Berka, Germany

Key Words
PKI-587 · Gedatolisib · mTOR inhibition · Everolimus · Gastroenteropancreatic neuroendocrine tumors · Signaling · 4E-BP1 · LCC-18 cell line

Abstract
Background: The characteristic clinical heterogeneity and mostly slow-growing behavior of gastroenteropancreatic neuroendocrine neoplasms (GEP-NENs) cause problems in finding appropriate treatments. Thus, the current therapy options are not satisfactory. PKI-587 is a highly potent, novel dual inhibitor of PI3K and mTORC1/C2. ***Aim:*** We assessed the effects of PKI-587 in different GEP-NEN tumor models, including the poorly differentiated cell line LCC-18, and compared them with those of the established mTORC1 inhibitor everolimus. ***Methods:*** We treated BON, QGP-1, KRJ-I, and LCC-18 cell lines with increasing concentrations of the inhibitor PKI-587, and compared the results with those of everolimus and DMSO. We assessed the impact of the treatments on viability (WST-1 assay), on apoptotic processes (caspase 3/7 assay, JC-1), and on cell cycle regulation (flow cytometry). We determined alterations in signaling mediators by phosphor-specific Western blot analysis and conducted multiplexed gene expression analysis (nCounter® technology). ***Results:*** In all cell lines, PKI-587 dose-dependently inhibited proliferation, whereas everolimus was less effective. Treatment with PKI-587 led to cell cycle arrest and induction of apoptosis and successfully suppressed activity of the direct mTORC1 target 4E-BP1, a crucial factor for tumor genesis only partially inhibited by everolimus. Gene expression analyses revealed relevant changes of RAS, MAPK, STAT, and PI3K pathway genes after treatment. Treatment-dependent and cell line-characteristic effects on AKT/Rb/E2F signaling regarding cell cycle control and apoptosis are extensively discussed in this paper. ***Conclusion:*** PI3K/mTOR dual targeting is a promising new therapeutic approach in neuroendocrine tumor disease that should be evaluated in further clinical trials.

KARGER

E-Mail karger@karger.com
www.karger.com/nen

Patricia Grabowski
Department of Gastroenterology, Infectious Diseases, Rheumatology CC13
Charité – Universitätsmedizin Berlin, Hindenburgdamm 30
DE–12203 Berlin (Germany)
E-Mail Patricia.Grabowski@charite.de

Introduction

Current Therapy Options for Gastroenteropancreatic Neuroendocrine Neoplasms and Their Pathogenesis

The rare tumor entity of gastroenteropancreatic neuroendocrine neoplasm (GEP-NEN) shows heterogeneity in its clinical behavior and lacks proper therapeutic options. A small, aggressive subgroup shows high proliferation rates, but most GEP-NENs demonstrate slow-growing characteristics, which makes them inaccessible to classical chemotherapies [1]. Despite their increasing incidence, GEP-NENs are counted among the rare neoplastic diseases. However, regarding their prevalence, they are the second most common malignancy in the gastrointestinal system [2].

Previous developments of molecular targeting substances have led to the approval of two members of this compound class for treatment of GEP-NENs. These are everolimus, an inhibitor of mTOR (mechanistic target of rapamycin) [3–5], and sunitinib, a multikinase inhibitor. Both compounds are approved only for the subgroup of progressive neuroendocrine pancreatic tumors [6–8]. Everolimus showed disease-stabilizing activity in intestinal and bronchial tumors as well, but better responses are rare (RADIANT-4 [9, 10]).

The pathogenesis and regulation of proliferation of GEP-NENs are not well investigated. While causal mutations have rarely been found, several pathways were shown to have a determining influence on extended cell growth [reviewed in 1]. Among these, the PI3K/AKT (phosphatidylinositol-4,5-bisphosphate 3-kinase/protein kinase B) signaling cascade, which regulates mTOR, is regarded as an important switch point for protein translation and therefore inducing proliferation and survival [11, 12] (fig. 1).

Everolimus and Its Limitations

The key mediator mTOR serves as a target for the approved inhibitor everolimus (also known as RAD001) and builds two distinct complexes, mTORC1 and mTORC2 (mTOR complex 1 and mTOR complex 2), with different binding partners and target structures [13]. Everolimus selectively inhibits the function of mTORC1 by interfering with raptor (regulatory-associated protein of mTOR)-dependent complex building and therefore prohibiting phosphorylation of the direct targets p70S6K (ribosomal protein S6 kinase, 70 kDa) and 4E-BP1 (eukaryotic translation initiation factor 4E-binding protein) [14].

However, several factors limit the efficacy of treatment with everolimus. Because of the mTORC1 selectivity, activating feedback occurs via mTORC2. Particularly the activation of upstream PI3K/AKT signaling through p70S6K/mTORC2/AKT but also through p70S6K/IRS-1 (insulin receptor substrate 1)/PI3K are considered to be crucial in this context (fig. 1) [15–18]. Further, it was reported that rapamycin analogs like everolimus only partially inhibit mTORC1, leading to rephosphorylation of 4E-BP1 even though raptor-dependent inhibition of p70S6K is maintained [19, 20]. Comparing p70S6K and 4E-BP1, the former turned out to be dispensable for tumor genesis, while 4E-BP1 and its impact via cap-dependent translation was described as a 'funnel factor' for cancer cell growth and progression [21] and was associated with malignancy and adverse prognosis [22]. Use of an inhibitor occupying the catalytic site of mTOR was shown to prevent 4E-BP1 rephosphorylation [21].

PKI-587 and the Aim of the Investigation

A more novel approach to avoid these limitations of feedback and the merely partial inhibition of mTORC1 is the development of dual PI3K/mTOR inhibitors such as PKI-587 by Pfizer (PF-05212384, gedatolisib). These compounds are working ATP competitively [23] and are therefore equally effective in both complexes of mTOR, mTORC1 and mTORC2.

In a recently published, first-in-human phase I clinical trial, its safety risk was classified as manageable [24]. Other preclinical studies reported an efficacy of PKI-587 in vitro and in vivo [25], but observations of PKI-587 activating other pathways [e.g., MAPK (mitogen-activated protein kinases) signaling] were mentioned as well [26].

Because we consider PKI-587 as a promising compound for treating GEP-NENs, we assessed its in vitro impact on several GEP-NEN cell lines and compared it with everolimus as the reference standard. In our study, we did not restrict ourselves to tumor models of typical slow-growing behavior (BON, KRJ-I, and QGP-1) but also included poorly differentiated, fast-proliferating LCC-18 cells, representing a rare and aggressive tumor subset. We investigated antiproliferative effects, the appearance of apoptosis, and cytotoxic events and performed cell cycle analyses. On the molecular level we conducted phospho-specific Western blot and gene expression analyses in order to gain basic insights into the characteristic behavior of the different tumor subtypes.

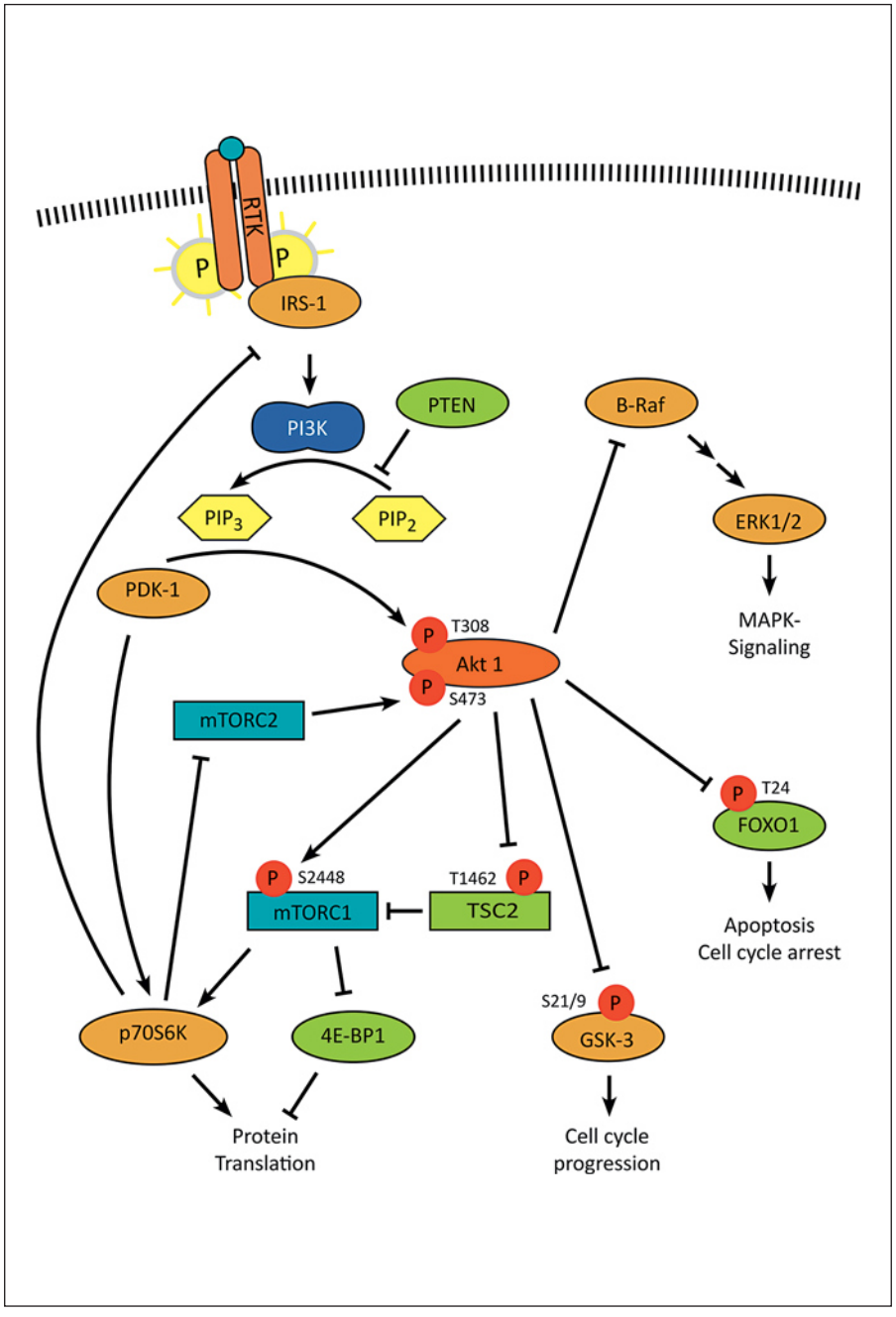

Fig. 1. PI3K/Akt/mTOR signaling is highly activated in GEP-NEN [1, 14]. Extracellular signals, bound to RTK (receptor tyrosine kinases), lead to activation of PI3K via IRS-1, and therefore to phosphorylation of PIP_2 [phosphatidylinositol (3,4)-bisphosphate] to PIP_3 [phosphatidylinositol (3,4,5)-trisphosphate] [54–56]. Constitutively active PDK-1 (3-phosphoinositide-dependent protein kinase-1) requires PIP_3 to phosphorylate – and hence activate – Akt, stimulated by prior Akt phosphorylation at Ser473 through mTORC2 [37, 57]. Active Akt phosphorylates a wide range of substrates (e.g., mTORC1), mostly inhibiting their activity, and therefore stimulates protein translation and the cell cycle and inhibits apoptotic processes [1]. mTORC1 is the target complex for both inhibitors of this study. Everolimus (RAD001) is an allosteric raptor-dependent inhibitor of mTORC1, whereas PKI-587 inhibits the catalytic activity of mTOR in both complexes [14, 23]. Crucial targets of mTOR are p70S6K and 4E-BP1. Phosphorylation of p70S6K by mTOR (Thr389) affects ribosomal protein S6, leading to protein translation [58, 59]. 4E-BP1 is a translation suppressor complexed with eIF4E (eukaryotic translation initiation factor 4E) to prevent cap-dependent translational activity. Phosphorylation of 4E-BP1 causes dissociation of the complex, relieving the inhibitory property [60]. mTORC2 is a complex including rictor (rapamycin-insensitive companion of mechanistic target of rapamycin) and is located upstream of Akt, leading to its phosphorylation at Ser473 [61]. As p70S6K is able to disrupt mTORC2, inhibition of p70S6K subsequently leads to Akt activation. This mechanism is regarded as an important feedback loop limiting the efficacy of mTORC1-specific RAD001 treatment [62]. Other important treatment escape mechanisms are activation of Akt via p70S6K/IRS-1/PI3K or activation of connected MAPK signaling [63, 64].

Materials and Methods

Cell Culture

For all in vitro experiments we employed several GEP-NEN cell line models representing different tumor subtypes. In particular, we used pancreatic BON [27, 28] and QGP-1 [29, 30] cells, ileal KRJ-I [31, 32] cells, and colonic LCC-18 [33] cells.

BON and KRJ-I cell lines were grown in DMEM/Ham's F12 (1:1) medium (Biochrom GmbH), QGP-1 in RPMI medium, and LCC-18 in DMEM medium (both PAA Laboratories GmbH). All media contained 10% FBS Gold (PAA Laboratories GmbH; one single batch for all experiments of this project), 1% penicillin/streptomycin (PAA Laboratories GmbH), and stable glutamine (RPMI and DMEM, also 25 mM HEPES; Biochrom GmbH). The cells received fresh medium twice a week and were held in exponential growth stadium (split once or twice a week). Confluence never exceeded 80% and culture periods were less than 10 weeks. In a regular, recurring procedure, we tested the cell lines for maintenance of specific neuroendocrine marker expression (e.g., chromogranin A, synaptophysin, syntaxin, and synaptobrevin)

by immunofluorescence microscopy. After their receipt in 2012 and 2013, all cell lines were authenticated or verified as unique by the DSMZ (The Leibniz Institute DSMZ – German Collection of Microorganisms and Cell Cultures GmbH, Braunschweig, Germany).

Reagents and Antibodies

The ATP-competitive, dual PI3K/mTOR inhibitor PKI-587 (gedatolisib, PF-05212384) was kindly provided by Pfizer Inc. (Milwaukee, Wis., USA). RAD001 (everolimus) was purchased from Cell Signaling Technology Inc.

Primary antibody against GAPDH was purchased from GeneTex Inc.; all other primary antibodies were purchased from Cell Signaling Technology Inc. The secondary antibodies swine anti-rabbit IgG-HRP and goat anti-mouse IgG-HRP were purchased from DAKO Deutschland GmbH.

Cell Viability Assay

Cells were seeded into 96-well plates, at 7,000–20,000 cells per well, and were left to adhere overnight. For the viability assay, cells were incubated with PKI-587 or RAD001 at eight different concentrations (0.01 nM to 5 μM, assessed for each cell line separately in preliminary testing) or with DMSO as a control (in quintuplicate) for 24, 48, and 96 h. The cell proliferation reagent WST-1 (Roche Diagnostics GmbH) was added according to the manufacturer's instructions. Measurement of absorption was followed by use of a Tecan Sunrise microplate reader (Tecan Trading AG). Each experiment was replicated 3 times independently.

Based on the viability data, we calculated the dose-response curve (GraphPad Prism 6) and determined the IC_{50} (relative IC_{50}, concentration of half-maximal effect [34]), C_{mid} (ca. 80% of the maximal effect, IC_{20}), and C_{max} (concentration of maximal response), considering different incubation times regarding the different requirements of the following experiments.

Multiplexed Viability, Cytotoxicity, and Apoptosis Assay

Cells were seeded into 96-well plates, at 7,000–15,000 cells per well, and were left to adhere overnight. The cells were incubated with PKI-587 or RAD001 at low (IC_{50}) and high (C_{max}) concentrations or with DMSO as a control (in triplicate) for 12 and 36 h. A fluorescence reagent mix for detection of viability and cytotoxicity (different wave lengths) and, later, a chemiluminescence reagent for detection of caspase 3/7 activity were added following the manufacturer's instructions (ApoTox-Glo Triplex Assay; Promega). Measurements were conducted using Tecan Infinite M200 (fluorescence) and Berthold Centro LB 960 plate readers. This experiment was performed 3 times independently.

Cell Cycle Analysis and Determination of Mitotic Index

Cells were seeded into 3.5-cm dishes, at 125,000–500,000 cells per dish, and were left to adhere overnight and incubated with PKI-587 or RAD001 at low (IC_{50}) and high (C_{max}) concentrations or with DMSO as a control for 48 h (all cell lines) and 96 h (just QGP-1 and LCC-18), respectively, in four biological replicates. Fixing and staining of each sample was accomplished as described previously [35]. Mitotic cells were dyed with mitosis-specific Phospho(Ser10)-Histone H3 primary antibody (1:1,600; Cell Signaling Technology Inc., No. 3377) and Alexa Fluor 488 goat anti-rabbit secondary antibody (1:500; Invitrogen, No. A11008); propidium iodide (Invitrogen) was used to quantify the DNA content of the cells. Fluorescence signals were detected by flow cytometry (BD FACSCalibur and attendant CellQuest Pro software; analyzed by FlowJo 8.7 software).

Assessment of Mitochondrial Membrane Potential $\Delta\psi_m$

Cells were seeded into 3.5-cm dishes, at 375,000 cells per dish, and were left to adhere overnight and incubated with PKI-587 or RAD001 at low (IC_{50}) and high (C_{max}) concentrations or with DMSO as a control for 16 h, respectively, in four biological replicates. The samples were incubated with JC-1 reagent (5 μM; AAT Bioquest) for 30 min at 37°C; CCCP (carbonyl cyanide *m*-chlorophenyl hydrazone, 50 μM; Abcam Biochemicals) functioned as a positive control. Fluorescence signals were detected by flow cytometry (BD FACSCalibur and attendant CellQuest Pro software; analyzed by FlowJo 8.7 software).

Western Blot

Following the incubation of cells with PKI-587, RAD001, or DMSO control at intermediate concentrations (C_{mid}) for 24 h, the cells were lysed in NP-40 buffer. The content of total protein was assessed using the Bradford method; 20 μg protein was used per lane. SDS-PAGE and Western blot were performed using a standard protocol. Membranes were blocked in 5% milk/TBS-T for 60 min and incubated with dilutions of primary antibody overnight. After incubation with secondary HRP-labeled antibody, detection followed using the ECL Prime Western Blotting Reagent (Amersham, GE Healthcare) with a Fujifilm LAS 4000 luminescent image analyzer. For re-probing, antibody binding was removed with acidic glycine buffer (pH 2.3). Always four biological replicates were detected simultaneously. Densitometric analysis was conducted with Fujifilm Multigauge version 3.0 software, and band density was normalized with Coomassie total protein stain ratios for each lane. The densitometric data from the four replicates were averaged and compared with the control.

Analysis of Gene Expression (NanoString®, nCounter® Technology)

Cells (only KRJ-I, LCC-18, and QGP-1, since p53-mutated BON cells do not provide added information) were seeded in 6-cm dishes ($1.5–4 \times 10^6$ cells/dish) and incubated with PKI-587 or RAD001 at intermediate concentrations (C_{mid}) or with control for 60 h, respectively, in two biological replicates.

For extraction of RNA we used the RNeasy Mini Kit (Qiagen), carrying out the instructions of the manufacturer; the total RNA content of each sample was assessed using a NanoDrop 2000c Spectrophotometer (Thermo Fisher Scientific). We used 60 ng RNA per sample for processing the nCounter® PanCancer Pathway Panel gene expression analysis (NanoString®). This innovative technology contains 730 different probes binding complementary to corresponding target mRNAs (hybridization at 65°C overnight). The probes were labeled with gene-specific fluorescence bar codes and immobilized on a coated slide. Sample preparation was conducted with nCounter® PrepStation 5s, and microscopy scanning of the bar code signals with nCounter® Digital Analyzer 5s (NanoString®).

The data were analyzed by first principal component analysis using nSolver® 2.5 PanCancer Pathway Analysis Module software (NanoString®). The resulting absolute log fold change data on the single genes were summed up into pathway scores.

Statistical Analyses

For statistical analysis, we used Microsoft Excel and GraphPad Prism 6 analysis software (San Diego, Calif., USA). The data passed a Kolmogorov-Smirnov test (with Dallal-Wilkinson-Lilliefors p value) for a Gaussian distribution, appropriate for data sets below 20 data points. Outliers were identified by Grubbs' test with $\alpha = 0.05$.

Dose-response curves were fitted to the measured data using the method of least squares with variable slope; goodness of fit was quantified with R^2 and sums of squares. For detection of significant differences between two or more data groups, we used ANOVA with or without repeated measures (depending on the experimental design) with a p value of 0.05.

Results

Reduction of Cell Viability by PKI-587 in Neuroendocrine Cells (WST-1 Assay)

Incubation of the four cell lines with everolimus (RAD001) or PKI-587 shows a time- and concentration-dependent decrease in cell viability for both treatments. In comparison, this effect of the dual PI3K/mTOR inhibitor PKI-587 was more distinct than that of RAD001 as an mTORC1-selective inhibitor. PKI-587 reduced the amount of living cells by 61–94%, whereas RAD001 reduced it only by 47–52% (fig. 2a).

IC_{50} of PKI-587 in Neuroendocrine Cell Lines

The concentration of half-maximal effect (relative IC_{50} [34]) was determined for both substances under the same experimental conditions based on WST-1 data. PKI-587 showed higher IC_{50} values (25–250 nM) than RAD001 (1–2.5 nM). For C_{max}, the concentration of maximal effect, we chose a low concentration of the lower plateau of the dose-response curve. The intermediate concentration, C_{mid}, was determined relative to IC_{20}, the concentration of 80% of the maximal effect (fig. 2b). The dose-response curves are shown in the online supplementary material (for all online suppl. material, see www.karger.com/doi/10.1159/000448843).

Apoptosis Induction through PKI-587 Treatment (JC-1, Flow Cytometry)

To investigate the occurrence of early apoptotic processes, we assessed the mitochondrial membrane integrity (JC-1, flow cytometry) after treatment of cell lines with RAD001 or PKI-587 for 16 h. Significant changes in the mitochondrial membrane potential ($\Delta\psi_m$) emerged through PKI-587 treatment at high concentrations (C_{max}) in BON and LCC-18 cells. An increase in apoptotic cells was also detectable in KRJ-I cells, but it was not significant (p = 0.09) (fig. 2c).

Assessment of Viability, Apoptosis, and Cytotoxicity by the Multiplexed ApoTox-Glo Assay

Viability. The viability data obtained with this assay subsequently confirmed the WST-1-derived data (data not shown).

Apoptosis. We detected caspase 3/7 activity after 36 h of treatment of the cell lines with RAD001 or PKI-587. At high concentrations (C_{max}), the dual inhibitor PKI-587 caused significant increases in apoptosis in BON, KRJ-I, and LCC-18 cells. RAD001 induced a significantly higher caspase 3/7 activity only in KRJ-I cells (fig. 2c). These data confirm the findings from the JC-1 assay of membrane potential integrity.

Cytotoxicity. Measurement of cytotoxicity after 12 h of treatment did not show any increase or decrease in dead cell protease versus the control (data not shown).

PKI-587 Causes Stronger Attenuation of Cell Cycle and G_0/G_1 Arrest

The flow cytometry cell cycle studies after PKI-587 treatment of cells revealed dose- and time-dependent alterations in proliferation. G_0/G_1 arrest occurred along with decreasing amounts of cells in the S, G_2, and M phases. Particularly in the pancreatic cell lines BON and QGP-1, this effect showed significance. These effects could be detected after RAD001 treatment as well, but they were notably weaker (fig. 3a, b).

In addition to these findings, flow cytometry analysis revealed apoptosis in terms of sub-G_1 peaks caused by PKI-587 treatment in the two intestinal cell lines KRJ-I and LCC-18 (fig. 3c).

Fig. 2. a, **b** We treated cell lines with different concentrations of everolimus (RAD001), PKI-587, or vehicle control for 0, 24, 48, and 96 h and assessed cell viability with the WST-1 assay (Roche). **a** Maximally reached effects on viability in percent of control (indicated by the lower plateau of the dose-response curve; mean ± SD). Left: RAD001 (BON: 50%; KRJ-I: 52%; LCC-18: 50%; QGP-1: 47%). Right: PKI-587 (BON: 94%; KRJ-I: 61%; LCC-18: 90%; QGP-1: 78%). **b** IC_{50}, C_{mid}, and C_{max} were determined by nonlinear fitting of the dose-response curves (also refer to the online suppl. material). **c** The cell lines were treated with RAD001 (RAD; IC_{50} and C_{max}), PKI-587 (PKI; IC_{50} and C_{max}), or control for 16 h (JC-1) or 36 h (caspase 3/7 activity). Subsequently, we detected cells with an altered mitochondrial membrane potential via JC-1 staining and flow cytometry analysis or luminescent signals of caspase 3/7 activity, respectively. JC-1: PKI-587 treatment showed significant results for BON (10.6% of cells; control: 5.5%) and LCC-18 cells (4.9% of cells; control: 3.1%); RAD001 significantly increased the apoptosis rate of KRJ-I cells (27.7% of cells; control: 21.6%). * $p \leq 0.05$, ** $p \leq 0.01$, *** $p \leq 0.001$: significant difference vs. control.

(For figure see next page.)

Efficacy

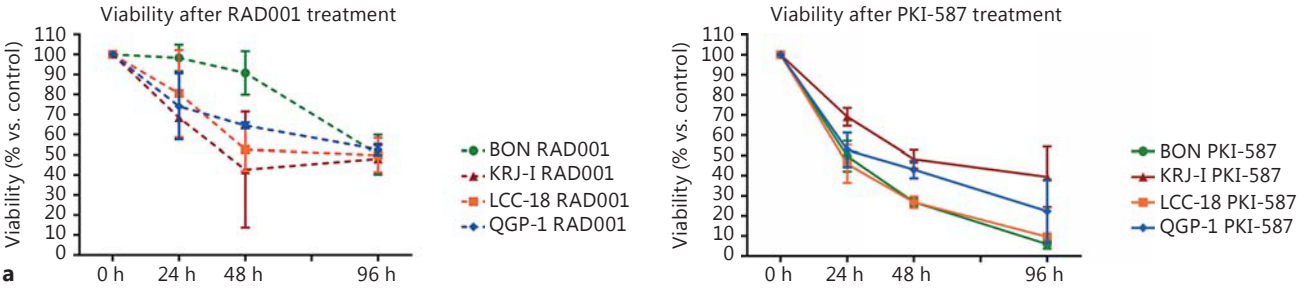

a

Concentrations of substances

b

		BON	KRJ-I	LCC-18	QGP-1
PKI-587	IC_{50}	250 nM	25 nM	250 nM	50 nM
	C_{mid}	1,000 nM	500 nM	1,000 nM	500 nM
	C_{max}	10,000 nM	1,000 nM	10,000 nM	1,000 nM
RAD001	IC_{50}	1 nM	2.5 nM	2.5 nM	2.5 nM
	C_{mid}	100 nM	100 nM	100 nM	100 nM
	C_{max}	500 nM	500 nM	500 nM	500 nM

Apoptosis

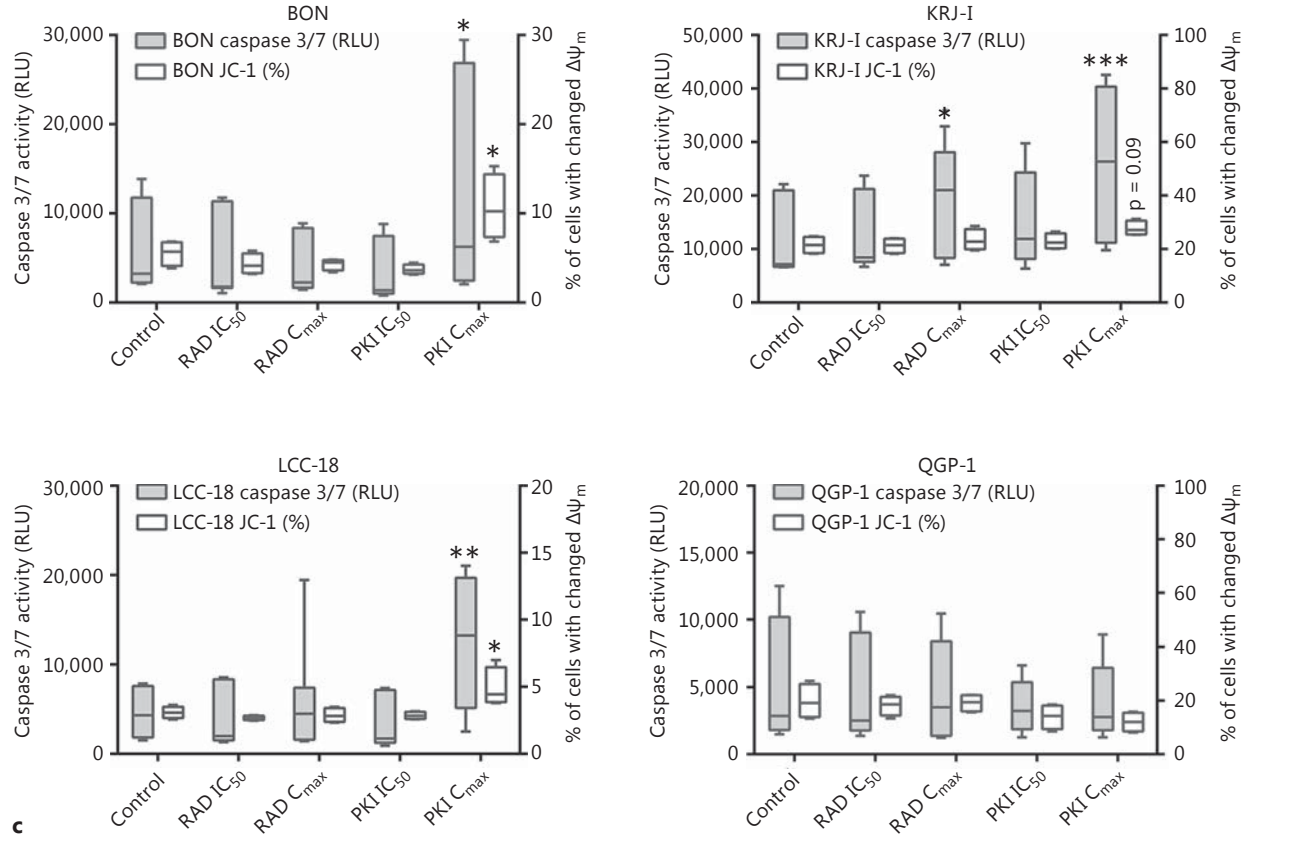

c

2

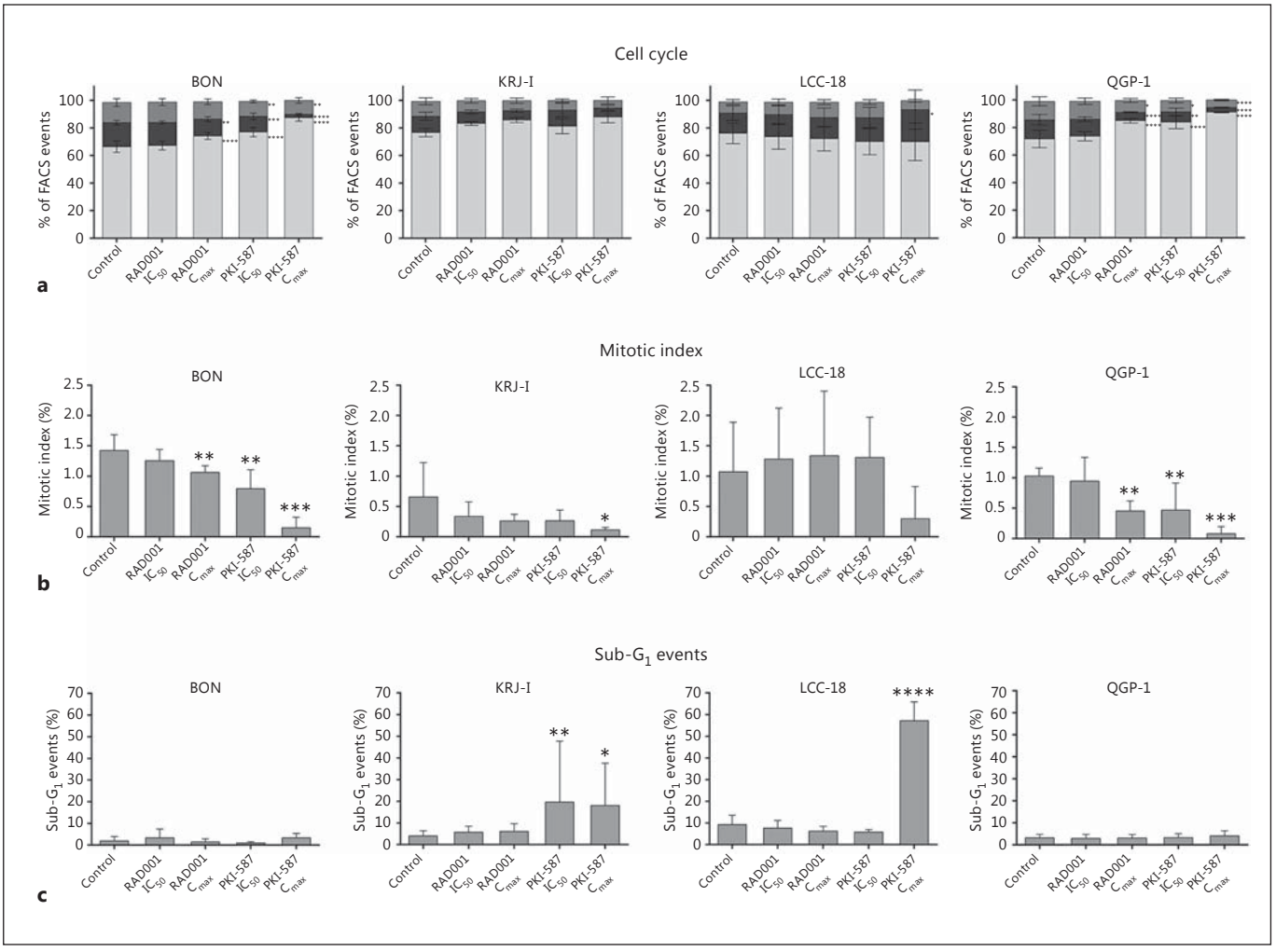

Fig. 3. Cell lines were treated with everolimus (RAD001; IC_{50} and C_{max}) or PKI-587 (IC_{50} and C_{max}) for 48 h (BON and KRJ-I) or 96 h (LCC-18 and QGP-1). Cells were stained with PI (DNA content) and mitosis-specific Phospho(Ser10)-Histone H3 immunostain followed by flow cytometry assessment (analysis solely included single cells). According to the stain, cells were divided into groups of several cell cycle phases (FlowJo software), given in percent of all detected cells (mean ± SD). For the sub-G_1 peak, we detected smaller apoptotic bodies, stated in percent of all detected events (mean + SD). **a** Cell cycle. **b** Mitotic index. **c** Sub-G_1 events. * $p \leq 0.05$, ** $p \leq 0.01$, *** $p \leq 0.001$, **** $p \leq 0.0001$: significant difference vs. control.

Western Blot Analyses

Detailed data are listed in table 1; exemplary bands (one of the four replicates) are shown in figure 4.

AKT Activation. The aim of dual inhibition by PKI-587 is to avoid the limiting feedback activation of AKT. Therefore, we analyzed its direct targets mTORC1, TSC2 (tuberous sclerosis complex 2/tuberin), GSK-3 (glycogen synthase kinase 3), and FOXO1 (forkhead box protein O1), as well as their phosphorylations (fig. 1). In summary, everolimus treatment had almost no detectable effect on AKT target phosphorylation. The only exception was a slight increase in the phosphorylation of GSK-3α and GSK-3β in KRJ-I and QGP-1 cells (fig. 4a). Further, we detected an elevation of the pan-AKT protein amount after everolimus treatment in the pancreatic cell lines BON and QGP-1 (fig. 4b). In the slow-growing cell lines KRJ-I and QGP-1, the PKI-587-induced AKT activity mainly went along with increased GSK-3 phosphorylation, and additionally, in KRJ-I cells further protein phosphorylations were induced (mTOR, TSC2, and FOXO1). In the two other cell lines, BON and LCC-18, the PKI-587-induced effects focused on the target FOXO1 (fig. 4a).

Proof of Principle. Downstream target proteins of mTOR and PI3K were analyzed. Phospho-4E-BP1 bands

Table 1. Summary of Western blot data clustered according to distinct issues

	BON		KRJ-I		LCC-18		QGP-1	
	RAD001	PKI-587	RAD001	PKI-587	RAD001	PKI-587	RAD001	PKI-587
Proof of principle								
p4E-BP1 (S65)	–	– – –*	– –*	– – –*	+	–	– –	– – –*
4E-BP1	0	– – –*	-	-	+	0	0	– –
pp70S6K (T389)	– – –*	– – –	– – –*	– – –*	– – –*	0	– – –*	– – –*
p70S6K	0	+	0	0	0	0	0	0
pAkt (S473)	–	–	– – –*	– – –	0	0	0	0
pAkt (T308)	0	0	0	0	0	0	0	0
pan-Akt	+ + +*	+ +	0	0	0	0	+	0
Akt activation								
pmTOR (S2448)	0	0	0	+ +	0	0	-	0
mTOR	+	+ +	0	–	0	0	0	0
pTSC2 (T1462)	0	0	0	+	0	0	0	0
TSC2	0	0	0	0	+	–	0	– – –*
pFOXO1 (T24)	0	+ + +*	0	+	0	+ +	0	0
FOXO1	0	+ + +*	0	0	0	0	+	+
pGSK-3α (S21)	0	0	+	+ +	0	0	+	+ + +*
pGSK-3β (S9)	0	0	+	+ +	0	0	+	+ + +*
GSK-3β	0	0	0	0	0	0	0	0
Cell cycle								
pRb (S780)	0	+	– – –	– –	0	0	– – –*	– – –*
Rb	–	– –	– – –*	– – –*	– – –	– – –	– –	– – –
MAPK signaling								
pERK1/2 (T202/204)	+ +	+ + +*	+	+ +	0	+	0	+ + +*
ERK1/2	+	0	–	0	–	– –	0	0

The cell lines were incubated with everolimus (RAD001; C_{mid}) or PKI-587 (C_{mid}) vs. control for 24 h. Densitometric data on the band intensity of four independent replicates were normalized to Coomassie total protein stain, averaged, and compared with the control. The values describe the impact of treatments on particular proteins regarding the relative data level and p value. – (light blue), – – (middle blue), – – – (dark blue) = Decreased band density vs. control, several intensity grades; + (light red), + + (middle red), + + + (dark red) = increased band density vs. control, several intensity grades; 0 = no difference from control. * Significant difference from control ($p \leq 0.05$).

consistently showed differences between the two treatments (fig. 4b, bands exemplarily shown for BON and QGP-1 cells).

Cell Cycle. A reduced band density of the negative cell cycle regulator Rb (retinoblastoma protein) was detected, and for KRJ-I and QGP-1 cells additionally lowered phospho-Rb levels (fig. 4c).

MAPK Signaling. A greater induction of ERK1/2 (extracellular signal-regulated kinase) phosphorylation was measurable for PKI-587 treatment (fig. 4d).

Gene Expression Analyses

Gene expressions of the cell lines QGP-1, KRJ-I, and LCC-18 were screened with innovative NanoString® nCounter® technology after incubation with RAD001 or PKI-587 to detect treatment-induced alterations in gene regulation. The panel includes 730 relevant genes out of 13 different canonical cancer-associated pathways (nCounter®, PanCancer pathway panel).

Fig. 4. Cell lines were treated with everolimus (RAD001; C_{mid}) or PKI-587 (C_{mid}) versus control for 24 h. We analyzed cell lysates using the Western blot method and conducted immunodetection of several proteins. **a** Analysis of direct target proteins of Akt and their phosphorylations. **b** Analysis of proteins and their phosphorylations downstream from the compound targets mTOR and PI3K. **c** Analysis of the cell cycle-relevant protein Rb. Treatment caused a decrease in Rb and phospho-Rb chemiluminescence. **d** Analysis of ERK1/2, mediator of the MAPK pathway. PKI-587 treatment caused an increase in ERK phosphorylation.

(For figure see next page.)

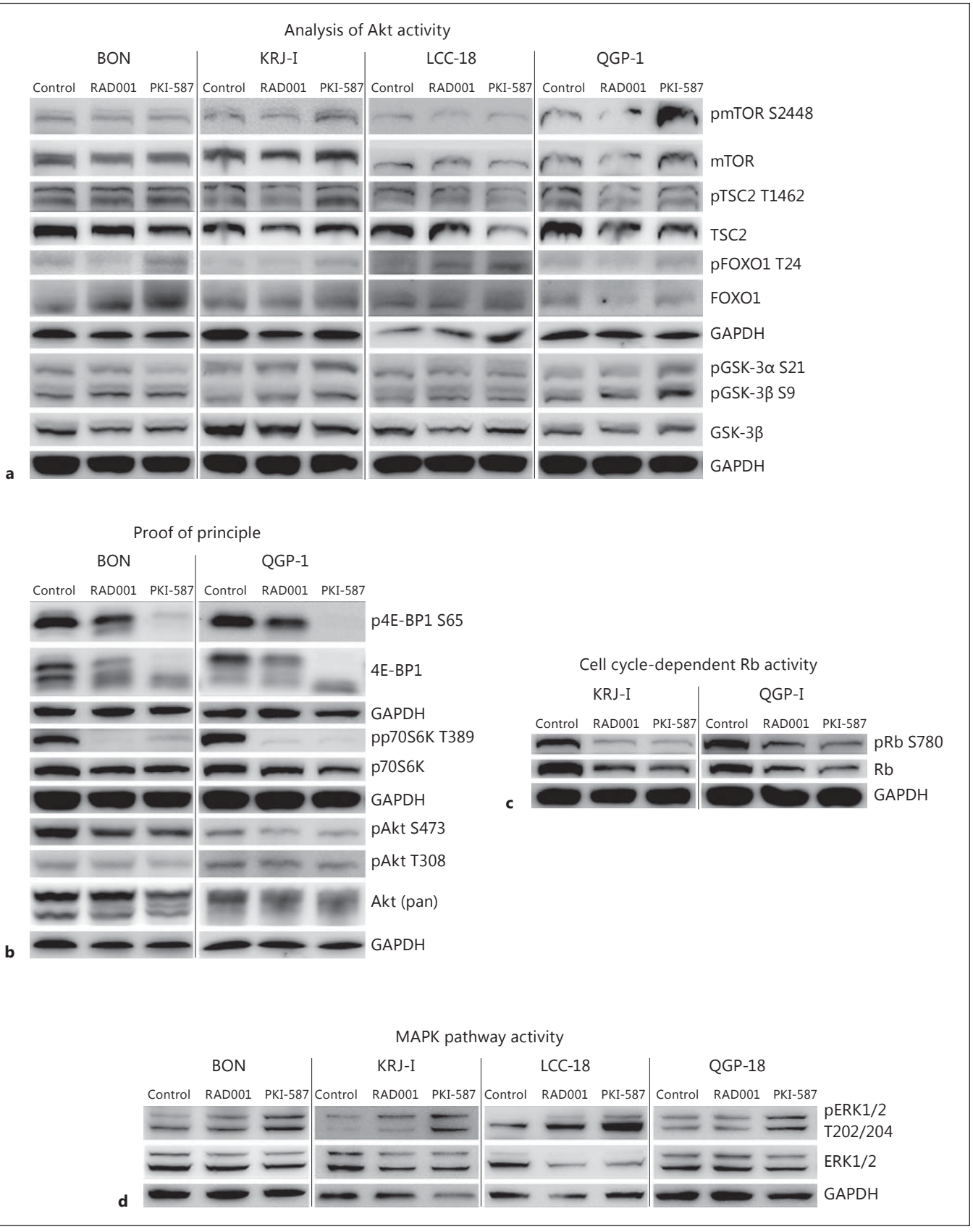

4

Neuroendocrinology 2017;105:90–104
DOI: 10.1159/000448843

Pathway scores

Pathways	KRJ-I RAD001 score	KRJ-I RAD001 genes	KRJ-I PKI-587 score	KRJ-I PKI-587 genes	LCC-18 RAD001 score	LCC-18 RAD001 genes	LCC-18 PKI-587 score	LCC-18 PKI-587 genes	QGP-1 RAD001 score	QGP-1 RAD001 genes	QGP-1 PKI-587 score	QGP-1 PKI-587 genes
Apoptosis			2.73	2			3.90	1	1.28	2	6.70	7
cell cycle	7.07	3	2.91	3					17.01	12	71.01	26
ChromMod	3.61	2	2.79	1					0.66	2	8.99	6
DNARepair			2.47	2	0.82	1	0.88	1	10.60	8	52.31	16
Hedgehog									5.01	2	6.65	2
MAPK	13.21	7	16.99	9	9.38	3	0.83	1	12.37	10	28.55	19
Notch	1.91	3	2.92	2	1.96	1	0.89	1	4.55	2	6.64	4
PI3K	11.83	8	23.68	10	5.32	2	3.37	2	10.69	9	41.06	23
RAS	4.03	2	10.99	6	8.27	3	2.78	3	8.58	5	27.95	16
STAT	14.59	5	26.53	9	1.44	1	3.26	3	2.45	3	16.66	11
TGFB			1.03	1					1.98	2	7.40	3
TXmisReg	6.89	2	9.26	4	1.44	1	2.20	2	8.87	7	26.93	10
Wnt	3.03	1	3.99	3	4.37	1			8.37	5	11.64	6
total	66.16	30	103.57	33	33.00	9	14.21	14	91.15	54	305.79	111

a

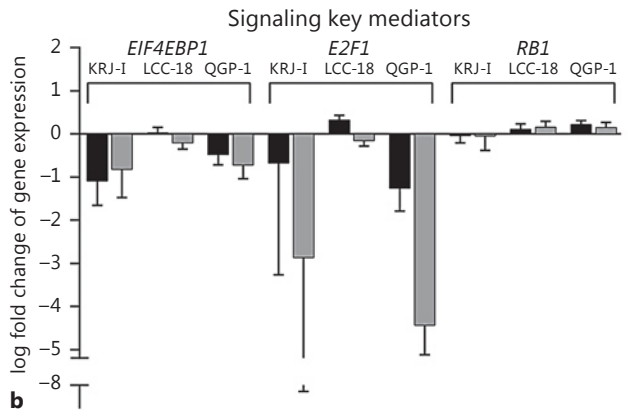

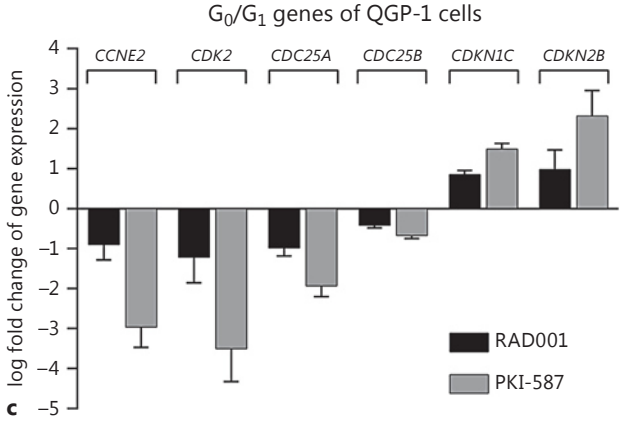

Fig. 5. Treatment-induced alterations in gene expression. GEP-NEN cell lines were treated (for 60 h) with everolimus (RAD001; C_{mid}), PKI-587 (C_{mid}), or control. Extracted mRNA was analyzed with the NanoString® nCounter® technology. The differential expression with regard to the impact of treatments vs. control was calculated by nSolver software. **a** For separating the major differentially expressed genes, we excluded genes with a fold change of less than 50% and p value of more than 0.05 and clustered them into 13 different pathways (based on KEGG, Reactome, and GO annotations; genes participating in several pathways were considered in each of them; total ≠ sum). Pathway scores indicate the intensity of the change in expression caused by treatment (sum of absolute log fold change). The column 'genes' shows the number of included genes of this pathway. The intensity of the green color indicates the height of the score/number of genes. **b** log fold change of the relevant signaling genes (mean ± SD). **c** Genes linked to G_0/G_1 arrest of QGP-1 cells (mean ± SD).

We selected all genes with a fold change of more than 50% combined with p values lower than 0.05 to discover major differentially expressed genes. We clustered the relevant genes to pathways and calculated a pathway score (fig. 5a). We precisely listed the genes affected by treatments and their log fold change intensity in the online supplementary material.

The result is that PKI-587 treatment caused relevant gene alterations more intensely than everolimus, and more genes were affected. For QGP-1 cells, we detected the greatest score for cell cycle-regulating genes. In addition, several genes related to G_0/G_1 arrest in QGP-1 cells were separately analyzed (fig. 5).

Discussion

PKI-587 Is Superior to Everolimus Treatment in Cell Growth Inhibition and Induction of Apoptosis

Comparing the maximal inducible effect of the two substances, cells responded notably better to the ATP-competitive dual PI3K/mTOR inhibitor PKI-587 than to everolimus as an mTORC1-selective inhibitor (fig. 2a), which is consistent with the very recent findings published by Vandamme et al. [36]. However, higher concentrations of PKI-587 are needed to become therapeutically relevant (see the IC_{50} values in fig. 2b), especially in BON and LCC-18 cells. These assessed dosages are consistent with tolerable drug concentrations used in humans in clinical trials [5, 24].

The measured effect of decreased cell viability is composed of apoptotic processes and of growth inhibition via cell cycle restriction regulated by intracellular signaling networks. Despite reaching a better efficacy with PKI-587 treatment in all four NEN cell lines, the effects on signaling vary characteristically between the different cell line models. Understanding the distinct tumor models might help in developing specific markers to predict the response of a patient to a certain treatment.

KRJ-I cells have the slowest-growing characteristics, and they show the smallest advantage of the dual inhibitor PKI-587 over the selective mTORC1 inhibitor everolimus. The advantage of PKI-587 in BON or LCC-18 cells is greater (fig. 2a). In our study, LCC-18 cells also showed the greatest propensity to induce apoptosis after treatment (fig. 2c, 3c), but they did not display G_0/G_1 arrest like the other cell lines (fig. 3a). Whereas in QGP-1 cells the efficacy of treatment is solely based on restriction of the cell cycle, apoptotic processes were not detectable. The BON and KRJ-I cell lines revealed both cell cycle restriction and apoptotic processes.

In the following, we will discuss this behavior of the different tumor types referring to our protein and gene expression analyses and to known mutations of the cell lines. Because the response of the aggressive cell line LCC-18 was also satisfactory but vastly different in its underlying mechanism from the other cell lines, we analyzed its results in a separate section.

Proof of Principle of PKI-587 in Neuroendocrine Cells: The mTORC1 Target 4E-BP1, a Crucial Factor for Malignancy and Treatment Response

In our study, the mediator 4E-BP1 emerged as an important factor for the antitumoral activity of PKI-587 treatment. The effect on 4E-BP1 protein correlates with the response to PKI-587 treatment and its advantage over everolimus (regarding cell cycle restriction).

Western blot analyses revealed that everolimus inhibits mTORC1 only partially in GEP-NEN cells in vitro, whereas PKI-587 is able to prevent the rapamycin-typical rephosphorylation of 4E-BP1 (table 1). This advantage of PKI-587 was differentiated depending on the cell type and correlates with the cell cycle-regulating mechanisms leading to G_0/G_1 arrest. In KRJ-I cells, both treatments showed a similar inhibition of 4E-BP1 phosphorylation, and the reduction of viability as well as induction of G_0/G_1 arrest were nearly identical, whereas BON cells responded much better to PKI-587, with strongly reduced phospho-4E-BP1 levels compared with everolimus. These findings confirm the partial inhibition of mTORC1 by everolimus as a crucial limiting factor of this treatment [19, 21].

In addition, gene expression of 4E-BP1, compared between cell lines, correlates with malignity. Highly proliferating, poorly differentiated LCC-18 cells showed sixfold higher amounts of *EIF4EBP1* mRNA than slowly growing KRJ-1 cells (data not shown). Treatment-induced downregulation of 4E-BP1 mRNA expression (gene: *EIF4EBP1*; fig. 5b) also correlates with treatment response with regard to viability (except LCC-18 cells). These findings provide a reason to investigate 4E-BP1 further as a prognostic marker.

The mTORC1 Target p70S6K

Phosphorylation of the second mTORC1 target p70S6K was equally reduced by both treatments (except in LCC-18 cells; table 1); thus, there is no evidence for p70S6K to play a role in the advantage of PKI-587 treatment in GEP-NEN cells.

Everolimus successfully inhibits the phosphorylation of this target by disrupting the mTORC1 complex, and PKI-587 shows the same effectiveness by active site occupation of the mTOR kinase.

Efficacy of PKI-587 Independent of mTORC2 Inhibition in GEP-NEN Cells

Against our expectations, we saw an equivalent behavior with both treatments: a decrease in AKT phosphorylation at Ser473 in BON and KRJ-I cells, and no effect in LCC-18 and QGP-1 cells. Only the results for KRJ-I cells were clear enough to be significant (Western blot; table 1).

For BON and KRJ-I cells, we assume an everolimus-induced inhibition of mTORC2 suppressing Ser473 phosphorylation of AKT, as it is a rapamycin analog. Similar results caused by rapamycin were published [37, 38], although mTORC2 is generally accepted as being rapalog

insensitive. For LCC-18 and QGP-1 cells, we possibly did not reach the required concentrations of both substances, since there are reports of increased concentrations to be necessary for inhibition of the mTORC2-dependent phosphorylation of AKT at Ser473 [39].

No Experimental Proof of PKI-587 Inhibition of PI3K in GEP-NEN Cells

According to the PI3K-inhibitory feature of PKI-587 proven in a cell-free assay of Venkatesan et al. [23], we expected to find a decrease in AKT phosphorylation at Thr308, but averaging the four biological replicates we were not able to detect any convincing changes (Western blot; table 1). Thus, the effects of PKI-587 on proliferation and survival seem to be independent of PI3K inhibition in our cell lines. Soares et al. [26] recently published similar results concerning dual PI3K/mTOR inhibition. They postulated that growth-inhibitory effects are PI3K independent. Instead, they assumed mTORC2 dependence, which is not consistent with our findings in the GEP-NEN cell lines (see previous subsection).

Induction of ERK Signaling and Minor Relevance of Feedback AKT Activation in GEP-NEN Cells

Because of several cross-activating connections between the PI3K/AKT/mTOR and other mitogen pathways, the dual inhibition of PI3K/mTOR can lead to increased activity in ERK signaling [26, 40]. For all four cell lines, our data ascertained PKI-587-induced activation of ERK signaling and therefore activation of MAPK signaling as an escape mechanism (Western blot; table 1).

The assumption that the everolimus-induced AKT activation due to feedback stimulation poses a considerable limitation to treatment [15–18] cannot be confirmed by our results. The Western blot data indicate that both treatments slightly enhance the phosphorylation of different AKT targets – surprisingly, to a greater extent with PKI-587 than with everolimus. Because we could not detect any activating AKT phosphorylations at Ser473 and Thr308 (Western blot; table 1), the phosphorylations of mTOR, FOXO1, and GSK-3 probably were caused by other kinases than AKT mediated by treatment-induced ERK signaling [41–44].

Treatment-Induced G_0/G_1 Arrest and Decrease in Mitotic Index

The cellular task of the tumor suppressor Rb is complexing and thereby inhibiting the cell cycle-regulating transcription factors E2F1/2/3. Phosphorylation of Rb through cyclin/CDK (cyclin-dependent kinase) complexes, stimulated via AKT, led to disruption of the complex and therefore to cell cycle progression [45]. We detected a downscaled amount of Rb protein for all four cell lines, with hardly any difference between the two treatments (Western blot; table 1), while Rb mRNA expression remained unaffected (fig. 5b). The distinctly decreased phosphorylation status of Rb in the low-proliferating KRJ-I and QGP-1 cells suggests a lower transcriptional activity of E2F1/2/3 and, thus, cell cycle deceleration [45].

The observed differences concerning the intensity of cell cycle restriction (or induction of apoptosis, as discussed later) between the two treatments may arise from distinct conditions such as the composition of interacting proteins, altered posttranslational modifications (e.g., acetylations), or the epigenetic regulation of gene expression [45]. Possibly, the abovementioned PKI-587-induced suppression of cap-dependent protein translation via 4E-BP1 is a further factor influencing the efficacy of treatments.

Affirmatively, differences between the two treatments were discernible in the mRNA expression of several proliferation-related genes in QGP-1 cells (fig. 5c). Expression of *E2F1*, physiologically upregulated for G_1/S transition [46], was suppressed, corresponding to PKI-587-induced G_0/G_1 arrest. Further, the genes of cyclin E2 *(CCNE2)* and CDK2 *(CDK2)*, also necessary for passing the G_1/S checkpoint, and the genes of the CDK2-activating proteins cdc25A (cell division cycle homolog A; gene: *CDC25A*) and cdc25B *(CDC25B)* were remarkably downregulated after PKI-587 incubation. Accordingly, expression of the genes of the cyclin D-CDK4/6 complex inhibitors p57 (cyclin-dependent kinase inhibitor 1C; gene: *CDKN1C*) and p15 (cyclin-dependent kinase inhibitor 2B; gene: *CDKN2B*) was upregulated (fig. 5c).

Further, it is likely that FOXO1 also participates in the induction of G_0/G_1 arrest, as the abundance of FOXO1 protein was increased in BON and QGP-1 cells after PKI-587 treatment (table 1). This is one of the major functions of this transcription factor [47] and is associated with elevated p15 mRNA levels [48].

Treatment-Induced Apoptotic Processes

As shown in the cell cycle analyses, the factors Rb/E2F and FOXO1 and their modulations caused by treatments play a crucial role in the cell cycle regulation of GEP-NEN cells. Moreover, these mediators also participate in apoptotic processes [45–47]. Another well-known inducer of apoptosis is the tumor suppressor p53 (tumor protein p53), interacting with both E2F and FOXO1 [46, 47, 49].

FOXO1 and p53 mutually control the induction of apoptosis in reply to cellular stress by transcriptional regulation of apoptotic target genes depending on the cellular context [47]. The aberrantly activated AKT signaling of GEP-NEN might prevent this FOXO-mediated apoptosis. On the other hand, the deregulated activity of E2F1 is able to induce the expression of several proapoptotic genes via p53 or independently of p53 [45, 46].

Inability of QGP-1 Cells to Induce Apoptosis

Although the clinical incidence of p53 mutations is low in GEP-NENs, recent studies have revealed several loss-of-function mutations in cell lines, leading to conformational changes in the DNA-binding domain of p53 (LCC-18) or to truncated (BON) or completely lost expression of the p53 protein (QGP-1) [49–52]. QGP-1 cells in particular seem to be incapable of inducing apoptotic processes. In addition, we observed a lack of caspase 8 and Fas receptor mRNA expression and a comparatively low expression of members of the TNF receptor superfamily in QGP-1 cells (data not shown). All of these findings probably combine in the QGP-1-characteristic prohibition of apoptosis.

Treatment-Induced Regulation of Gene Expression

After a gene expression analysis of the 730 cancer pathway genes in three of the cell lines with and without treatment, we included only differentially expressed genes with significant values and a fold change (treatment vs. control) of 50% or more. Further, we functionally analyzed the intensity of the differential expression using pathway scores.

QGP-1 cells showed the most notably affected gene expression pattern after treatment with regard to both the pathway scores and the number of differentially expressed genes (fig. 5a). Treatment of this cell line particularly interferes with genes participating in cell cycle regulation, confirming our findings of G_0/G_1 arrest (fig. 3, 5c). KRJ-I cells revealed a similar pattern to QGP-1 cells, but it was clearly weaker and without notable results for the cell cycle-related genes. In both cell lines, PKI-587 treatment caused a stronger change in expression of MAPK, PI3K, RAS, and STAT pathway genes than did RAD001 treatment, reflecting the overall stronger effects of PKI-587 compared with everolimus (fig. 5a).

Variational Response of LCC-18 Cells Representing Poorly Differentiated GEP-NENs

Treatment of LCC-18 cells with PKI-587 successfully reduced their viability more than did treatment with everolimus (fig. 2a). However, there was no association of treatment efficacy with the differing effects concerning 4E-BP1 phosphorylation; surprisingly, everolimus treatment even increased the amount of phospho-4E-BP1 (table 1).

PKI-587 treatment of LCC-18 cells caused apoptosis, but the efficacy of everolimus treatment – not inducing apoptosis, cytotoxicity, or cell cycle arrest but reducing viability – raises the question of how the treatments work. In LCC-18 cells, an unusual form of cell cycle slowdown might occur, without the accumulation of cells in one of the cell cycle phases [53]; however, the knowledge about the possible underlying mechanisms is insufficient.

Conclusion

The dual PI3K/mTOR inhibitor PKI-587 is a promising compound for the treatment of GEP-NENs; it showed good results in our in vitro investigation and displayed a greater efficacy than the approved mTOR inhibitor everolimus. The reduction of cell viability is based on apoptotic processes and cell cycle restriction; whereas BON and KRJ-I cell lines showed both effects, QGP-1 cells were unable to induce apoptosis. PKI-587 treatment of the poorly differentiated cell line LCC-18 successfully decreased cell viability as well, but the underlying mechanisms differed greatly from those in the BON, KRJ-I, and QGP-1 cell lines. The complex processes behind these distinct responses are poorly understood, but phosphorylation of 4E-BP1 and the Rb/E2F axis as well as subsequent modulation of gene expression seem to play crucial roles. Thus, further investigations concerning the different tumor subtypes are required to predict a patient's response to a compound. Because of the convincing efficacy of PKI-587 in GEP-NEN cell models revealed in our study, indicating that PKI-587 is a promising therapy option for GEP-NEN disease, we recommend subsequent in vivo studies of this substance.

Acknowledgements

This study was financially supported by the Theranostics Research Network and the Sonnenfeld-Stiftung Berlin. The BON cells were a generous gift from C.M. Townsend (University of Texas, Galveston, Tex., USA). KRJ-I midgut NET cells were generated by R. Pfragner (Medical University of Graz, Graz, Austria) and kindly provided by I. Modlin (Yale University, New Haven, Conn., USA).

References

1 Briest F, Grabowski P: PI3K-AKT-mTOR-signaling and beyond: the complex network in gastroenteropancreatic neuroendocrine neoplasms. Theranostics 2014;4:336–365.
2 Schimmack S, Svejda B, Lawrence B, Kidd M, Modlin IM: The diversity and commonalities of gastroenteropancreatic neuroendocrine tumors. Langenbecks Arch Surg 2011;396:273–298.
3 Pavel ME, Hainsworth JD, Baudin E, Peeters M, Hörsch D, Winkler RE, Klimovsky J, Lebwohl D, Jehl V, Wolin EM, Öberg K, Van Cutsem E, Yao JC: Everolimus plus octreotide long-acting repeatable for the treatment of advanced neuroendocrine tumours associated with carcinoid syndrome (RADIANT-2): a randomised, placebo-controlled, phase 3 study. Lancet 2011;378:2005–2012.
4 Yao JC, Lombard-Bohas C, Baudin E, Kvols LK, Rougier P, Ruszniewski P, Hoosen S, St Peter J, Haas T, Lebwohl D, Van Cutsem E, Kulke MH, Hobday TJ, O'Dorisio TM, Shah MH, Cadiot G, Luppi G, Posey JA, Wiedenmann B: Daily oral everolimus activity in patients with metastatic pancreatic neuroendocrine tumors after failure of cytotoxic chemotherapy: a phase II trial. J Clin Oncol 2010;28:69–76.
5 Yao JC, Shah MH, Ito T, Bohas CL, Wolin EM, Van Cutsem E, Hobday TJ, Okusaka T, Capdevila J, de Vries EG, Tomassetti P, Pavel ME, Hoosen S, Haas T, Lincy J, Lebwohl D, Öberg K: Everolimus for advanced pancreatic neuroendocrine tumors. N Engl J Med 2011;364:514–523.
6 Faivre S, Delbaldo C, Vera K, Robert C, Lozahic S, Lassau N, Bello C, Deprimo S, Brega N, Massimini G, Armand JP, Scigalla P, Raymond E: Safety, pharmacokinetic, and antitumor activity of SU11248, a novel oral multitarget tyrosine kinase inhibitor, in patients with cancer. J Clin Oncol 2006;24:25–35.
7 Kulke MH, Lenz HJ, Meropol NJ, Posey J, Ryan DP, Picus J, Bergsland E, Stuart K, Tye L, Huang X, Li JZ, Baum CM, Fuchs CS: Activity of sunitinib in patients with advanced neuroendocrine tumors. J Clin Oncol 2008;26:3403–3410.
8 Raymond E, Dahan L, Raoul JL, Bang YJ, Borbath I, Lombard-Bohas C, Valle J, Metrakos P, Smith D, Vinik A, Chen JS, Hörsch D, Hammel P, Wiedenmann B, Van Cutsem E, Patyna S, Lu DR, Blanckmeister C, Chao R, Ruszniewski P: Sunitinib malate for the treatment of pancreatic neuroendocrine tumors. N Engl J Med 2011;364:501–513.
9 From ECC 2015 – Neuroendocrine Cancer: RADIANT-4 trial – NET improvement with everolimus? Nat Rev Clin Oncol 2015;12:684.
10 Yao JC, Fazio N, Singh S, Buzzoni R, Carnaghi C, Wolin E, Tomasek J, Raderer M, Lahner H, Voi M, Pacaud LB, Rouyrre N, Sachs C, Valle JW, Delle Fave G, Van Cutsem E, Tesselaar M, Shimada Y, Oh DY, Strosberg J, Kulke MH, Pavel ME: Everolimus for the treatment of advanced, non-functional neuroendocrine tumours of the lung or gastrointestinal tract (RADIANT-4): a randomised, placebo-controlled, phase 3 study. Lancet 2016;387:968–977.
11 Porta C, Paglino C, Mosca A: Targeting PI3K/AKT/mTOR signaling in cancer. Front Oncol 2014;4:64.
12 Showkat M, Beigh MA, Andrabi KI: mTOR signaling in protein translation regulation: implications in cancer genesis and therapeutic interventions. Mol Biol Int 2014;2014:686984.
13 Wullschleger S, Loewith R, Hall MN: TOR signaling in growth and metabolism. Cell 2006;124:471–484.
14 Houghton PJ: Everolimus. Clin Cancer Res 2010;16:1368–1372.
15 Svejda B, Kidd M, Kazberouk A, Lawrence B, Pfragner R, Modlin IM: Limitations in small intestinal neuroendocrine tumor therapy by mTOR kinase inhibition reflect growth factor-mediated PI3K feedback loop activation via ERK1/2 and AKT. Cancer 2011;117:4141–4154.
16 Zitzmann K, Rüden J, Brand S, Göke B, Lichtl J, Spöttl G, Auernhammer CJ: Compensatory activation of Akt in response to mTOR and Raf inhibitors – a rationale for dual-targeted therapy approaches in neuroendocrine tumor disease. Cancer Lett 2010;295:100–109.
17 Ginion A, Auquier J, Benton CR, Mouton C, Vanoverschelde JL, Hue L, Horman S, Beauloye C, Bertrand L: Inhibition of the mTOR/p70S6K pathway is not involved in the insulin-sensitizing effect of AMPK on cardiac glucose uptake. Am J Physiol Heart Circ Physiol 2011;301:H469–H477.
18 Kuo SH, Hsu CH, Chen LT, Lu YS, Lin CH, Yeh PY, Jeng HJ, Gao M, Yeh KH, Cheng AL: Lack of compensatory pAKT activation and eIF4E phosphorylation of lymphoma cells towards mTOR inhibitor, RAD001. Eur J Cancer 2011;47:1244–1257.
19 Choo AY, Yoon SO, Kim SG, Roux PP, Blenis J: Rapamycin differentially inhibits S6Ks and 4E-BP1 to mediate cell-type-specific repression of mRNA translation. Proc Natl Acad Sci USA 2008;105:17414–17419.
20 Ismail HMS: Downstream the mTOR: S6 kinases between divergence and redundancy. J Biochem Pharmacol Res 2013;1:94–105.
21 Hsieh AC, Costa M, Zollo O, Davis C, Feldman ME, Testa JR, Meyuhas O, Shokat KM, Ruggero D: Genetic dissection of the oncogenic mTOR pathway reveals druggable addiction to translational control via 4EBP-eIF4E. Cancer Cell 2010;17:249–261.
22 Armengol G, Rojo F, Castellví J, Iglesias C, Cuatrecasas M, Pons B, Baselga J, Ramón y Cajal S: 4E-binding protein 1: a key molecular 'funnel factor' in human cancer with clinical implications. Cancer Res 2007;67:7551–7555.
23 Venkatesan AM, Dehnhardt CM, Delos Santos E, Chen Z, Dos Santos O, Ayral-Kaloustian S, Khafizova G, Brooijmans N, Mallon R, Hollander I, Feldberg L, Lucas J, Yu K, Gibbons J, Abraham RT, Chaudhary I, Mansour TS: Bis(morpholino-1,3,5-triazine) derivatives: potent adenosine 5′-triphosphate competitive phosphatidylinositol-3-kinase/mammalian target of rapamycin inhibitors: discovery of compound 26 (PKI-587), a highly efficacious dual inhibitor. J Med Chem 2010;53:2636–2645.
24 Shapiro GI, Bell-McGuinn KM, Molina JR, Bendell J, Spicer J, Kwak EL, Pandya SS, Millham R, Borzillo G, Pierce KJ, Han L, Houk BE, Gallo JD, Alsina M, Braña I, Tabernero J: First-in-human study of PF-05212384 (PKI-587), a small-molecule, intravenous, dual inhibitor of PI3K and mTOR in patients with advanced cancer. Clin Cancer Res 2015;21:1888–1895.
25 Mallon R, Feldberg LR, Lucas J, Chaudhary I, Dehnhardt C, Santos ED, Chen Z, dos Santos O, Ayral-Kaloustian S, Venkatesan A, Hollander I: Antitumor efficacy of PKI-587, a highly potent dual PI3K/mTOR kinase inhibitor. Clin Cancer Res 2011;17:3193–3203.
26 Soares HP, Ming M, Mellon M, Young SH, Han L, Sinnet-Smith J, Rozengurt E: Dual PI3K/mTOR inhibitors induce rapid overactivation of the MEK/ERK pathway in human pancreatic cancer cells through suppression of mTORC2. Mol Cancer Ther 2015;14:1014–1023.
27 Parekh D, Ishizuka J, Townsend CM Jr, Haber B, Beauchamp RD, Karp G, Kim SW, Rajaraman S, Greeley G Jr, Thompson JC: Characterization of a human pancreatic carcinoid in vitro: morphology, amine and peptide storage, and secretion. Pancreas 1994;9:83–90.
28 Evers BM, Townsend CM Jr, Upp JR, Allen E, Hurlbut SC, Kim SW, Rajaraman S, Singh P, Reubi JC, Thompson JC: Establishment and characterization of a human carcinoid in nude mice and effect of various agents on tumor growth. Gastroenterology 1991;101:303–311.
29 Iguchi H, Hayashi I, Kono A: A somatostatin-secreting cell line established from a human pancreatic islet cell carcinoma (somatostatinoma): release experiment and immunohistochemical study. Cancer Res 1990;50:3691–3693.
30 Kaku M, Nishiyama T, Yagawa K, Abe M: Establishment of a carcinoembryonic antigen-producing cell line from human pancreatic carcinoma. Gan 1980;71:596–601.
31 Modlin IM, Kidd M, Pfragner R, Eick GN, Champaneria MC: The functional characterization of normal and neoplastic human enterochromaffin cells. J Clin Endocrinol Metab 2006;91:2340–2348.
32 Pfragner R, Wirnsberger G, Niederle B, Behmel A, Rinner I, Mandl A, Wawrina F, Luo J, Adamiker D, Hoger H, Ingolic E, Schauenstein K: Establishment of a continuous cell line from a human carcinoid of the small intestine (KRJ-I). Int J Oncol 1996;8:513–520.

33 Lundqvist M, Mark J, Funa K, Heldin NE, Morstyn G, Wedell B, Layton J, Öberg K: Characterisation of a cell line (LCC-18) from a cultured human neuroendocrine-differentiated colonic carcinoma. Eur J Cancer 1991;27:1663–1668.
34 Sebaugh JL: Guidelines for accurate EC50/IC50 estimation. Pharm Stat 2011;10:128–134.
35 Briest F, Berg E, Grass I, Freitag H, Kaemmerer D, Lewens F, Christen F, Arsenic R, Altendorf-Hofmann A, Kunze A, Sänger J, Knösel T, Siegmund B, Hummel M, Grabowski P: FOXM1: a novel drug target in gastroenteropancreatic neuroendocrine tumors. Oncotarget 2015;6:8185–8199.
36 Vandamme T, Beyens M, de Beeck KO, Dogan F, van Koetsveld PM, Pauwels P, Mortier G, Vangestel C, de Herder W, Van Camp G, Peeters M, Hofland LJ: Long-term acquired everolimus resistance in pancreatic neuroendocrine tumours can be overcome with novel PI3K-AKT-mTOR inhibitors. Br J Cancer 2016;114:650–658.
37 Sarbassov DD, Ali SM, Sengupta S, Sheen JH, Hsu PP, Bagley AF, Markhard AL, Sabatini DM: Prolonged rapamycin treatment inhibits mTORC2 assembly and Akt/PKB. Mol Cell 2006;22:159–168.
38 Sarbassov DD, Guertin DA, Ali SM, Sabatini DM: Phosphorylation and regulation of Akt/PKB by the rictor-mTOR complex. Science 2005;307:1098–1101.
39 Serra V, Markman B, Scaltriti M, Eichhorn PJ, Valero V, Guzman M, Botero ML, Llonch E, Atzori F, Di Cosimo S, Maira M, Garcia-Echeverria C, Parra JL, Arribas J, Baselga J: NVP-BEZ235, a dual PI3K/mTOR inhibitor, prevents PI3K signaling and inhibits the growth of cancer cells with activating PI3K mutations. Cancer Res 2008;68:8022–8030.
40 Gedaly R, Angulo P, Hundley J, Daily MF, Chen C, Evers BM: PKI-587 and sorafenib targeting PI3K/AKT/mTOR and Ras/Raf/MAPK pathways synergistically inhibit HCC cell proliferation. J Surg Res 2012;176:542–548.
41 Jacobs KM, Bhave SR, Ferraro DJ, Jaboin JJ, Hallahan DE, Thotala D: GSK-3β: a bifunctional role in cell death pathways. Int J Cell Biol 2012;2012:930710.
42 Parrales A, López E, Lee-Rivera I, López-Colomé AM: ERK1/2-dependent activation of mTOR/mTORC1/p70S6K regulates thrombin-induced RPE cell proliferation. Cell Signal 2013;25:829–838.
43 Asada S, Daitoku H, Matsuzaki H, Saito T, Sudo T, Mukai H, Iwashita S, Kako K, Kishi T, Kasuya Y, Fukamizu A: Mitogen-activated protein kinases, Erk and p38, phosphorylate and regulate Foxo1. Cell Signal 2007;19:519–527.
44 Sutherland C, Leighton IA, Cohen P: Inactivation of glycogen synthase kinase-3 beta by phosphorylation: new kinase connections in insulin and growth-factor signalling. Biochem J 1993;296(pt 1):15–19.
45 Polager S, Ginsberg D: E2F – at the crossroads of life and death. Trends Cell Biol 2008;18:528–535.
46 Lavia P, Jansen-Dürr P: E2F target genes and cell-cycle checkpoint control. Bioessays 1999;21:221–230.
47 Zhang X, Tang N, Hadden TJ, Rishi AK: Akt, FoxO and regulation of apoptosis. Biochim Biophys Acta 2011;1813:1978–1986.
48 Katayama K, Nakamura A, Sugimoto Y, Tsuruo T, Fujita N: FOXO transcription factor-dependent p15(INK4b) and p19(INK4d) expression. Oncogene 2008;27:1677–1686.
49 Briest F, Grabowski P: The p53 network as therapeutic target in gastroenteropancreatic neuroendocrine neoplasms. Cancer Treat Rev 2015;41:423–430.
50 Briest F, Grass I, Möbs M, Christen F, Mende S, Kaemmerer D, Freitag H, Lewens F, Worpenberg L, Iwaszkiewicz S, Sänger J, Kunze A, Siegmund B, Hummel M, Grabowski P: Targeting the MDM2-p53-FOXM1 axis is highly effective in p53 wild type GEP-NENs. Endocr Relat Cancer 2016, submitted.
51 Vandamme T, Peeters M, Dogan F, Pauwels P, Van Assche E, Beyens M, Mortier G, Vandeweyer G, de Herder W, Van Camp G, Hofland LJ, Op de Beeck K: Whole-exome characterization of pancreatic neuroendocrine tumor cell lines BON-1 and QGP-1. J Mol Endocrinol 2015;54:137–147.
52 Bartz C, Ziske C, Wiedenmann B, Moelling K: p53 tumour suppressor gene expression in pancreatic neuroendocrine tumour cells. Gut 1996;38:403–409.
53 Schauen M, Spitkovsky D, Schubert J, Fischer JH, Hayashi J, Wiesner RJ: Respiratory chain deficiency slows down cell-cycle progression via reduced ROS generation and is associated with a reduction of p21CIP1/WAF1. J Cell Physiol 2006;209:103–112.
54 Franke TF, Kaplan DR, Cantley LC, Toker A: Direct regulation of the Akt proto-oncogene product by phosphatidylinositol-3,4-bisphosphate. Science 1997;275:665–668.
55 Nicholson KM, Anderson NG: The protein kinase B/Akt signalling pathway in human malignancy. Cell Signal 2002;14:381–395.
56 Park HK, Ahima RS: Leptin signaling. F1000Prime Rep 2014;6:73.
57 Osaki M, Oshimura M, Ito H: PI3K-Akt pathway: its functions and alterations in human cancer. Apoptosis 2004;9:667–676.
58 Nojima H, Tokunaga C, Eguchi S, Oshiro N, Hidayat S, Yoshino K, Hara K, Tanaka N, Avruch J, Yonezawa K: The mammalian target of rapamycin (mTOR) partner, raptor, binds the mTOR substrates p70 S6 kinase and 4E-BP1 through their TOR signaling (TOS) motif. J Biol Chem 2003;278:15461–15464.
59 Faivre S, Kroemer G, Raymond E: Current development of mTOR inhibitors as anticancer agents. Nat Rev Drug Discov 2006;5:671–688.
60 Mader S, Lee H, Pause A, Sonenberg N: The translation initiation factor eIF-4E binds to a common motif shared by the translation factor eIF-4 gamma and the translational repressors 4E-binding proteins. Mol Cell Biol 1995;15:4990–4997.
61 Bhaskar PT, Hay N: The two TORCs and Akt. Dev Cell 2007;12:487–502.
62 Liu P, Guo J, Gan W, Wei W: Dual phosphorylation of Sin1 at T86 and T398 negatively regulates mTORC2 complex integrity and activity. Protein Cell 2014;5:171–177.
63 Easton JB, Kurmasheva RT, Houghton PJ: IRS-1: auditing the effectiveness of mTOR inhibitors. Cancer Cell 2006;9:153–155.
64 Guan KL, Figueroa C, Brtva TR, Zhu T, Taylor J, Barber TD, Vojtek AB: Negative regulation of the serine/threonine kinase B-Raf by Akt. J Biol Chem 2000;275:27354–27359.

PLOS ONE

RESEARCH ARTICLE

The selective PI3Kα inhibitor BYL719 as a novel therapeutic option for neuroendocrine tumors: Results from multiple cell line models

Svenja Nölting[1,2], Jakob Rentsch[3], Helma Freitag[3], Katharina Detjen[3], Franziska Briest[3,4,5], Markus Möbs[6], Victoria Weissmann[7], Britta Siegmund[3], Christoph J. Auernhammer[1,2], Elke Tatjana Aristizabal Prada[1], Michael Lauseker[8], Ashley Grossman[9], Samantha Exner[3], Christian Fischer[3], Carsten Grötzinger[3], Jörg Schrader[7,10☯], Patricia Grabowski[3,4☯]*, on behalf of the GERMAN NET-Z study group[¶]

1 Department of Internal Medicine II, Klinikum der Universität München (KUM), Ludwig-Maximilians-Universität München, München, Bavaria, Germany, **2** Department of Internal Medicine IV, Klinikum der Universität München (KUM), Ludwig-Maximilians-Universität München, München, Bavaria, Germany, **3** Dept. of Gastroenterology, CC13 (CBF and CVK), Charité - Universitätsmedizin Berlin, Berlin, Germany, **4** Dept. of Gastroenterology and Endocrinology, Zentralklinik Bad Berka GmbH, Bad Berka, Germany, **5** Dept. of Chemistry and Biochemistry, Freie Universität (FU) Berlin, Berlin, Germany, **6** Institute of Pathology, Charité - Universitätsmedizin Berlin, Berlin, Germany, **7** Department of General, Visceral and Thoracic Surgery, University Medical Center Hamburg-Eppendorf, Hamburg, Germany, **8** Institute for Medical Information Sciences, Biometry, and Epidemiology, Ludwig-Maximilians-Universität München, München, Bavaria, Germany, **9** Oxford Centre for Diabetes, Endocrinology and Metabolism, University of Oxford, Oxford, United Kingdom and Neuroendocrine Tumour Centre, Royal Free Hospital, London, United Kingdom, **10** Medical Department I, University Medical Center Hamburg-Eppendorf, Hamburg, Germany

☯ These authors contributed equally to this work.
¶ Complete membership of the author group can be found in the Acknowledgments.
* patricia.grabowski@charite.de

OPEN ACCESS

Citation: Nölting S, Rentsch J, Freitag H, Detjen K, Briest F, Möbs M, et al. (2017) The selective PI3Kα inhibitor BYL719 as a novel therapeutic option for neuroendocrine tumors: Results from multiple cell line models. PLoS ONE 12(8): e0182852. https://doi.org/10.1371/journal.pone.0182852

Editor: Aamir Ahmad, University of South Alabama Mitchell Cancer Institute, UNITED STATES

Received: April 11, 2017

Accepted: July 25, 2017

Published: August 11, 2017

Data Availability Statement: All relevant data are within the paper and its Supporting Information files.

Funding: This work has been supported by a grant from NOVARTIS (YING Investigator program) to JS and from the Roggenbruck Foundation (Hamburg, Germany) to JS. The funders had no role in study design, data collection and analysis, decision to publish, or preparation of the manuscript. "Zentralklinik Bad Berka GmbH, Germany" is a communal hospital of the Rhön-

Abstract

Background/Aims

The therapeutic options for metastatic neuroendocrine tumors (NETs) are limited. As PI3K signaling is often activated in NETs, we have assessed the effects of selective PI3Kp110α inhibition by the novel agent BYL719 on cell viability, colony formation, apoptosis, cell cycle, signaling pathways, differentiation and secretion in pancreatic (BON-1, QGP-1) and pulmonary (H727) NET cell lines.

Methods

Cell viability was investigated by WST-1 assay, colony formation by clonogenic assay, apoptosis by caspase3/7 assay, the cell cycle by FACS, cell signaling by Western blot analysis, expression of chromogranin A and somatostatin receptors 1/2/5 by RT-qPCR, and chromogranin A secretion by ELISA.

Results

BYL719 dose-dependently decreased cell viability and colony formation with the highest sensitivity in BON-1, followed by H727, and lowest sensitivity in QGP-1 cells. BYL719

Klinikum AG and provided support in the form of salaries for authors [FB,PG], but did not have any additional role in the study design, data collection and analysis, decision to publish, or preparation of the manuscript. The specific roles of these authors are articulated in the author contributions section.

Competing interests: CJA has received research contracts (Ipsen, Novartis), lecture honoraria (Ipsen, Novartis, Pfizer, Amgen, Roche, Falk) and advisory board honoraria (Novartis). JS has received travel assistance, speakers honoraria and research funding from Novartis and travel assistance and speakers honoraria from Ipsen. PG has received research contracts (Ipsen, Novartis) and lecture honoraria (Ipsen, Novartis). SN has received travel assistance, speakers honoraria and research funding from Novartis and travel assistance and speakers honoraria from Ipsen. ABG has received lecture fees and advisory board honoraria from Novartis. The authors declare that there is no conflict of interest that would prejudice the impartiality of this scientific work. This does not alter the authors' adherence to PLOS ONE policies on sharing data and materials. "Zentralklinik Bad Berka GmbH, Germany" is a communal hospital of the Rhön-Klinikum AG and provided support in the form of salaries for authors [FB,PG]. This does not alter the authors' adherence to PLOS ONE policies on sharing data and materials.

induced apoptosis and G0/G1 cell cycle arrest associated with increased p27 expression. Western blots showed inhibition of PI3K downstream targets to a varying degree in the different cell lines, but IGF1R activation. The most sensitive BON-1 cells displayed a significant, and H727 cells a non-significant, GSK3 inhibition after BYL719 treatment, but these effects do not appear to be mediated through the IGF1R. In contrast, the most resistant QGP-1 cells showed no GSK3 inhibition, but a modest *activation*, which would partially counteract the other anti-proliferative effects. Accordingly, BYL719 enhanced neuroendocrine differentiation with the strongest effect in BON-1, followed by H727 cells indicated by induction of chromogranin A and somatostatin receptor 1/2 mRNA-synthesis, but not in QGP-1 cells. In BON-1 and QGP-1 cells, the BYL719/everolimus combination was synergistic through simultaneous AKT/mTORC1 inhibition, and significantly increased somatostatin receptor 2 transcription compared to each drug separately.

Conclusion

Our results suggest that the agent BYL719 could be a novel therapeutic approach to the treatment of NETs that may sensitize NET cells to somatostatin analogs, and that if there is resistance to its action this may be overcome by combination with everolimus.

Introduction

Neuroendocrine tumors (NET) are a heterogeneous group of malignancies. The therapy of choice for limited non-metastatic disease is surgery, but therapeutic options of metastatic disease are limited, as recently reviewed [1]. Low to intermediate grade metastatic NET may be managed by active surveillance, somatostatin analogs, loco-regional therapy, peptide receptor radionuclide therapy (PRRT), chemotherapy or molecular targeted therapy. If they progress and become more aggressive, chemotherapy shows only limited success (reviewed in [1]). However, several important molecular pathways involved in the pathogenesis and progression of NET have been identified to date, and open up new avenues for targeted therapies, including the tyrosine kinase inhibitor (TKI) sunitinib [2] or the mTORC1 inhibitor everolimus [3–5].

Besides the RAS/RAF/MEK/ERK or JNK pathways, one of the central signaling pathways is the phosphatidyl-inositol-3 kinase (PI3K)/AKT/mTOR sequence, which is frequently over-activated in NETs [6–14].

In brief, PI3K—encoded by the *PI3KCA* gene—is activated by different receptor tyrosine kinases (such as IGFR, EGFR, VEGFR, FGFR, RET) and in turn activates AKT which leads to inhibition of TSC1/2 and consequently to disinhibition/activation of *mTORC1/p70S6K*, phosphorylation of 4EBP1, activation of eIF-4E, cell proliferation and tumor growth (analogous to RAS/RAF/MEK/ERK signaling). RAS and PI3K may activate each other. Accordingly, the mTORC1 inhibitor everolimus has shown significant efficacy in NETs *in vitro*, *in vivo* and in clinical studies [1, 6], and has been approved for the treatment of pancreatic [5] and, very recently, of gastrointestinal and lung NETs [3, 4]. However, mTORC1 inhibition leads to a compensatory activation of PI3K/AKT signaling via p70S6K and IRS-1 activation, associated with an increase in $pAKT^{T308}$ (via PI3K/PDK1), $pAKT^{S473}$ (via mTORC2) and RAS/RAF/MEK/ERK signaling [15–19] (Fig 1). This compensatory up-regulation of PI3K/AKT and RAS/RAF/MEK/ERK may cause tumor cell resistance of initially sensitive cells [18–26]. Thus,

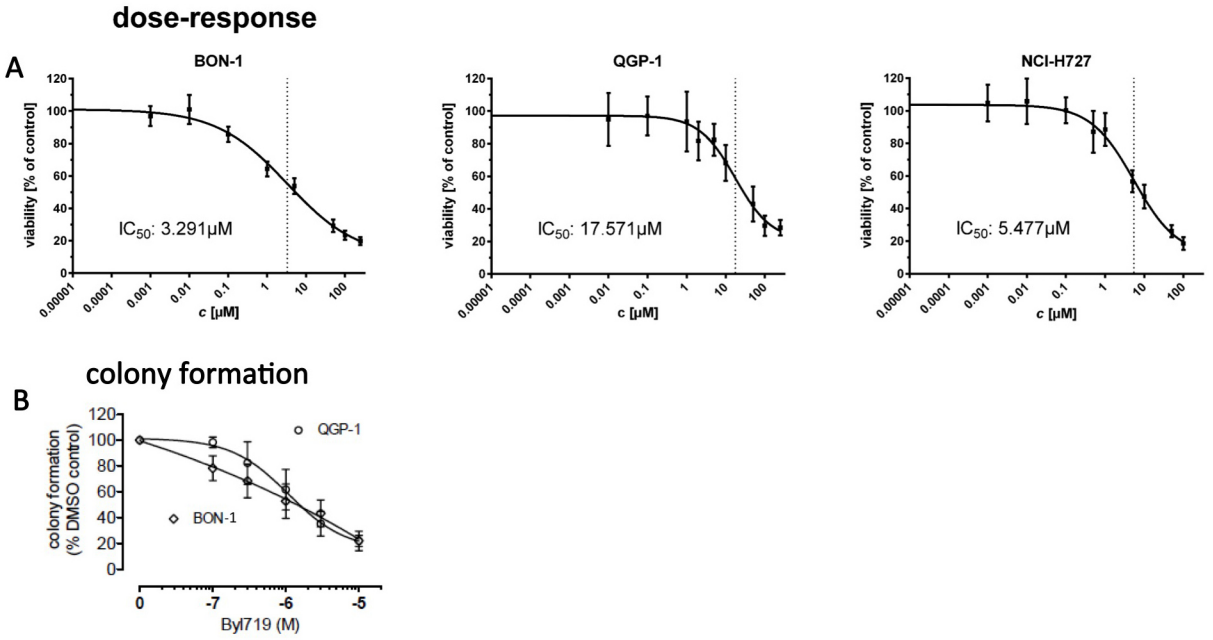

Fig 1. A: We treated cell lines with 9 different concentrations of BYL719 or vehicle control for 96 h and assessed cell viability with the WST-1 assay (Roche). Viability of treated cells was stated in percent vs. control (mean ± standard deviation (SD)). Dose-response curves and IC_{50} were calculated with GraphPad Prism software. B: In BON-1 and QGP-1 cells, colony formation was dose dependently reduced down to 22% of vehicel controls, with IC50 values of 1,3 µM and 1,8 µM, respectively. Data are presented as mean±SD of at least three independent experiments with five replicates per data point.

https://doi.org/10.1371/journal.pone.0182852.g001

it could be speculated that PI3K inhibitors working more upstream may bypass this mechanism of resistance and be more effective than mTORC1-inhibition alone. Indeed, different panPI3K inhibitors (LY294002, BKM120) or the dual PI3K/mTORC1/2 inhibitor BEZ235 alone and in combination with mTORC1 inhibitors and a MEK inhibitor, respectively, have shown anti-tumor potential in NET cells *in vitro* and *in vivo* [17, 18, 27–31]. In pancreatic NET cells, a synergistic effect of everolimus plus BEZ235 has been reported [18]. However, global clinical development of BEZ235—the most effective agent in pancreatic NET cells *in vitro* [18]—has been terminated, and two clinical trials in pancreatic NETs were stopped early due to poor tolerability, frequent treatment discontinuation, a non-fulfilled statistical endpoint and, moreover, no clear superiority to everolimus [24]. However, selective inhibition of the PI3Kα/110α-subunit—the predominant catalytic isoform in neuroendocrine pancreatic β-cells [32] involved in glucose homeostasis regulation [33, 34] and angiogenesis [35]—may be more effective and have a better safety profile than panPI3K inhibitors.

BYL719 is a selective PI3Kα inhibitor [36, 37] which has shown anti-proliferative activity in the pancreatic NET cell lines BON-1 and QGP-1 in a recent study [18]. BON-1 cells were more sensitive to BYL719 than QGP-1 cells in that study [18]. Notably, in pancreatic NET cells, the selective PI3Kα inhibitor BYL719 led to an additional weak inhibition of mTORC1 at 10 µM; in contrast, the panPI3K inhibitor BKM120 did not induce supplementary mTORC1 inhibition. BKM120 plus everolimus was not synergistic, whereas BYL719 plus everolimus was not tested in NET cells [18].

On the basis of that previous study, which showed anti-proliferative effects and partial PI3K/mTORC1 inhibition in BON-1 and QGP-1 cells after BYL719 treatment [18], we have now investigated the effects of the selective PI3Kα inhibitor BYL719 on pancreatic (BON-1, QGP-1) and lung (H727) NET cells in detail. Besides exploring its influence on cell viability,

colony formation and PI3K/AKT/mTORC1/2-signaling, we also investigated the effects on other signaling pathways, such as IGF1 and GSK3, assessing compensatory signaling pathway activations and downstream targets; these included apoptosis, cell cycle, cell differentiation [somatostatin receptor (SSTR)1/2/5 expression], chromogranin A (CgA) expression and secretion. Moreover, we tested the combination treatment of BYL719 with everolimus in NET cell lines, since additional mTORC1 inhibition has been shown to enhance sensitivity to BYL719 in breast cancer cells [38]. The aim of our study was to assess the efficacy of the PI(3)Kα inhibitor BYL719 in different NET cell lines and to determine the underlying mechanisms of action in order to explain the different cell line sensitivities, and to see if we could overcome partial resistance via combination treatments. We hypothesized that BYL719 might be effective at inhibiting the proliferation of NET cells to a different extent depending on cell line, and that partial resistance may be overcome by combination treatments.

Our results showed for the first time that the selective PI3Kα or BYL719 led to GSK3 inhibition and induction of re-differentiation with a significant increase of SSTR1/2 transcription in pancreatic BON-1 and pulmonary H727 cells associated with higher efficacy of BYL719 and higher cell line sensitivity, compared to QGP-1 cells. In contrast, the lower sensitivity of QGP-1 cells to BYL719 was associated with absent GSK3 inhibition and an absence of re-differentiation; partial resistance to BYL719 could be overcome by combination with everolimus via simultaneous PI3K/mTORC1 inhibition and hence strongly increased SSTR2 transcription. Thus, BYL719 might be an effective therapy for NETs, especially in combination with everolimus, and might sensitize NET cells to somatostatin analogs.

This study was a collaborative effort of five German research groups with complementary expertise in preclinical studies on NET cell lines. The long-term goal is the establishment of a preclinical collaborative network (NET-Z) that would provide an efficient and fast preclinical evaluation of novel drug candidates for clinical trials.

Materials and methods

Cell lines and drugs

Pancreatic neuroendocrine tumor cell lines BON-1 [39] and QGP-1 [40] (both obtained from Japanese Collection of Research Bioresources) and the typical bronchial carcinoid-NET cell line NCI-H727 (H727) [41] (purchased from ATCC, Manassas, VA) underwent authentication at the DSMZ (Braunschweig, Germany, in 2014), and their neuroendocrine features were confirmed by immunocytochemistry. Participating researchers received cell aliquots of the same passage together with SOPs for culture procedures. Cell lines had been tested for *PIK3CA* mutations by panel sequencing (Ion Seq Torrent Lung and Colon Panel v2). No *PIK3CA* mutations had been detected. BYL719 is a selective PI3Kα inhibitor developed by Novartis Pharma. All cell lines have been treated with different concentrations (10 nM– 250 μM) of BYL719 (kindly provided by Novartis) versus DMSO control for several time periods according to assay type. Everolimus was purchased from Selleckchem (Munich, Germany) and used in concentrations between 1 and 10nM.

Cell viability

For determination of cell viability, the WST-1 Assay (Roche) was utilized according to the manufacturer's instructions followed by calculation of IC_{50} and IC_{85}. The relative IC_{50} and IC_{85} values (indicating the concentration of half-maximal and 85% of maximal effect) were determined by non-linear regression using GraphPad Prism 6 software (mean of three independent experiments, 95% CI). Cells were incubated with 9 different concentrations of BYL719 (1nM-250μM) against vehicle control for 96h. The procedure of experiments and

analysis of results were conducted as described previously [42]. For statistical analysis, we used Microsoft Excel and GraphPad Prism 6 analysis software (San Diego, Calif., USA). The data passed a Kolmogorov-Smirnov test (with Dallal-Wilkinson-Lilliefors p value) for a Gaussian distribution, appropriate for data sets below 20 data points. Outliers were identified by Grubbs' test with $\alpha = 0.05$. Dose-response curves were fitted to the measured data using the method of least squares with variable slope; goodness of fit was quantified with R^2 and sums of squares. For detection of significant differences between two or more data groups, we used ANOVA followed by the Dunnett's test with a p value of <0.05. Data are presented as mean±standard deviation (SD) of at least three independent experiments with five replicates per data point.

For the combination experiments with BYL719/everolimus co-treatment, cell viability was assessed by "Cell Titer 96 Aqueous One Solution" MTS cell viability assay (Promega, Madison, WI, USA) according to the manufacturer's instructions as previously described in detail [43]. Cells were treated with various concentrations of 1 μM—20 μM BYL719, 1 nM -10 nM everolimus, or a combination of both drugs for the indicated incubation times. The low dose combination experiments of 1 μM BYL719 plus 1 nM everolimus were conducted in Hamburg with an incubation period of 120 h. The higher dose experiments were conducted in Munich with an incubation period of 144 h. To identify potential synergistic or antagonistic effects between BYL719 and everolimus on the natural logarithm of cell viability (ln cell viability), we used Linear Mixed Effects Models. BYL179, everolimus and the interactions between both were considered as fixed effects, the trial as a random effect. If a significant positive interaction between BYL179 and everolimus on cell survival was found, we concluded an antagonistic effect; if a significant negative interaction on cell survival was found, we concluded a synergistic effect. One model was estimated for each cell line. Statistical significance was defined at $p<0.05$. All computations were performed with R 3.2.2. For each MTS experiment, 4–6 independent samples per data point have been analyzed; each experiment was repeated at least two times in an independent manner.

Colony formation

Soft agar colony formation assays were used for assessment of anchorage-independent growth, as previously described [44]. Each experiment was repeated at least three times in an independent manner.

Cell cycle

For flow cytometry analysis of the cell cycle, cells were seeded and incubated with two different concentrations of BYL719 (IC_{50} and IC_{85} of the cell viability experiments for each cell line) against vehicle control for 72h. Detailed conditions and procedure of treatment, staining, measurement and analysis of results are described before [42]. DNA was stained with propidium iodide and mitotic cells were detected with an antibody against phospho-Histon H3. For statistical analysis, we used Microsoft Excel and GraphPad Prism 6 analysis software (San Diego, Calif., USA). The data passed a Kolmogorov-Smirnov test (with Dallal-Wilkinson-Lilliefors p value) for a Gaussian distribution, appropriate for data sets below 20 data points. Outliers were identified by Grubbs' test with $\alpha = 0.05$. For detection of significant differences between two or more data groups, we used ANOVA followed by the Dunnett's test with a p value of <0.05. Data are presented as percentage of all detected cells (about 50.000 cells) (mean ± SD) of at least four independent experiments.

Apoptosis

Caspase activity/apoptotic activity was determined using the Apo-One homogeneous caspase-3/7- Assay kit (Promega, #G7790): 10.000 cells per well were seeded, grown for 24 h and incubated for 24 h with different concentrations of BYL719. Concentrations of 10 μM (effective dose close to the IC50 of the cell viability experiments) and higher doses were tested. Caspase-3/7 activity was assessed following the manufacturer's instructions. For statistical analysis, *a priori* tests evaluating the normal distribution and homogeneity of variances were performed by the Kolmogorov-Smirnov-Test and the Levene′s Test of the SPSS statistical package SPSS (version 13.0 for Windows, SPSS Inc (2005), Chicago, USA). Non-parametric criteria were met; therefore, the Kruskal-Wallis followed by the Mann-Whitney test was performed. Statistical significance was assessed at $p<0.05$. Three independent samples per data point have been analyzed; each experiment was repeated at least two times in an independent manner. The results are displayed as mean ± SD.

Western blot technology

Western blot experiments were performed as previously described [45]. In brief, BON-1, H727 and QGP-1 cells were grown in 6-well plates for 24 h in complete medium. Afterwards, the medium was replaced by fresh 10% FBS medium and the respective doses of BYL719, everolimus or NVP-AEW541 were added for the respective incubation periods. In case of IGF1 stimulation, cells were pre-treated with the respective drugs for 48 h followed by IGF1 stimulation (50 ng/ml) for 30 minutes. After being washed twice in PBS, cells were lysed in 200 μl lysis buffer (M-PER ® Mammalian Protein Extraction Reagent containing HALT ™ protease & phosphatase inhibitor cocktail, Thermo Scientific, Rockford, USA). Lysates were centrifuged at 13,000 rpm for 10 min. Supernatants were adjusted to the same protein concentration (30–50 μg/50 μl) (Rotiquant Universal, Carl Roth, Karlsruhe, Germany). Equal amounts of protein were boiled for 5 minutes and denatured in Sodium dodecyl sulfate (SDS) sample buffer (0.25% Tris HCL, 40% glycerol, 2% SDS, 1% dithiothreitol, bromophenol blue, pH 8.8) before protein extracts were separated by SDS-PAGE and analysed by Western blot technology, as described before in detail [45].

The following primary antibodies were utilized: Primary monoclonal antibodies against pAKT (Ser473) (#4060), pAKT (Thr308) (#13038), AKT (#2920), pGSK3 (Ser21/9) (#8566), GSK3 (#5676), pERK1/2 (Thr202/Tyr204) (#4370), pp70S6K (Thr389) (#9234), p70S6K (#9202), pEGFR (Tyr1068) (#3777), EGFR (#4267), p4EBP1 (Ser65) (#9451), 4EBP1 (#9644), pS6 (Ser240/4) (#5364), S6 (#2317), p27 Kip1 (#3686), Caspase 3 (#9662), PARP (#9542), pChk1 (Ser345) (#2341), Chk1 (#2360), pRb (Ser780) (#9307), Cyclin D3 (#2936), pIGF1 (Tyr1131) (Tyr1146) (#3021), IGF1 (#3027) (all from Cell Signaling, Danvers, MA), Rb (#614602) (Biolegend, San Diego, USA), p21 Waf1/Cip1 (610233) (from BD Transduction Laboratories, Heidelberg, Germany), Actin (A5441) (Sigma, St. Louis, USA), Erk 1/2 (06–182) (Merck-Millipore, Darmstadt, Germany), SSTR2 (Abcam, Cambrdige, UK), GAPDH (Clone 6C5, Merck-Millipore, Darmstadt, Germany).

Actin was used as loading control. Peroxidase-conjugated polyclonal secondary antibody (1:25000) was incubated for 2 h, the blots were immersed in the chemiluminescent substrate SuperSignal West Dura (Thermo Scientific, Rockford, USA) and images were taken with an ECL Chemocam Imager (INTAS, Göttingen, Germany) or generated by using conventional X-ray films. Optical density of the approximately sized bands was densitometrically quantified using ImageJ 1.440 software (Wayne Rasband, National Institute of Health, USA). Band intensities were quantified from at least 3 independent experiments for each cell line and protein, and are described as the mean percentage relative to the untreated control (100%). We

performed statistical analysis according to the following method: A linear mixed effects model was estimated for the logarithm of the relative increase [compared to the respective control group] with the trial as random effect. The logarithm was chosen to account for the multiplicative nature of the data. Analogously, means and standard deviations are reported as geometric means and geometric standard deviations of the relative increase, respectively. A geometric mean of "1.0" has to be interpreted as "equal to the control group" and for the geometric standard deviation "1.0" refers to "no variation". We compared the phospho(p)-protein expression to the control to adequately assess the extent of activation or inhibition of signaling pathways after drug treatment and compare it between the different cell lines. All original uncropped Western blots are shown as supplementary Figures (S1–S23, S29 and S30 Figs).

Gene expression analysis of somatostatin receptors (*SSTR) 1/2/5* and chromogranin A (*CHGA)*

For monotherapy with BYL719 we evaluated an effective dose close to the IC50 of the cell viability experiments (10μM). For combination treatment we used concentrations that gave us a synergistic effect at the lowest dose, therefore achieving maximum synergistic effects but minimizing potential toxic side effects. Thus, tumor cells were treated for 96h with BYL719 at 10μM (monotherapy) or at 1μM BYL719 and 1nM everolimus (combination treatment). Total RNA was isolated from cell cultures using the Nucleo Spin RNA, DNA and protein purification Kit (Macherey-Nagel, Düren, Germany) according to the manufacturer's protocol. Total RNA was reverse-transcribed using the High Capacity cDNA Reverse Transcription Kit (Applied Biosystems, Foster City, CA) and a T3 Thermocycler (Biometra, Göttingen, Germany).

We used pre-validated TaqMan Primers for SSTR1, SSTR2, SSTR3, SSTR5 and GAPDH for real-time PCR. These primers were purchased from Applied Biosystems. Samples in duplicate were subjected to PCR in a Step One Plus Real-Time PCR System (Applied Biosystems). Values were expressed as (Ct) values normalized to housekeeping gene GAPDH using the $2^{-\Delta\Delta Ct}$ method. All graphs and statistical analysis were performed using GraphPad Prism 4 utilizing standard two-tailed unpaired Students t-test for normally distributed data. P-values <0.05 have been considered significant ($^{*}<0.05$; $^{**}<0.005$, $^{***}<0.001$). Data are presented as mean ± standard error of mean (SEM) of at least three independent experiments with three replicates per data point.

ChromograninA (CgA) ELISA

BON, H727 and QGP-1 cells were seeded in 24-well plates at a density of $2x10^5$ per well and grown for 24 h. Cells were treated with either 0.1% DMSO (vehicle control), PDBu (Phorbol-12,13-dibutyrate; Sigma-Aldrich, Deisenhofen, Germany) as a positive control for the induction of secretion or BYL719 for 24 h in growth medium. Media were collected and remaining cell debris was eliminated by centrifugation for 3 min at 200 x *g*. CgA concentration in the supernatants was measured using CgAnalyze Kit (DAKO, Hamburg, Germany) according to the manufacturer's protocol. Two independent experiments with three replicates per data point were analyzed.

Results

Cell viability, apoptosis and cell cycle

Significant reduction cell viability in NET cell lines in vitro. The pancreatic NET cell lines BON-1 and QGP-1 and the typical bronchial carcinoid cell line H727 were treated with

increasing doses of BYL719 for 96 h and cell viability was determined by the WST-1 assay. BON-1 cells showed the highest sensitivity to BYL719 with an IC_{50} of 3.29 μM, followed by H727 cells with an IC_{50} of 5.48 μM, and QGP-1 cells with the lowest sensitivity to BYL719 and an IC_{50} of 17.57 μM (Fig 1A).

The IC_{85} was 100 μM in all cell lines (Fig 1A): 96 h treatment with low doses of 1 μM BYL719 only led to a slight decrease in cell viability in all three cell lines (by 36%, 11% and 7% in BON-1, H727 and QGP-1 cells, respectively) (Fig 1A).

Colony formation assay demonstrated the efficacy of BYL719 in pancreatic NET cells with a higher sensitivity for BON-1 cells compared to QGP-1 cells. BYL719 dose-dependently reduced colony formation down to 22% of vehicle controls, with IC_{50} values of 1.3 μM (BON-1) and 1.8 μM (QGP-1) (Fig 1B). H727 cells did not form colonies.

Induction of apoptosis. Caspase 3 and 7 activity was measured by caspase3/7 assay after 24 h of treatment with increasing concentrations of BYL719: 10 μM and higher concentrations of BYL719 significantly induced apoptosis in all 3 cell lines, BON-1, QGP-1 and H727 cells. The strongest apoptosis induction was found in BON-1 cells, followed by H727 cells, with QGP-1 showing the least but still significant apoptosis. The data shown represent the mean ± SD (Fig 2).

Consistent with clear apoptosis induction, western blot analyses showed a dose-dependent significant increase of cleaved caspase-3 and cleaved PARP in all three cell lines after 24 h of treatment with BYL719 (S1 Table, Fig 3).

Cell cycle arrest in G_0/G_1. While p27 and p21 inhibit cell cycle progression by inhibition of cyclin dependent kinases, Cyclin D3 induces cell cycle progression from G_0/G_1- to S-phase,. Activation of the DNA-damage checkpoint marker CHK1 leads to cell cycle arrest, DNA-repair and if ineffective cell death to prevent damaged cells from cell cycle progression.

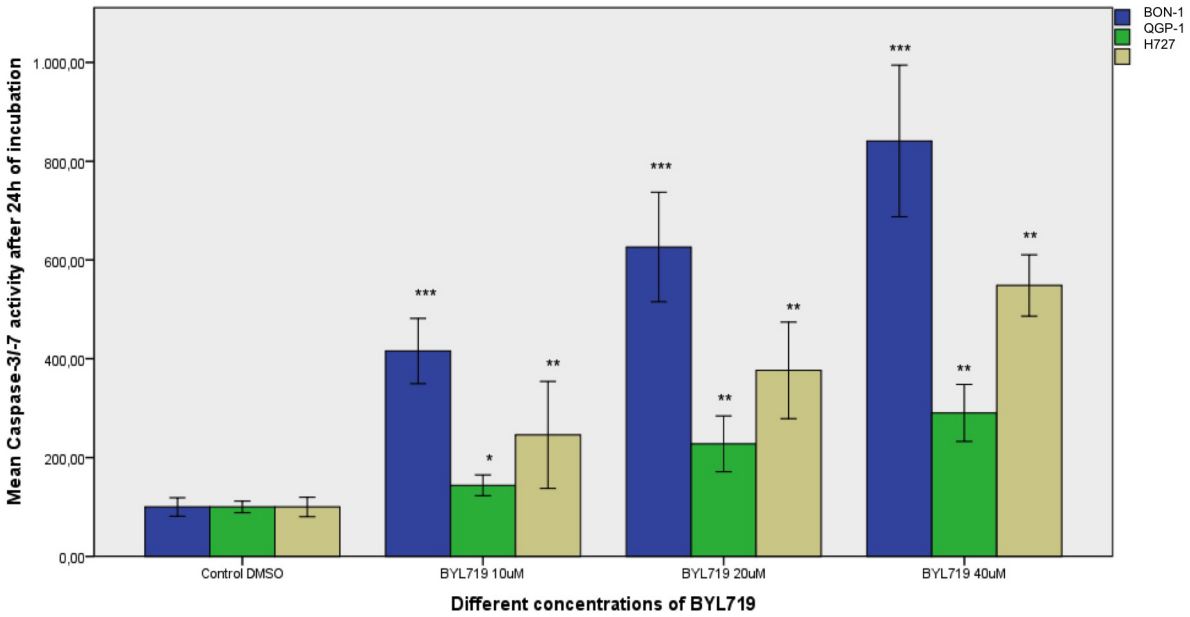

Fig 2. Assessment of apoptosis: Caspase 3/7 assay results after 24 h treatment with different doses of BYL719 are shown as mean percentage of caspase 3/7 activity referred to the untreated control (100%) ± SD: Strongest apoptosis was induced in BON-1 cells, followed by H727 cells. QGP-1 cells showed the least but still significant apoptosis. * $p<0.05$; ** $p\leq0.01$; *** $p\leq0.001$ (two independent experiments with three replicates per data point).

https://doi.org/10.1371/journal.pone.0182852.g002

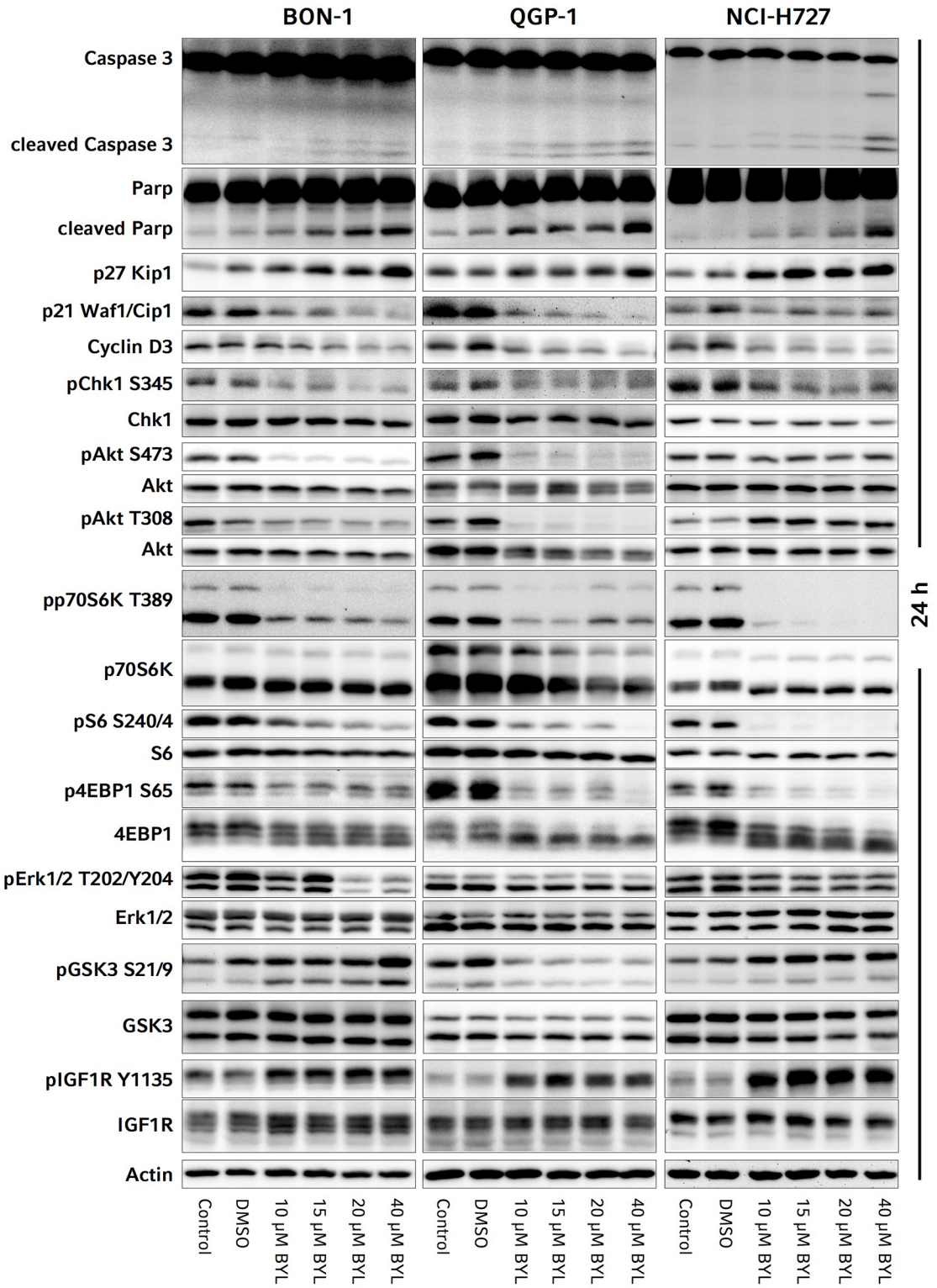

Fig 3. Representative western blots of the investigated signaling pathways, apoptosis and cell cycle markers in BON-1, QGP-1 and H727 cells: The means, standard deviations and p-values of the western blot quantification and statistical analysis from at least three independent replicates are given in S1 Table.

https://doi.org/10.1371/journal.pone.0182852.g003

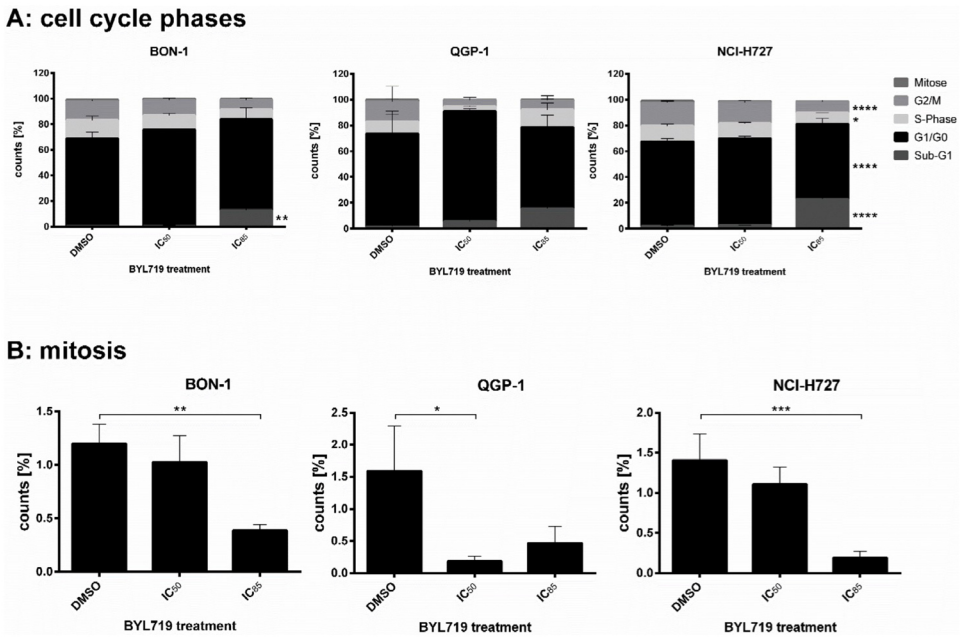

Fig 4. Cell lines were treated with BYL719 (IC_{50} and IC_{85}) for 72 h. Cells were stained with PI (DNA content) analysis solely included and mitosis-specific Phospho(Ser10)-Histone H3 immunostain followed by flow cytometry assessment (single cells). According to the stain, events were divided into cells of several cell cycle phases or were classified as sub-G1-events indicating cell death (FlowJo software), given in percent of all detected cells (mean ± SD) of at least four independent experiments. A: Cell cycle. B: Mitotic index. * $p<0.05$; ** $p\leq0.01$; *** $p\leq0.001$; **** $p\leq0.0001$.

https://doi.org/10.1371/journal.pone.0182852.g004

BON-1, QGP-1 and H727 cells were treated with BYL719 for 72 h and changes in cell cycle patterns were assessed by flow cytometry. BYL719 increased the G_0/G_1 fraction at IC_{50} concentrations indicating induction of G_0/G_1 cell cycle arrest. At higher doses (IC_{85}), a sub-G1 fraction suggested induction of cell death (Fig 4A).

Furthermore, the percentage of mitotic cells was assessed by mitotic index flow cytometry (mitotic index: percentage of cells which are in the mitotic phase). In all three cell lines the percentage of mitotic cells decreased at high dose of BYL719 treatment (mean of four independent experiments, including standard deviation) (Fig 4B).

Consistent with induction of G_0/G_1-cell cycle arrest, p27 was significantly increased after 24 h treatment in all three cell lines (S1 Table, Fig 3); the strongest up-regulation of p27 at 10–20 μM BYL719 was found in BON-1 cells (S1 Table, Fig 3). Moreover, there was a non-significant decrease of Cyclin D3 in all three cell lines, also promoting G_0/G_1-cell cycle arrest (S1 Table, Fig 3). According to the induction of apoptosis, as discussed below, there was a significant reduction of the cell cycle regulator p21 in all three cell lines after 24 h treatment (S1 Table, Fig 3).

We observed a significant inhibition of the DNA damage checkpoint marker Chk1 ($pChk1^{Ser345}$) after 24 h treatment in all three cell lines—in BON-1 cells at doses higher than 15 μM, in H727 and QGP-1 cells at all tested doses (S1 Table, Fig 3).

Signaling pathways

PI3K/AKT/mTORC1/2 and ERK signaling: Partial inhibition of PI3K/$AKT^{Ser473/Thr308}$, mTORC1 and ERK signaling. Activated/phosphorylated (p)AKT^{Ser473} indicates mTORC2-dependent PI3K/AKT activity, while $pAKT^{Thr308}$, which is mediated by PDK1, is a marker

PI3K/PDK1/AKT activity; pp70S6K, pS6 and p4EBP1 are downstream-targets of mTORC1 and markers of mTORC1 activation; pERK displays activation of RAS/RAF/ERK signaling.

In BON-1 and QGP-1 cells, there was a significant inhibition of AKT^{Ser473} at all tested doses (10–40 μM) of BYL719 after 24 h treatment; a lower and inconsistent inhibition of $PI3K/AKT^{Ser473}$ was seen in H727 cells with a statistical significance at doses higher than 15 μM (S1 Table, Fig 3). Similar results were found for $PI3K/AKT^{Thr308}$ with a significant inhibition in QGP-1 cells at all tested doses and in BON-1 cells at doses higher than 15 μM. In contrast, in H727 cells there was a non-significant activation of $PI3K/AKT^{Thr308}$ (S1 Table, Fig 3). In all three cell lines, mTORC1 was significantly inhibited after 24 h treatment with 10–40 μM BYL719 as demonstrated by significant reduction of pp70S6K, pS6 and p4EBP1 (S1 Table, Fig 3). The strongest decrease of pp70S6K and pS6 was found in H727 cells, followed by QGP-1 cells, and the lowest, but a significant decrease was still observed in BON-1 cells. The decrease of p4EBP1 was significant in H727 cells at all tested doses, but in BON-1 and QGP-1 cells only at the highest tested dose (S1 Table, Fig 3); We observed a slight inhibition of ERK signaling upon 24 h BYL719 treatment in all three cell lines with a statistical significance only at high doses (at 20 μM in BON-1 and 40 μM in QGP-1 and H727 cells) (S1 Table, Fig 3).

Inhibition of GSK3 in BON-1 and H727 cells, but not in QGP-1 cells. The growth-factor-induced PI3K/AKT signaling pathway phosphorylates and thereby inhibits GSK3 [46–48]. In our study GSK3α and β (GSK3) behaved similarly. We quantified both together and separately (S1 Table). Unexpectedly, despite significant PI3K/AKT inhibition after 24 h BYL719 treatment, there was a dose-dependent phosphorylation/inhibition of GSK3 in BON-1 and H727 cells with a significant inhibition of GSKα/β and especially GSK3 in BON-1 cells at doses higher than 10 μM (S1 Table, Fig 3); in QGP-1 cells, there was no inhibition, but a modest activation of GSK3 at doses higher than 10 μM BYL719 after 24 h treatment (S1 Table, Fig 3). Additional Western blot analysis with low dose treatment of 1 μM BYL719 was performed in the most sensitive cell line BON-1 as our cell line model: we showed no effects on pGSK3, compared to the control (S24 Fig). PGSK3 was increased in BON-1 cells at 2.5 μM BYL719 and higher doses (S25 Fig).

Receptor tyrosine kinases: Strong activation of IGF1R signaling. Phosphorylated (p) IGF1R and pEGFR are markers of activated receptor tyrosine kinases IGF1R and EGFR, respectively. IGF1R may also phosphorylate/inhibit GSK3 [46–48]. In BON-1, QGP-1 and H727 cells, IGF1R was significantly activated after treatment with 10–40 μM BYL719 for 24 h with strongest activation in H727 cells, followed by BON-1 cells and lowest activation in QGP-1 cells (S1 Table, Fig 3). Additional Western blot analysis after low dose treatment with 1 μM BYL719 still showed IGF1R activation in BON-1 cells as our cell line model (S24 Fig).

EGFR activity was not notably altered in any cell line.

Combination treatment of BYL719 with the specific IGF1R inhibitor NVP-AEW541. In order to prove a potential dependence of GSK3 phosphorylation on IGF1R activation in response to BYL719 treatment, we tested co-treatment of BYL719 with the specific IGF1R inhibitor NVP-AEW541 in all three cell lines for an incubation period of 48 h; surprisingly, such co-treatment showed at least additive inhibitory effects on BON-1, H727 and QGP-1 cell viability. We confirmed again that BYL719 led to phosphorylation/inhibition of GSK3 in BON-1 and H727 cells. However, unexpectedly, this inhibitory effect on GSK3 was even enhanced in both BON-1 and H727 cells by co-treatment with NVP-AEW541 (and not blocked), being accompanied by stronger IGF1R phosphorylation/activation after combination treatment. In QGP-1 cells neither drug alone nor the combination changed GSK3 phosphorylation: in QGP-1 cells NVP-AEW541 alone inhibited IGF1R phosphorylation/activation and co-treatment inhibited the BYL719-induced IGF1R activation. In QGP-1 and H727 cells total IGF1R expression was slightly increased after NVP-AEW541 treatment alone. H727 cells

showed a low baseline phosphorylation of the IGF1R. In BON-1 cells, which showed a very low baseline phosphorylation/activation of IGF1R, NVP-AEW541 did not change phosphorylation or total expression levels of IGF1R (S26 Fig).

The low baseline phosphorylation/activity of the IGF1R in BON1 and H727 cells might not have been sufficient to show the effects of specific IGF1R inhibition by NVP-AEW541; moreover, others have shown a dependence of GSK3 phosphorylation on IGF1R activity in medulloblastoma cells [49], but they stimulated their cells with IGF1 to demonstrate clear results. We therefore enhanced and optimized our experimental design by using IGF1 stimulation according to the previously-published experimental design [49]. We used a slightly lower dose of 10 μM BYL719 because we expected a much stronger IGF1R phosphorylation after IGF1 stimulation, and we wished to investigate if the absent effect of NVP-AEW541 on BYL719-induced GSK3 phosphorylation could also be observed at lower doses of 10 μM BYL719. We could then show strong baseline IGF1R phosphorylation/activity after IGF1 stimulation in all three cell lines, which could be clearly inhibited by NVP-AEW541 in all three cell lines. As expected, BYL719 led to strong IGF1R activation in all cell lines, and NVP-AEW541 prevented the BYL719-induced IGF1R activation. However, while the baseline phosphorylation of GSK3 increased after stimulation with IGF1 in all three cell lines, it was even more strongly increased after either NVP-AEW541 treatment or BYL719 treatment alone in BON-1 (especially GSK3β) and H727 cells. In QGP-1 cells no changes in GSK3 phosphorylation after drug treatment were seen, consistent with our previous results. Thus, despite IGF1R inhibition after combination treatment in all three cell lines, the phosphorylation/inhibition of GSK3 was even stronger after the combination treatment in H727 cells and not changed in BON-1 and QGP-1 cells compared to single BYL719 treatment (S27 Fig). Therefore, blockade of the IGF1R did not attenuate BYL719-induced GSK3 phosphorylation refuting our initial hypothesis of the dependence of BYL719-induced GSK3 phosphorylation on IGF1R activation in BON1 and H727 cells.

mRNA expression of NET markers *(SSTR1*, *SSTR2*, *SSTR5*, *CHGA)*: Induction of cell re-differentiation in BON-1 and H727 cells, but not in QGP-1 cells

Treatment of cells with 10 μM BYL719 for 96 h induced mRNA expression of genes related to neuroendocrine differentiation in BON-1 and H727 cells. Transcripts for CgA (*CHGA*), *SSTR1* and *SSTR2* were induced in H727 and BON-1 cells, whereas *SSTR5* was reduced. In particular, we observed a 2.5- (CI 1.8–3.1) and 4.5- (CI 2.6–6.3) fold induction of *SSTR2* mRNA upon BYL719 treatment in H727 and BON-1 cell, respectively ($p<0.001$). In contrast, in QGP-1 cells *SSTR1* transcripts were reduced, while *CHGA*, *SSTR2* and *SSTR5* were unaffected (Fig 5A). We also tested SSTR2 mRNA expression in all three cell lines after treatment with a low dose of 1 μM BYL719 for 96 h and found significant SSTR2 induction in BON-1 and H727 cells, but not in QGP-1 cells.

CgA secretion was not altered

To evaluate the influence of BYL719-induced cell differentiation and signaling on CgA secretion in neuroendocrine tumor cells, BON-1, H727 and QGP-1 cells were analyzed for their release of CgA when treated with either vehicle, the known PKC activator and secretagogue phorbol-12,13-dibutyrate (PDBu), or two concentrations of BYL719. As Fig 6 demonstrates, PDBu at a concentration of 1 μM was able to increase the concentration of secreted CgA in BON-1 cells from the basal value (366 ± 58 U/ml) about 5-fold (2061 ± 166 U/ml). PDBu also raised CgA levels in the medium of H727 (about 2-fold) and QGP-1 cells (about 1.5-fold). In

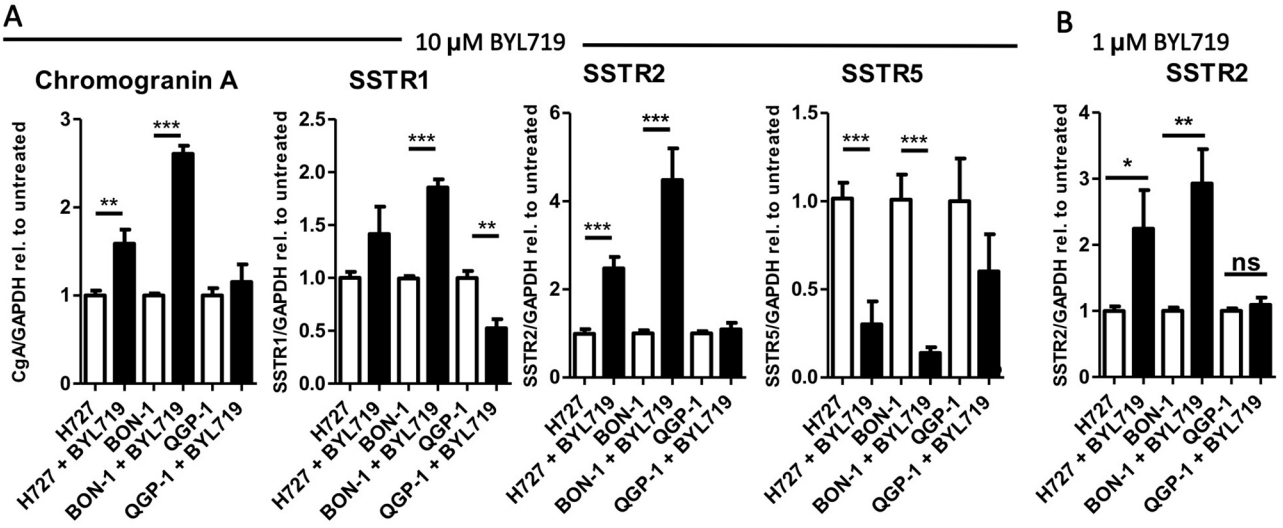

Fig 5. Neuroendocrine marker expression was increased by BYL719 treatment. A: BON-1, H727 and QGP-1 cells were treated with 10 µM BYL719 for 96 h and mRNA expression of Chromogranin A *(CHGA)*, *SSTR1*, *SSTR2* and *SSTR5* was analyzed by qPCR. B: BON-1, H727 and QGP-1 cells were treated with 1 µM BYL719 for 96 h and mRNA expression of *SSTR2* was analyzed by qPCR; Values are summarized from three independent experiments of three replicates per data point. * $p<0.05$; ** $p\leq0.01$; *** $p\leq0.001$.

https://doi.org/10.1371/journal.pone.0182852.g005

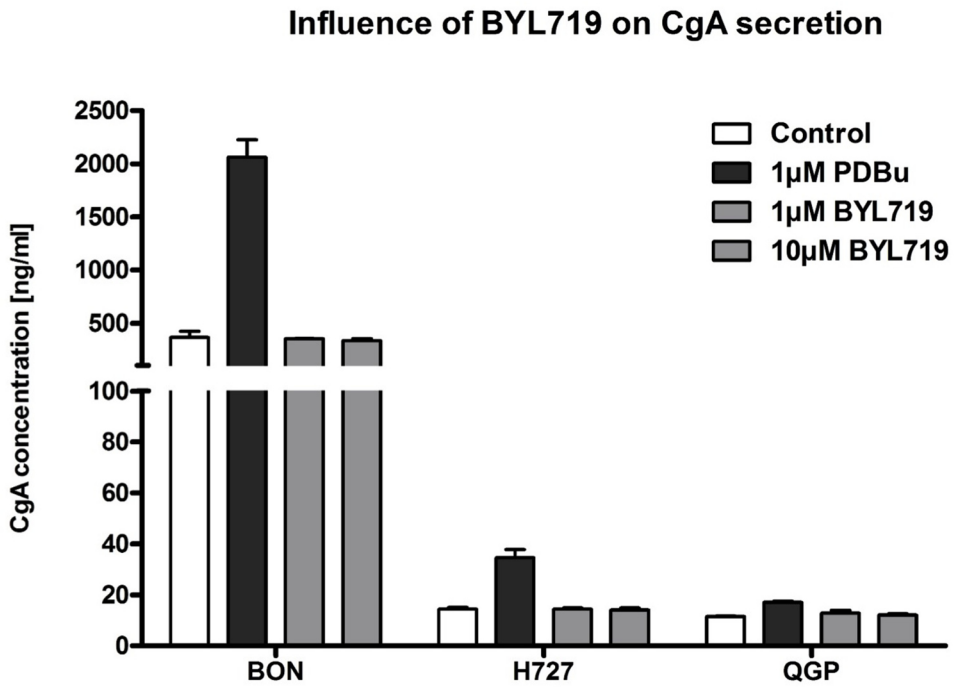

Fig 6. CgA secretion of NET cells was not altered by BYL719 treatment. BON-1, H727 and QGP-1 cells were treated with vehicle, PDBu (positive control) or BYL719 (1 µM, 10 µM) for 24 h; the supernatant was collected for CgA measurements (two independent experiments with three replicates per data point).

https://doi.org/10.1371/journal.pone.0182852.g006

contrast, BYL719 did not alter the concentration of CgA in either BON-1, H727 or QGP-1 cell supernatants at either 1 or 10 μM concentrations (Fig 6).

Synergistic effect of BYL719 plus everolimus in QGP-1 cells

Given earlier reports on synergistic effects of combination therapies with PI3K and mTOR inhibitors, we evaluated the potential of co-treatment of BYL719 and everolimus in our NET cell line models *in vitro*. In QGP-1 cells—showing the lowest sensitivity to BYL719 alone—a synergistic inhibitory effect of 1–20 μM BYL719 plus 1–10 nM everolimus on cell viability was found ($p \leq 0.01$) (Fig 7A).

In BON-1 cells, there was also a synergistic effect at low doses of 1 μM BYL719 plus 1 nM everolimus, and an additive effect of both treatments at higher doses (Fig 7A), whereas H727 cells did not respond to everolimus and no synergistic or additive effect was observed in the latter (data not shown). As described earlier, Western blot analysis showed a strong activation

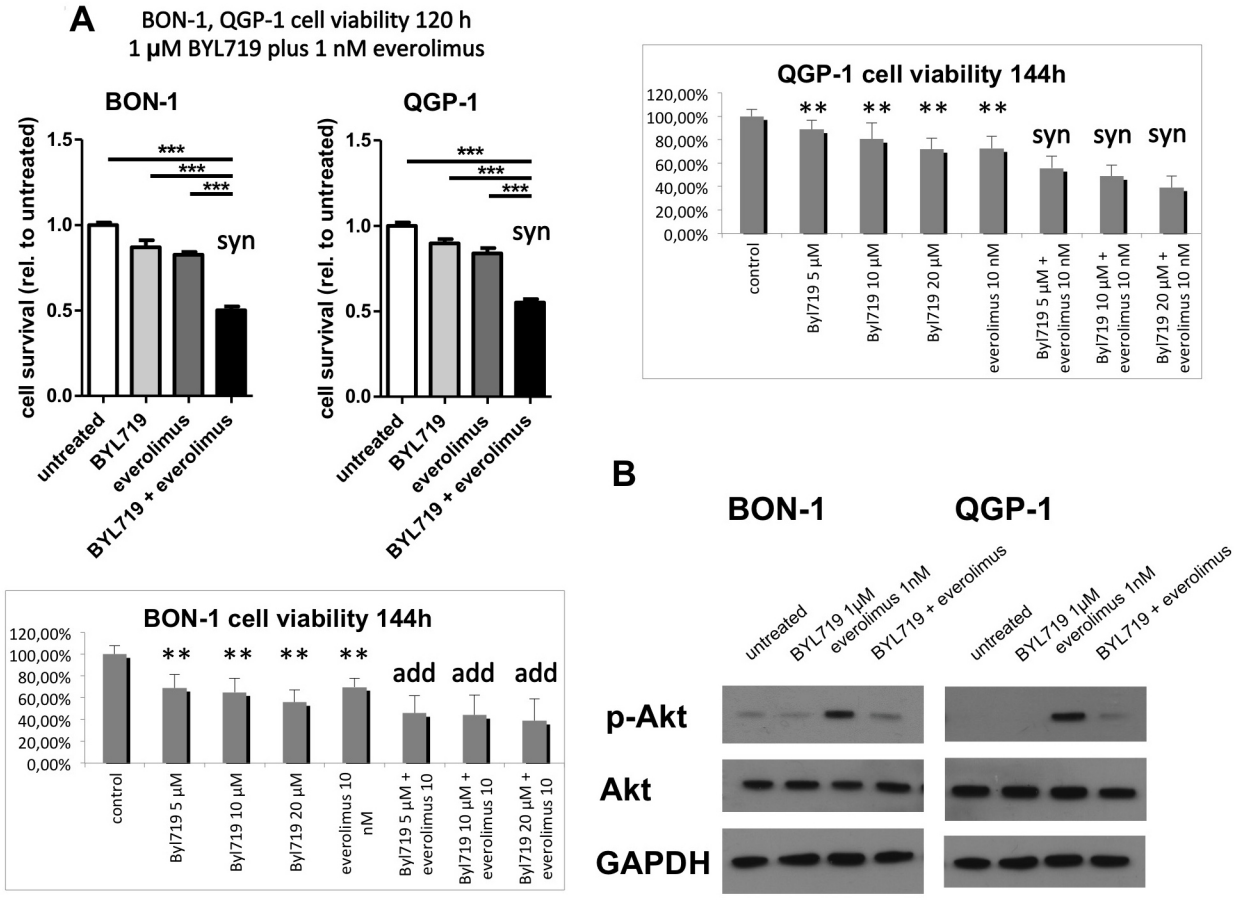

Fig 7. A: The combination therapy of BYL719 plus everolimus was synergistic in QGP-1 cells at all tested doses (1–20 μM BYL719 plus 1–10 nM everolimus) and in BON-1 cells at low doses (1 μM BYL719 plus 1 nM everolimus) ($p \leq 0.01$), and additive in BON-1 cells at higher doses. MTS cell viability assay data are shown as mean ± SD of 4–6 replicates per data point from two independent experiments, referred to the untreated control; syn: synergistic ($p \leq 0.01$); add: additive; **, *** highly significant, compared to the control (** $p \leq 0.01$, *** $p \leq 0.001$); B: Co-treatment of BON-1 and QGP-1 cells with BYL719 and everolimus prevented everolimus-induced AKT activation. Cells have been treated with 5 μM BYL719, 5 nM everolimus or the combination of both for 48h and subjected to western blot analysis of $pAKT^{Ser473}$, AKT and GAPDH. Representative Western Blot of three replicates.

https://doi.org/10.1371/journal.pone.0182852.g007

of AKT after treatment with everolimus alone, which was almost completely prevented by addition of a low dose of 5 μM BYL719 in BON-1 and QGP-1 cells (Fig 7B).

Moreover, 1 μM BYL719 plus 1 nM everolimus significantly more strongly induced *SSTR2* transcription compared to each drug separately in BON-1 (12.5-fold, CI 5.8–19.2) and QGP-1 cells (1.5-fold, CI 1.2–1.7) (Fig 8).

It should be noted that this synergism already occurred at doses (1 μM for BYL719 and 1 nM for everolimus), which do not influence cell viability as monotherapies.

Comparison of BYL719 versus the panPI3K inhibitor BKM120 in BON-1 cells

To prove the involvement of other PI3K subunit isoforms apart from PI3Kα in NET signaling, we compared the efficacy of the selective PI3Kα inhibitor BYL719 to the efficacy of the pan-PI3K inhibitor BKM120 in the most sensitive cell line BON-1 cells as our model, and found a much stronger inhibitory effect of BKM120 at low doses, compared to BYL719 (IC_{20} BKM120 at 72h 0.5 μM vs. IC_{20} BYL719 at 72 h 6.9 μM; IC_{50} BKM120 at 72 h 1.2 μM vs. IC_{50} BYL719 at 72 h not reached) (S28 Fig).

Discussion

Cell viability, apoptosis and cell cycle

BYL719 dose-dependently reduced NET cell viability and colony formation with highest sensitivity for BON-1, followed by H727 cells and with the lowest sensitivity for QGP-1 cells. Our data are consistent with a previous study showing higher sensitivity of BON-1 cells to BYL719 compared to QGP-1 cells [18]. Interestingly, colony formation was already suppressed at low doses (IC_{50} 1.3 μM in BON-1 and 1.8 μM in QGP-1 cells). The colony formation assay tests every cell in the population for its ability to undergo "unlimited" division and determines reproductive cell death after treatment with cytotoxic agents [50]. Therefore, colony formation may also reflect interactions between tumor cells and its microenvironment and might even better correlate with tumor growth *in vivo* than cell viability assays [51–53].

In all three NET cell lines investigated, BYL719 induced apoptosis associated with significantly increased caspase 3 and. cleaved PARP. The highest sensitivity to BYL719 correlated with strongest BYL719-induced apoptosis in BON-1 cells, followed by H727 cells and then QGP-1 cells.

Moreover, BYL719 induced cell cycle arrest in the G_0/G_1-phase in all three cell lines. This was consistent with a significant up-regulation of p27 in all cell lines investigated. The strongest BYL719-mediated increase of p27 after 24 h treatment was found in BON-1 cells. A positive correlation of loss of p27 and aggressiveness as well as increased cell cycle progression of gastroenteropancreatic NETs has previously been described [54].

After 24 h of BYL719 incubation, there was a significant decrease of activated DNA-damage checkpoint marker Chk1 in all three cell lines. Interestingly, inhibition of Chk1 has shown promising anti-cancer effects *in vitro* in a variety of p53 deficient human tumor cell lines through induction of caspase-3/7 dependent apoptosis, and especially sensitized colon tumors to chemotherapy *in vivo* [55, 56]. This may be an interesting additional effect in poorly differentiated neuroendocrine carcinomas (NECs) which regularly bear p53 mutations [57]. The observed significant decrease of the cell cycle inhibitor p21 may be due to PI3K/AKT inhibition by BYL719, since PI3K/AKT signaling increases p21 [58, 59]. The role of p21 has been a controversal topic in the literature [60]. On the one hand, it is a cell cycle inhibitor leading to cell cycle arrest and anti-proliferative signals. On the other hand, there is also evidence that

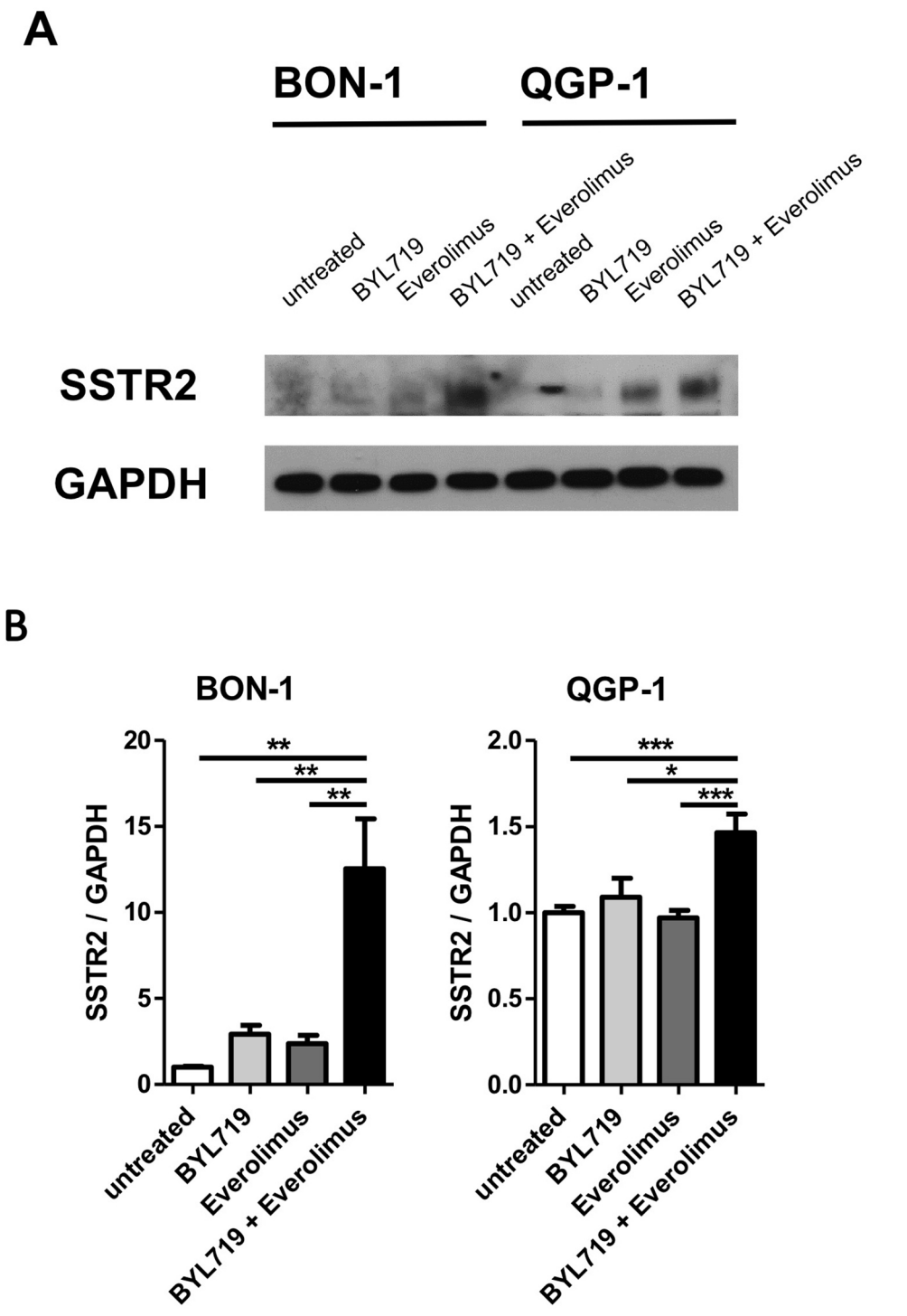

Fig 8. The combination therapy with BYL719 plus everolimus strongly induced SSTR2 expression in BON-1 and QGP-1 cells. Cells have been treated with 5 μM BYL719, 5 nM everolimus, or the combination of both for 48h (A) or with 1 μM BYL719, 1 nM everolimus or the combination of both for 96h (B). SSTR2 expression was analyzed by Western Blot (A) and qPCR (B). Representative western blot of two replicates; qPCR results are summarized from three independent experiments of three replicates. * $p<0.05$; ** $p\leq0.01$; *** $p\leq0.001$.

https://doi.org/10.1371/journal.pone.0182852.g008

p21 may inhibit apoptosis, promote tumor cell growth and cooperate with Chk1 to prevent apoptosis during DNA replication fork stress [59–63]. Therefore, the observed decrease of p21 due to partial PI3K/AKT inhibition together with a Chk1 inhibition may also have pro-apoptotic/anti-tumor effects.

Signaling pathways

Inhibition of PI3K/AKT/mTORC1/2 signaling. In all three cell lines, mTORC2-induced PI3K/AKT^{Ser473} signaling was significantly and partially, but not completely, inhibited by BYL719 treatment, and the inhibition was stronger in BON-1 and QGP-1, compared to H727 cells. Similar data were found for PI3K/PDK1/AKT^{Thr308} signaling with significant partial inhibition in BON-1 and QGP-1 cells, but even activation in H727 cells after 24 h of treatment with 10 μM BYL719. This suggests that, surprisingly, potent PI3K/AKT inhibition may not be crucial for BYL719 efficacy in NET cells. This indicates potential non-selective effects of BYL719 independent of the p110α subunit and the involvement of alternative signaling pathways, as discussed in detail below. Consistently, we could show only slight inhibitory effects of a low dose of 1 μM BYL719 alone on cell viability, also arguing for non-selective effects of BYL719 at higher doses.

Moreover, this indicates the potential importance of alternative PI3Kp110 catalytic subunit isoforms in NET signaling. PI3K110α (the catalytic subunit of class I PI3K) has been considered as the only relevant catalytic subunit in the context of cancer associated mutations [64] and has shown relevant anti-tumor potential in pancreatic NETs *in vitro* and *in vivo* [18, 65]. However, the other variants of the p110 catalytic subunit—β or δ—may be of importance and promote sustained activity of PI3K/AKT^{Ser473} and PI3K/AKT^{Thr308} despite PI3K110α inhibition. The δ isoform of the p110 catalytic subunit of PI3K has already shown anti-tumor potential in leukemia or in anaplastic thyroid carcinoma [66, 67]. The theory of potential involvement of alternative PI3K subunit isoforms in NET signaling was supported by a much stronger inhibitory effect of the panPI3K inhibitor BKM120, compared to BYL719, on BON-1 cell viability (IC_{20} BKM120 at 72h 0.5 μM vs. IC_{20} BYL719 at 72h 6.9 μM; IC_{50} BKM120 at 72h 1.2 μM vs. IC_{50} BYL719 at 72h not reached).

Interestingly, while we confirmed previous findings of a partial mTORC1 inhibition at 10 μM BYL719 in pancreatic NET cells [18], we noted that H727 cells showed more pronounced mTORC1 inhibition accompanied by higher PI3K/AKT activity in response to BYL719 treatment. Thus, our data might argue for a direct effect of BYL719 on mTORC1. In this context, PI3K knock-down experiments would seem to be a reasonable procedure to prove a direct impact of BYL719 on mTORC1 signaling and will be subject of further studies. However, with our current study we were not able to confirm a direct effect of BYL719 on mTORC1. BON-1 and QGP-1 cells behave very similarly with respect to the impact of BYL719 on PI3K/AKT/mTORC1 signaling although they showed different sensitivities. BON-1 cells showed lower inhibition on PI3K/AKT signaling, compared to QGP-1 cells, and the lowest inhibition of mTORC1 of all three cell lines, however, the highest sensitivity to BYL719 of all three cell lines. Hence, the extent of PI3K/AKT/mTORC1 inhibition did not seem to correlate with sensitivity to BYL719 in the different NET cell lines. This implicates another mechanism of action different from PI3K/AKT/mTORC1 signaling responsible for the different cell line sensitivities.

Inhibition of GSK3 in BON-1 and H727 cells, but not in QGP-1 cells at 24 h treatment. The most evident difference between the three cell lines which might correlate with different cell line sensitivities was found in GSK3 signaling. GSK3 is usually phosphorylated and inhibited by the growth factor induced PI3K/AKT signaling pathway [46–48]. Hence,

partial PI3K/AKT inhibition would be expected to lead to dephosphorylation/activation of GSK3. However, unexpectedly, despite partial PI3K/AKT inhibition, BYL719 treatment led to phosphorylation/inhibition of GSK3 in BON-1 and H727 cells with a significant and strongest inhibition, especially of GSK3β in the most sensitive BON-1 cell line. Hence, our study suggests an impact of BYL719 on GSK3 not directly linked to PI3K/AKT signaling. In contrast to GSK3 inhibition in BON-1 and H727 cells, there was *no phosphorylation/inhibition, but a modest activation* of GSK3 in the more resistant QGP-1 cells after BYL719 treatment.

The role of GSK3β in cancer has been discussed and remains controversial [46, 68]. Since GSK3β induces phosphorylation and degradation of its downstream targets, and some GSK3β substrates are key proteins for promoting cell survival, such as β-Catenin, Cyclin D1, eIF2B and MYC [46, 68, 69], it was initially considered as a tumor suppressor. However, in contrast, a tumor-*promoting* role of GSK3β has been reported in leukemia, glioblastoma, non-small cell lung cancer, BON-1, insulinoma and H727 cells as well as medullary thyroid carcinoma cells [70–75]. Accordingly, GSK3β inhibition has already shown anti-tumor potential with anti-proliferative and pro-apoptotic effects in neuroblastoma, BON-1, H727 and medullary thyroid carcinoma cells being accompanied by reduced expression of β-catenin and neuroendocrine tumor markers [70, 71, 76, 77]. GSK3β inhibition also displayed anti-proliferative effects in other tumor entities, including leukemia, non-small cell lung cancer, melanoma, prostate, pancreatic, colon and renal cell carcinoma [73, 75, 78–83]. Several studies have found that inhibition of GSK3β led to apoptosis through inhibition of NFκB, mitotic catastrophe in apoptosis-resistant cells, and cycle arrest due to the increase of CDK inhibitors including p27 *in vitro* and *in vivo* [46, 71, 84–88]. This is consistent with our findings of *strongest* GSK3 inhibition being associated with *highest sensitivity* to BYL719 and strongest induction of apoptosis in BON-1, compared to H727 and QGP-1 cells, after BYL719 treatment. One potential explanation for this effect of BYL719 on GSK3 would be IGF1 receptor activation in all three cell lines to a different extent in response to BYL719 treatment. This theory, however, could not be supported by our data, as discussed in detail below. A more detailed analysis of signaling effects is warranted in novel primary cell lines and primary tumor cell cultures to understand differences in signaling pathway alterations in NETs.

Compensatory activation of IGF1R. Svejda *et al*. have already reported a growth factor mediated feedback loop in NET cells after mTORC1 inhibition [19], as we observed with BYL719 in this study: we found a strong activation of IGF1R in all cell lines, which was already seen at low doses of 1 μM BYL719 arguing for a specific effect of PI3Kα inhibition on IGF1R signaling. In case of inappropriate strong mTORC1 activation, a negative feed-back effect on IGFR signaling has previously been described [89]. Therefore, the observed activation of IGF1 receptor might be due to PI3K/mTORC1 inhibition and might be a potential compensatory mechanism of the tumor cells. IGF1R activation seems to play an essential role in cancer cell proliferation of different tumor cell entities including BON-1 cells [90–94].

On the other hand, IGF1R is known to phosphorylate/inhibit GSK3 [47]. Therefore, we have tested a potential dependence of GSK3 phosphorylation on IGF1R signaling in our NET cell lines through co-treatment of BYL719 with the specific IGF1R inhibitor NVP-AEW541. Surprisingly, in BON-1 and H727 cells co-treatment with the specific IGF1R inhibitor NVP-AEW541 even led to an enhanced (not reduced) GSK3 phosphorylation/inhibition, compared to each drug separately, being associated with strongest IGF1R activation after combination treatment in BON-1 and H727 cells; in QGP-1 cells, absent GSK3 phosphorylation/inhibition, compared to the control, was accompanied by IGF1R inhibition after combination treatment. NVP-AWE541 alone seemed to lead to a compensatory increase of total IGF1R expression, potentially to compensate for the IGF1R inhibition, and thereby rendering cells more sensitive to BYL719-induced IGF1R activation.

However, the low baseline phosphorylation/activity of the IGF1R in BON1 and H727 cells might not have been sufficient to show the effects of specific IGF1R inhibition by NVP-AEW541; moreover, another group stimulated their cells with IGF1 to demonstrate the dependence of GSK3 phosphorylation on IGF1R activity in medulloblastoma cells [49],. Therefore, we modified our experimental setting by using IGF1 stimulation. IGF1 stimulation led to strong basal IGF1R phosphorylation/activity in all three cell lines, which could then be clearly inhibited by NVP-AEW541 in all three cell lines. BYL719 alone led to strong IGF1R phosphorylation/activation. However, despite clear IGF1R inhibition after combination treatment with NVP-AEW541 plus BYL719 in all three cell lines, the phosphorylation/inhibition of GSK3 was even stronger (not blocked) after the combination treatment in H727 cells and not changed in BON-1 and QGP-1 cells compared to single BYL719 treatment. Therefore, according to these data, blockade of the IGF1R did not attenuate BYL719-induced GSK3 phosphorylation. Due to optimizing our experimental design by IGF1 stimulation according to a previously published experimental design [49], we have refuted our initial hypothesis of the dependence of BYL719-induced GSK3 phosphorylation on IGF1R activation in BON1 and H727 cells. The mechanism through which BYL719 leads to GSK3 inhibition, thus still needs to be assessed and will be the subject of further studies. Essentially, the IGF1R does not appear to mediate the effect of Byl719 on the phosphorylation of GSK3.

Induction of cell re-differentiation in BON-1 and H727 cells, but not in QGP-1 cells

BYL719 induced neuroendocrine differentiation in BON-1 and H727 cells as indicated by increased expression of CgA (*CHGA-)*, *SSTR1*- and *SSTR2*-mRNA; *SSTR2* mRNA expression was already significantly induced at a low dose of 1 μM BYL719 arguing for a specific effect of PI3Kα inhibition on *SSTR2*-mRNA induction; in contrast, in QGP-1 cells, *SSTR1* transcripts were reduced, and *CHGA* and *SSTR2* were unaffected.

Although *CHGA*-mRNA was found to be upregulated by BYL719, the compound did not modulate CgA release from any of the cell lines studied. It was important to verify this, as Li et al. have reported that the p110 catalytic subunit of PI3K negatively regulated neurotensin secretion in BON-1 cells and that inhibition of p110 induced neurotensin release from these cells [95]. Likewise, inhibition of the PI3K/PDK1/AKT pathway has been shown to upregulate insulin secretion from pancreatic beta cells [96]. Potentiation of hormone hypersecretion in NET patients would be considered an unwanted side effect that could limit the application of this therapeutic principle. However, none of the three cell lines tested showed an increase of CgA secretion under BYL719 treatment. In clinical practice, CgA is a marker for NETs in terms of progression and changes in response to therapy, but has low sensitivity for diagnosis, especially when the tumor burden is low. It tends to be higher in more differentiated tumors, but there is considerable variability and in general it is not universally useful in determining the degree of tumor differentiation [97].

In contrast, SSTR1/2 expression seems to be a more suitable marker for cell differentiation. In general, almost 100% of low (G1) and intermediate grade (G2) NETs show SSTR expression, but high grade NETs and neuroendocrine carcinomas (NECs) (G3) show lesser expression. Hence, in less differentiated tumors SSTR expression is less frequent and SSTR density is lower. Moreover, SSTR expression is less frequently seen in pancreatic than in gastrointestinal tumors, as reviewed in [98]. Furthermore, SSTR2 expression positively correlated with better prognosis In NET patients [99, 100]. Therefore, re-differentiation of tumor cells with an increase of SSTR2 expression, as we observed after BYL719 and after BYL719/everolimus

combination treatment (discussed below) *in vitro*, might lead to better differentiated tumors and improve the prognosis of NET patients if transferable to humans. Moreover, the increased SSTR1/2 expression upon BYL719 exposure could potentially be exploited for co-treatments with somatostatin analogs. It also seems an interesting option to increase SSTR2 mediated tracer uptake for imaging studies and peptide radioreceptor ligand therapy (PRRT). Interestingly, SSTR5 seems to be differentially regulated compared to SSTR1 and SSTR2.

GSK3 inhibition might promote neuronal and pancreatic NET cell differentiation, as described previously [101, 102]. Therefore, pronounced BYL719-induced inhibition of GSK3 in BON-1 and H727 cells may contribute to enhanced tumor cell differentiation; accordingly, there was no inhibition, but even a slight activation of GSK3 in QGP-1 cells after 24 h BYL719 treatment associated with decreased cell differentiation.

Potentially, the BYL719-induced cell differentiation in BON-1 and H727 cells reflects re-differentiation of tumor cells. A re-differentiation of thyroid carcinoma cells upon growth arrest has been described previously [103]. Indeed, it has recently been reported, that treatment of BON-1 cells with HDAC inhibitors can potently induce SSTR2 expression coinciding with a profound proliferative arrest of the tumor cells [104].

Synergistic effect of BYL719 plus everolimus in QGP-1 cells

Although there was just a slight effect of a low dose of 1 μM BYL719 alone on BON-1 and no relevant effect on QGP-1 cell viability, there was a synergistic effect of 1 μM BYL719 in combination with the mTORC1-inhibitor everolimus (1 nM) in both cell lines. This may be explained by additional everolimus-mediated mTORC1 inhibition rendering cells more sensitive to BYL719, as previously reported for breast cancer cells [38], and BYL719-mediated prevention of everolimus-induced AKT activation [16–18], as now shown in our cells. Moreover, in another study on BON-1 cells (submitted data) we have shown a much stronger phosphorylation/inhibition of GSK3 after 72 h BYL719/everolimus combination treatment (by 2507%), compared to each drug separately (by 195% and 298%, respectively). This again supports the concept of combining targeted therapies in NETs, as previously shown to be effective: Combined inhibition of mTORC1/2, PI3K/mTORC1/2, PI3K/mTORC1/2/ERK or EGFR/PI3K/mTORC1 has shown promising anti-tumor potential in NETs *in vitro* [18, 28, 42, 45, 105]. Of note implementing combination therapies could dramatically reduce the doses of single agent treatment, as we observed synergistic effects already at subtherapeutic doses in monotherapy. Moreover, since these synergistic effects already occurred at low doses of both drugs, the synergism might be a specific effect of simultaneous inhibition of the PI3Kα subunit by BYL719 and of mTORC1 by everolimus. Nevertheless, harmful side effects of combined treatments should be evaluated in animal studies.

Furthermore, we found that the synergism of 1 μM BYL719 plus 1 nM everolimus was associated with induction of cell re-differentiation and a significant increase of SSTR2 expression in QGP-1 and BON-1 cells, compared to each drug separately, potentially sensitizing cells to somatostatin analogs.

No synergistic or additive effect of the BYL719/everolimus combination was found in H727 cells. This is consistent with our finding of lower PI3K/AKT^{Ser473} inhibition and even activation of PI3K/AKT^{Thr308} associated with stronger mTORC1 inhibition by BYL719 alone in H727 cells.

Conclusions

The selective PI3Kα inhibitor BYL719 significantly reduced cell viability and colony formation in all NET cell lines investigated, with the highest sensitivity in BON-1, followed by H727 cells,

and a much lower sensitivity in QGP-1 cells. The highest sensitivity of BON-1, followed by H727 cells, might be due to stronger BYL719-induced apoptosis as a potential consequence of GSK3 inhibition and tumor cell re-differentiation with significant SSTR1/2 up-regulation, in contrast to lower apoptosis induction, absent GSK3 inhibition and absent re-differentiation in QGP-1 cells [71, 72, 85, 101, 106, 107]. Thus, BYL719 may sensitize neuroendocrine tumor cells to therapy with somatostatin analogs or PRRT, depending on the specific cell line. Moreover, BYL719/everolimus combination treatment showed synergistic effects in BON-1 and the more resistant QGP-1 cells and might help to overcome everolimus or BYL719 resistance through simultaneous AKT/mTORC1 inhibition. The BYL719/everolimus combination also enhanced cell differentiation with significant SSTR2 up-regulation in BON-1 and QGP-1 cells, compared to each drug separately.

In summary, our suggested hypothesis and our data indicate that BYL719 might be an interesting novel therapeutic option for NETs, especially in combination with the approved and promising somatostatin analogs or everolimus, which merits clinical therapeutic consideration. However, our data also confirm the importance of individualized targeted therapies depending on tumor entity.

Supporting information

S1 Fig. Uncropped western blots.
(TIF)

S2 Fig. Uncropped western blots.
(TIF)

S3 Fig. Uncropped western blots.
(TIF)

S4 Fig. Uncropped western blots.
(TIF)

S5 Fig. Uncropped western blots.
(TIF)

S6 Fig. Uncropped western blots.
(TIF)

S7 Fig. Uncropped western blots.
(TIF)

S8 Fig. Uncropped western blots.
(TIF)

S9 Fig. Uncropped western blots.
(TIF)

S10 Fig. Uncropped western blots.
(TIF)

S11 Fig. Uncropped western blots.
(TIF)

S12 Fig. Uncropped western blots.
(TIF)

S13 Fig. Uncropped western blots.
(TIF)

S14 Fig. Uncropped western blots.
(TIF)

S15 Fig. Uncropped western blots.
(TIF)

S16 Fig. Uncropped western blots.
(TIF)

S17 Fig. Uncropped western blots.
(TIF)

S18 Fig. Uncropped western blots.
(TIF)

S19 Fig. Uncropped western blots.
(TIF)

S20 Fig. Uncropped western blots.
(TIF)

S21 Fig. Uncropped western blots.
(TIF)

S22 Fig. Uncropped western blots.
(TIF)

S23 Fig. Uncropped western blots.
(TIF)

S24 Fig. Western blot 1 μM and higher concentrations of BYL719 pGSK3 and pIGF1R.
(TIF)

S25 Fig. Western blot 2.5 μM and higher concentrations of BYL719 pGSK3 and pIGF1R.
(TIF)

S26 Fig. Western blot NVP-AEW541 plus BYL719 without IGF1 stimulation.
(TIF)

S27 Fig. Western blot NVP-AEW541 plus BYL719 with IGF1 stimulation.
(TIFF)

S28 Fig. Comparison of the effects of BYL719 versus BKM120 on BON-1 cell viability.
(TIF)

S29 Fig. Uncropped western blots.
(TIF)

S30 Fig. Uncropped western blots.
(TIF)

S1 Table. Densitometry analysis of the performed western blots. Band intensities were quantified from at least 3 independent experiments for each cell line and protein, and are expressed as the mean percentage relative to the untreated control (100%). The means and standard deviations are reported as geometric means and geometric standard deviations of the

relative increase, respectively. A geometric mean of "1.0" has to be interpreted as "equal to the control group" and for the geometric standard deviation "1.0" refers to "no variation". Statistically significantly different results in comparison to the control are shown as p-values, considering $p<0.05$ as significant.
(XLSX)

Acknowledgments

This work has been supported by a grant from NOVARTIS (YING Investigator program) to JS and PG from the Roggenbruck Foundation (Hamburg, Germany) to JS. We thank Julian Maurer and Gerald Spöttl, Klinikum der Universität München (KUM), and Martina Fahl, Universitätsklinikum Hamburg-Eppendorf (UKE), for technical support.

The following authors are members of the GERMAN NET-Z study group: Svenja Nölting[1,2], Katharina Detjen[3], Christoph J Auernhammer[1,2], Christian Fischer[3], Carsten Grötzinger[3], Patricia Grabowski[3,4] and Jörg Schrader[5,6]. The lead authors of the GERMAN NET-Z study group are Patricia Grabowski[3,4] and Jörg Schrader[5,6].

Affiliations of the authors belonging to the GERMAN NET-Z study group:

[1]Department of Internal Medicine II, Klinikum der Universität München (KUM), Ludwig-Maximilians-Universität München, Bavaria, Germany;

[2]Department of Internal Medicine IV, Klinikum der Universität München (KUM), Ludwig-Maximilians-Universität München, Bavaria, Germany;

[3]Dept. of Gastroenterology, CC13 (CBF and CVK), Charité - Universitätsmedizin Berlin, Germany;

[4]Dept. of Gastroenterology and Endocrinology, Zentralklinik Bad Berka GmbH, Germany;

[5]Department of General, Visceral and Thoracic Surgery, University Medical Center Hamburg-Eppendorf, Hamburg, Germany;

[6]Medical Department I, University Medical Center Hamburg-Eppendorf, Hamburg, Germany;

Author Contributions

Conceptualization: Svenja Nölting, Jörg Schrader.

Data curation: Svenja Nölting, Jakob Rentsch, Helma Freitag.

Formal analysis: Michael Lauseker.

Funding acquisition: Jörg Schrader, Patricia Grabowski.

Investigation: Svenja Nölting, Jakob Rentsch, Helma Freitag, Katharina Detjen, Franziska Briest, Markus Möbs, Victoria Weissmann, Britta Siegmund, Christoph J. Auernhammer, Elke Tatjana Aristizabal Prada, Samantha Exner, Christian Fischer, Carsten Grötzinger, Jörg Schrader, Patricia Grabowski.

Project administration: Svenja Nölting, Patricia Grabowski.

Writing – original draft: Svenja Nölting, Carsten Grötzinger, Jörg Schrader.

Writing – review & editing: Svenja Nölting, Ashley Grossman, Jörg Schrader, Patricia Grabowski.

References

1. Papaxoinis G, Syrigos K, Saif MW. Novel therapeutic approaches and mechanisms in neuroendocrine tumors: the role of targeted agents. Discov Med. 2016; 21(117):391–402. PMID: 27355335.

2. Raymond E, Dahan L, Raoul JL, Bang YJ, Borbath I, Lombard-Bohas C, et al. Sunitinib malate for the treatment of pancreatic neuroendocrine tumors. N Engl J Med. 2011; 364(6):501–13. https://doi.org/10.1056/NEJMoa1003825 PMID: 21306237.
3. Yao JC, Fazio N, Singh S, Buzzoni R, Carnaghi C, Wolin E, et al. Everolimus for the treatment of advanced, non-functional neuroendocrine tumours of the lung or gastrointestinal tract (RADIANT-4): a randomised, placebo-controlled, phase 3 study. Lancet. 2016; 387(10022):968–77. https://doi.org/10.1016/S0140-6736(15)00817-X PMID: 26703889.
4. Pavel ME, Hainsworth JD, Baudin E, Peeters M, Horsch D, Winkler RE, et al. Everolimus plus octreotide long-acting repeatable for the treatment of advanced neuroendocrine tumours associated with carcinoid syndrome (RADIANT-2): a randomised, placebo-controlled, phase 3 study. Lancet. 2011; 378(9808):2005–12. https://doi.org/10.1016/S0140-6736(11)61742-X PMID: 22119496.
5. Yao JC, Shah MH, Ito T, Bohas CL, Wolin EM, Van Cutsem E, et al. Everolimus for advanced pancreatic neuroendocrine tumors. N Engl J Med. 2011; 364(6):514–23. https://doi.org/10.1056/NEJMoa1009290 PMID: 21306238.
6. Wolin EM. PI3K/Akt/mTOR pathway inhibitors in the therapy of pancreatic neuroendocrine tumors. Cancer Lett. 2013; 335(1):1–8. https://doi.org/10.1016/j.canlet.2013.02.016 PMID: 23419523.
7. Jiao Y, Shi C, Edil BH, de Wilde RF, Klimstra DS, Maitra A, et al. DAXX/ATRX, MEN1, and mTOR pathway genes are frequently altered in pancreatic neuroendocrine tumors. Science (New York, NY). 2011; 331(6021):1199–203. Epub 2011/01/22. https://doi.org/10.1126/science.1200609 PMID: 21252315.
8. Banck MS, Kanwar R, Kulkarni AA, Boora GK, Metge F, Kipp BR, et al. The genomic landscape of small intestine neuroendocrine tumors. J Clin Invest. 2013; 123(6):2502–8. https://doi.org/10.1172/JCI67963 PMID: 23676460.
9. Pitt SC, Davis R, Kunnimalaiyaan M, Chen H. AKT and PTEN expression in human gastrointestinal carcinoid tumors. Am J Transl Res. 2009; 1(3):291–9. PMID: 19956439.
10. Missiaglia E, Dalai I, Barbi S, Beghelli S, Falconi M, della Peruta M, et al. Pancreatic endocrine tumors: expression profiling evidences a role for AKT-mTOR pathway. J Clin Oncol. 2010; 28(2):245–55. https://doi.org/10.1200/JCO.2008.21.5988 PMID: 19917848.
11. Tan HL, Sood A, Rahimi HA, Wang W, Gupta N, Hicks J, et al. Rb loss is characteristic of prostatic small cell neuroendocrine carcinoma. Clin Cancer Res. 2014; 20(4):890–903. https://doi.org/10.1158/1078-0432.CCR-13-1982 PMID: 24323898.
12. Kasajima A, Pavel M, Darb-Esfahani S, Noske A, Stenzinger A, Sasano H, et al. mTOR expression and activity patterns in gastroenteropancreatic neuroendocrine tumours. Endocr Relat Cancer. 2011; 18(1):181–92. https://doi.org/10.1677/ERC-10-0126 PMID: 21159731.
13. Qian ZR, Ter-Minassian M, Chan JA, Imamura Y, Hooshmand SM, Kuchiba A, et al. Prognostic significance of MTOR pathway component expression in neuroendocrine tumors. J Clin Oncol. 2013; 31(27):3418–25. https://doi.org/10.1200/JCO.2012.46.6946 PMID: 23980085.
14. Geis C, Fendrich V, Rexin P, Di Fazio P, Bartsch DK, Ocker M, et al. Ileal neuroendocrine tumors show elevated activation of mammalian target of rapamycin complex. J Surg Res. 2015; 194(2):388–93. https://doi.org/10.1016/j.jss.2014.10.052 PMID: 25439321.
15. Carracedo A, Ma L, Teruya-Feldstein J, Rojo F, Salmena L, Alimonti A, et al. Inhibition of mTORC1 leads to MAPK pathway activation through a PI3K-dependent feedback loop in human cancer. Journal of Clinical Investigation. 2008; 118(9):3065–74. https://doi.org/10.1172/JCI34739 PMID: 18725988
16. O'Reilly KE, Rojo F, She QB, Solit D, Mills GB, Smith D, et al. mTOR inhibition induces upstream receptor tyrosine kinase signaling and activates Akt. Cancer Research. 2006; 66(3):1500–8. https://doi.org/10.1158/0008-5472.CAN-05-2925 PMID: 16452206
17. Zitzmann K, Ruden J, Brand S, Goke B, Lichtl J, Spottl G, et al. Compensatory activation of Akt in response to mTOR and Raf inhibitors—a rationale for dual-targeted therapy approaches in neuroendocrine tumor disease. Cancer Letters. 2010; 295(1):100–9. https://doi.org/10.1016/j.canlet.2010.02.018 PMID: 20356670
18. Passacantilli I, Capurso G, Archibugi L, Calabretta S, Caldarola S, Loreni F, et al. Combined therapy with RAD001 e BEZ235 overcomes resistance of PET immortalized cell lines to mTOR inhibition. Oncotarget. 2014; 5(14):5381–91. https://doi.org/10.18632/oncotarget.2111 PMID: 25026292.
19. Svejda B, Kidd M, Kazberouk A, Lawrence B, Pfragner R, Modlin IM. Limitations in small intestinal neuroendocrine tumor therapy by mTor kinase inhibition reflect growth factor-mediated PI3K feedback loop activation via ERK1/2 and AKT. Cancer. 2011; 117(18):4141–54. https://doi.org/10.1002/cncr.26011 PMID: 21387274.
20. Capozzi M, Caterina I, De Divitiis C, von Arx C, Maiolino P, Tatangelo F, et al. Everolimus and pancreatic neuroendocrine tumors (PNETs): Activity, resistance and how to overcome it. Int J Surg. 2015; 21 Suppl 1:S89–94. https://doi.org/10.1016/j.ijsu.2015.06.064 PMID: 26123382.

21. Tijeras-Raballand A, Neuzillet C, Couvelard A, Serova M, de Gramont A, Hammel P, et al. Resistance to targeted therapies in pancreatic neuroendocrine tumors (PNETs): molecular basis, preclinical data, and counteracting strategies. Target Oncol. 2012; 7(3):173–81. https://doi.org/10.1007/s11523-012-0229-6 PMID: 22923165.

22. Iida S, Miki Y, Ono K, Akahira J, Nakamura Y, Suzuki T, et al. Synergistic anti-tumor effects of RAD001 with MEK inhibitors in neuroendocrine tumors: a potential mechanism of therapeutic limitation of mTOR inhibitor. Molecular and Cellular Endocrinology. 2012; 350(1):99–106. https://doi.org/10.1016/j.mce.2011.11.024 PMID: 22178087

23. Francois RA, Maeng K, Nawab A, Kaye FJ, Hochwald SN, Zajac-Kaye M. Targeting Focal Adhesion Kinase and Resistance to mTOR Inhibition in Pancreatic Neuroendocrine Tumors. J Natl Cancer Inst. 2015; 107(8). https://doi.org/10.1093/jnci/djv123 PMID: 25971297.

24. Fazio N. Neuroendocrine tumors resistant to mammalian target of rapamycin inhibitors: A difficult conversion from biology to the clinic. World J Clin Oncol. 2015; 6(6):194–7. https://doi.org/10.5306/wjco.v6.i6.194 PMID: 26677429.

25. Bago-Horvath Z, Sieghart W, Grusch M, Lackner A, Hayden H, Pirker C, et al. Synergistic effects of erlotinib and everolimus on bronchial carcinoids and large-cell neuroendocrine carcinomas with activated EGFR/AKT/mTOR pathway. Neuroendocrinology. 2012; 96(3):228–37. https://doi.org/10.1159/000337257 PMID: 22378048.

26. Capurso G, Fendrich V, Rinzivillo M, Panzuto F, Bartsch DK, Delle Fave G. Novel molecular targets for the treatment of gastroenteropancreatic endocrine tumors: answers and unsolved problems. Int J Mol Sci. 2012; 14(1):30–45. https://doi.org/10.3390/ijms14010030 PMID: 23344019.

27. Gagliano T, Bellio M, Gentilin E, Mole D, Tagliati F, Schiavon M, et al. mTOR, p70S6K, AKT, and ERK1/2 levels predict sensitivity to mTOR and PI3K/mTOR inhibitors in human bronchial carcinoids. Endocr Relat Cancer. 2013; 20(4):463–75. https://doi.org/10.1530/ERC-13-0042 PMID: 23653462.

28. Nolting S, Garcia E, Alusi G, Giubellino A, Pacak K, Korbonits M, et al. Combined blockade of signalling pathways shows marked anti-tumour potential in phaeochromocytoma cell lines. Journal of Molecular Endocrinology. 2012; 49(2):79–96. https://doi.org/10.1530/JME-12-0028 PMID: 22715163

29. Valentino JD, Li J, Zaytseva YY, Mustain WC, Elliott VA, Kim JT, et al. Cotargeting the PI3K and RAS pathways for the treatment of neuroendocrine tumors. Clin Cancer Res. 2014; 20(5):1212–22. https://doi.org/10.1158/1078-0432.CCR-13-1897 PMID: 24443523.

30. Djukom C, Porro LJ, Mrazek A, Townsend CM Jr., Hellmich MR, Chao C. Dual inhibition of PI3K and mTOR signaling pathways decreases human pancreatic neuroendocrine tumor metastatic progression. Pancreas. 2014; 43(1):88–92. https://doi.org/10.1097/MPA.0b013e3182a44ab4 PMID: 24263107.

31. Couderc C, Poncet G, Villaume K, Blanc M, Gadot N, Walter T, et al. Targeting the PI3K/mTOR pathway in murine endocrine cell lines: in vitro and in vivo effects on tumor cell growth. Am J Pathol. 2011; 178(1):336–44. https://doi.org/10.1016/j.ajpath.2010.11.023 PMID: 21224070.

32. Schrader J, Niebel P, Rossi A, Archontidou-Aprin E, Horsch D. Differential signaling by regulatory subunits of phosphoinositide-3-kinase influences cell survival in INS-1E insulinoma cells. Exp Clin Endocrinol Diabetes. 2015; 123(2):118–25. https://doi.org/10.1055/s-0034-1390461 PMID: 25393342.

33. Sopasakis VR, Liu P, Suzuki R, Kondo T, Winnay J, Tran TT, et al. Specific roles of the p110alpha isoform of phosphatidylinsositol 3-kinase in hepatic insulin signaling and metabolic regulation. Cell Metab. 2010; 11(3):220–30. https://doi.org/10.1016/j.cmet.2010.02.002 PMID: 20197055.

34. Knight ZA, Gonzalez B, Feldman ME, Zunder ER, Goldenberg DD, Williams O, et al. A pharmacological map of the PI3-K family defines a role for p110alpha in insulin signaling. Cell. 2006; 125(4):733–47. https://doi.org/10.1016/j.cell.2006.03.035 PMID: 16647110.

35. Graupera M, Guillermet-Guibert J, Foukas LC, Phng LK, Cain RJ, Salpekar A, et al. Angiogenesis selectively requires the p110alpha isoform of PI3K to control endothelial cell migration. Nature. 2008; 453(7195):662–6. https://doi.org/10.1038/nature06892 PMID: 18449193.

36. Fritsch C, Huang A, Chatenay-Rivauday C, Schnell C, Reddy A, Liu M, et al. Characterization of the novel and specific PI3Kalpha inhibitor NVP-BYL719 and development of the patient stratification strategy for clinical trials. Mol Cancer Ther. 2014; 13(5):1117–29. https://doi.org/10.1158/1535-7163.MCT-13-0865 PMID: 24608574.

37. Furet P, Guagnano V, Fairhurst RA, Imbach-Weese P, Bruce I, Knapp M, et al. Discovery of NVP-BYL719 a potent and selective phosphatidylinositol-3 kinase alpha inhibitor selected for clinical evaluation. Bioorg Med Chem Lett. 2013; 23(13):3741–8. https://doi.org/10.1016/j.bmcl.2013.05.007 PMID: 23726034.

38. Elkabets M, Vora S, Juric D, Morse N, Mino-Kenudson M, Muranen T, et al. mTORC1 inhibition is required for sensitivity to PI3K p110alpha inhibitors in PIK3CA-mutant breast cancer. Sci Transl Med. 2013; 5(196):196ra99. https://doi.org/10.1126/scitranslmed.3005747 PMID: 23903756.

39. Evers BM, Townsend CM Jr., Upp JR, Allen E, Hurlbut SC, Kim SW, et al. Establishment and characterization of a human carcinoid in nude mice and effect of various agents on tumor growth. Gastroenterology. 1991; 101(2):303–11. PMID: 1712329.

40. Kaku M, Nishiyama T, Yagawa K, Abe M. Establishment of a carcinoembryonic antigen-producing cell line from human pancreatic carcinoma. Gan. 1980; 71(5):596–601. PMID: 7227711.

41. Cakir M, Grossman A. The molecular pathogenesis and management of bronchial carcinoids. Expert Opin Ther Targets. 2011; 15(4):457–91. https://doi.org/10.1517/14728222.2011.555403 PMID: 21275849.

42. Freitag H, Christen F, Lewens F, Grass I, Briest F, Iwaszkiewicz S, et al. Inhibition of mTORs Catalytic Site by PKI-587 is a Promising Therapeutic Option for Gastroenteropancreatic Neuroendocrine Tumor Disease. Neuroendocrinology. 2016. https://doi.org/10.1159/000448843 PMID: 27513674.

43. Reuther C, Heinzle V, Nolting S, Herterich S, Hahner S, Halilovic E, et al. The HDM2 (MDM2) Inhibitor NVP-CGM097 Inhibits Tumor cell Proliferation and Shows Additive Effects with 5-Fluorouracil on the p53—p21—Rb—E2F1 Cascade in the p53wildtype Neuroendocrine Tumor Cell Line GOT1. Neuroendocrinology. 2016. https://doi.org/10.1159/000453369 PMID: 27871087.

44. Plath T, Detjen K, Welzel M, von Marschall Z, Murphy D, Schirner M, et al. A novel function for the tumor suppressor p16(INK4a): induction of anoikis via upregulation of the alpha(5)beta(1) fibronectin receptor. J Cell Biol. 2000; 150(6):1467–78. PMID: 10995450.

45. Nolting S, Maurer J, Spottl G, Aristizabal Prada ET, Reuther C, Young K, et al. Additive Anti-Tumor Effects of Lovastatin and Everolimus In Vitro through Simultaneous Inhibition of Signaling Pathways. PLoS One. 2015; 10(12):e0143830. https://doi.org/10.1371/journal.pone.0143830 PMID: 26636335.

46. Maurer U, Preiss F, Brauns-Schubert P, Schlicher L, Charvet C. GSK-3—at the crossroads of cell death and survival. J Cell Sci. 2014; 127(Pt 7):1369–78. https://doi.org/10.1242/jcs.138057 PMID: 24687186.

47. Cross DA, Alessi DR, Vandenheede JR, McDowell HE, Hundal HS, Cohen P. The inhibition of glycogen synthase kinase-3 by insulin or insulin-like growth factor 1 in the rat skeletal muscle cell line L6 is blocked by wortmannin, but not by rapamycin: evidence that wortmannin blocks activation of the mitogen-activated protein kinase pathway in L6 cells between Ras and Raf. Biochem J. 1994; 303 (Pt 1):21–6. PMID: 7945242.

48. Cross DA, Alessi DR, Cohen P, Andjelkovich M, Hemmings BA. Inhibition of glycogen synthase kinase-3 by insulin mediated by protein kinase B. Nature. 1995; 378(6559):785–9. https://doi.org/10.1038/378785a0 PMID: 8524413.

49. Urbanska K, Trojanek J, Del Valle L, Eldeen MB, Hofmann F, Garcia-Echeverria C, et al. Inhibition of IGF-I receptor in anchorage-independence attenuates GSK-3beta constitutive phosphorylation and compromises growth and survival of medulloblastoma cell lines. Oncogene. 2007; 26(16):2308–17. https://doi.org/10.1038/sj.onc.1210018 PMID: 17016438.

50. Franken NA, Rodermond HM, Stap J, Haveman J, van Bree C. Clonogenic assay of cells in vitro. Nat Protoc. 2006; 1(5):2315–9. https://doi.org/10.1038/nprot.2006.339 PMID: 17406473.

51. Hanahan D, Weinberg RA. Hallmarks of cancer: the next generation. Cell. 2011; 144(5):646–74. https://doi.org/10.1016/j.cell.2011.02.013 PMID: 21376230.

52. Ungefroren H, Sebens S, Seidl D, Lehnert H, Hass R. Interaction of tumor cells with the microenvironment. Cell Commun Signal. 2011; 9:18. https://doi.org/10.1186/1478-811X-9-18 PMID: 21914164.

53. Zhou C, Ji J, Cai Q, Shi M, Chen X, Yu Y, et al. MTA2 enhances colony formation and tumor growth of gastric cancer cells through IL-11. BMC Cancer. 2015; 15:343. https://doi.org/10.1186/s12885-015-1366-y PMID: 25929737.

54. Grabowski P, Schrader J, Wagner J, Horsch D, Arnold R, Arnold CN, et al. Loss of nuclear p27 expression and its prognostic role in relation to cyclin E and p53 mutation in gastroenteropancreatic neuroendocrine tumors. Clin Cancer Res. 2008; 14(22):7378–84. https://doi.org/10.1158/1078-0432.CCR-08-0698 PMID: 19010853.

55. Bryant C, Rawlinson R, Massey AJ. Chk1 inhibition as a novel therapeutic strategy for treating triple-negative breast and ovarian cancers. BMC Cancer. 2014; 14:570. https://doi.org/10.1186/1471-2407-14-570 PMID: 25104095.

56. Massey AJ, Stokes S, Browne H, Foloppe N, Fiumana A, Scrace S, et al. Identification of novel, in vivo active Chk1 inhibitors utilizing structure guided drug design. Oncotarget. 2015; 6(34):35797–812. https://doi.org/10.18632/oncotarget.5929 PMID: 26437226.

57. Konukiewitz B, Schlitter AM, Jesinghaus M, Pfister D, Steiger K, Segler A, et al. Somatostatin receptor expression related to TP53 and RB1 alterations in pancreatic and extrapancreatic neuroendocrine neoplasms with a Ki67-index above 20. Mod Pathol. 2017. https://doi.org/10.1038/modpathol.2016.217 PMID: 28059098.

58. Xu Y, Li N, Xiang R, Sun P. Emerging roles of the p38 MAPK and PI3K/AKT/mTOR pathways in oncogene-induced senescence. Trends Biochem Sci. 2014; 39(6):268–76. https://doi.org/10.1016/j.tibs.2014.04.004 PMID: 24818748.

59. Hollander MC, Blumenthal GM, Dennis PA. PTEN loss in the continuum of common cancers, rare syndromes and mouse models. Nat Rev Cancer. 2011; 11(4):289–301. https://doi.org/10.1038/nrc3037 PMID: 21430697.

60. Abbas T, Dutta A. p21 in cancer: intricate networks and multiple activities. Nat Rev Cancer. 2009; 9 (6):400–14. https://doi.org/10.1038/nrc2657 PMID: 19440234.

61. Almond JB, Cohen GM. The proteasome: a novel target for cancer chemotherapy. Leukemia. 2002; 16(4):433–43. https://doi.org/10.1038/sj.leu.2402417 PMID: 11960320.

62. Rodriguez R, Meuth M. Chk1 and p21 cooperate to prevent apoptosis during DNA replication fork stress. Mol Biol Cell. 2006; 17(1):402–12. https://doi.org/10.1091/mbc.E05-07-0594 PMID: 16280359.

63. Janicke RU, Sohn D, Essmann F, Schulze-Osthoff K. The multiple battles fought by anti-apoptotic p21. Cell Cycle. 2007; 6(4):407–13. https://doi.org/10.4161/cc.6.4.3855 PMID: 17312393.

64. Briest F, Grabowski P. PI3K-AKT-mTOR-signaling and beyond: the complex network in gastroenteropancreatic neuroendocrine neoplasms. Theranostics. 2014; 4(4):336–65. https://doi.org/10.7150/thno.7851 PMID: 24578720.

65. Soler A, Figueiredo AM, Castel P, Martin L, Monelli E, Angulo-Urarte A, et al. Therapeutic Benefit of Selective Inhibition of p110alpha PI3-Kinase in Pancreatic Neuroendocrine Tumors. Clin Cancer Res. 2016; 22(23):5805–17. https://doi.org/10.1158/1078-0432.CCR-15-3051 PMID: 27225693.

66. Brown JR. The PI3K pathway: clinical inhibition in chronic lymphocytic leukemia. Semin Oncol. 2016; 43(2):260–4. https://doi.org/10.1053/j.seminoncol.2016.02.004 PMID: 27040704.

67. Bu Q, You F, Pan G, Yuan Q, Cui T, Hao L, et al. MiR-125b inhibits anaplastic thyroid cancer cell migration and invasion by targeting PIK3CD. Biomed Pharmacother. 2017; 88:443–8. https://doi.org/10.1016/j.biopha.2016.11.090 PMID: 28122310.

68. Takahashi-Yanaga F. Activator or inhibitor? GSK-3 as a new drug target. Biochem Pharmacol. 2013; 86(2):191–9. https://doi.org/10.1016/j.bcp.2013.04.022 PMID: 23643839.

69. Takahashi-Yanaga F, Sasaguri T. GSK-3beta regulates cyclin D1 expression: a new target for chemotherapy. Cell Signal. 2008; 20(4):581–9. https://doi.org/10.1016/j.cellsig.2007.10.018 PMID: 18023328.

70. Greenblatt DY, Ndiaye M, Chen H, Kunnimalaiyaan M. Lithium inhibits carcinoid cell growth in vitro. Am J Transl Res. 2010; 2(3):248–53. PMID: 20589165.

71. Kunnimalaiyaan M, Vaccaro AM, Ndiaye MA, Chen H. Inactivation of glycogen synthase kinase-3beta, a downstream target of the raf-1 pathway, is associated with growth suppression in medullary thyroid cancer cells. Mol Cancer Ther. 2007; 6(3):1151–8. https://doi.org/10.1158/1535-7163.MCT-06-0665 PMID: 17363508.

72. Desai SS, Modali SD, Parekh VI, Kebebew E, Agarwal SK. GSK-3beta protein phosphorylates and stabilizes HLXB9 protein in insulinoma cells to form a targetable mechanism of controlling insulinoma cell proliferation. J Biol Chem. 2014; 289(9):5386–98. https://doi.org/10.1074/jbc.M113.533612 PMID: 24425879.

73. Zeng J, Liu D, Qiu Z, Huang Y, Chen B, Wang L, et al. GSK3beta overexpression indicates poor prognosis and its inhibition reduces cell proliferation and survival of non-small cell lung cancer cells. PLoS One. 2014; 9(3):e91231. https://doi.org/10.1371/journal.pone.0091231 PMID: 24618715.

74. Atkins RJ, Stylli SS, Luwor RB, Kaye AH, Hovens CM. Glycogen synthase kinase-3beta (GSK-3beta) and its dysregulation in glioblastoma multiforme. J Clin Neurosci. 2013; 20(9):1185–92. https://doi.org/10.1016/j.jocn.2013.02.003 PMID: 23768967.

75. Wang Z, Smith KS, Murphy M, Piloto O, Somervaille TC, Cleary ML. Glycogen synthase kinase 3 in MLL leukaemia maintenance and targeted therapy. Nature. 2008; 455(7217):1205–9. https://doi.org/10.1038/nature07284 PMID: 18806775.

76. Carter YM, Kunnimalaiyaan S, Chen H, Gamblin TC, Kunnimalaiyaan M. Specific glycogen synthase kinase-3 inhibition reduces neuroendocrine markers and suppresses neuroblastoma cell growth. Cancer Biol Ther. 2014; 15(5):510–5. https://doi.org/10.4161/cbt.28015 PMID: 24521712.

77. Dent P. New methods to control neuroblastoma growth. Cancer Biol Ther. 2014; 15(5):481–2. https://doi.org/10.4161/cbt.28465 PMID: 24618834.

78. Bilim V, Ougolkov A, Yuuki K, Naito S, Kawazoe H, Muto A, et al. Glycogen synthase kinase-3: a new therapeutic target in renal cell carcinoma. Br J Cancer. 2009; 101(12):2005–14. https://doi.org/10.1038/sj.bjc.6605437 PMID: 19920820.

79. Madhunapantula SV, Sharma A, Gowda R, Robertson GP. Identification of glycogen synthase kinase 3alpha as a therapeutic target in melanoma. Pigment Cell Melanoma Res. 2013; 26(6):886–99. https://doi.org/10.1111/pcmr.12156 PMID: 24034838.

80. Marchand B, Tremblay I, Cagnol S, Boucher MJ. Inhibition of glycogen synthase kinase-3 activity triggers an apoptotic response in pancreatic cancer cells through JNK-dependent mechanisms. Carcinogenesis. 2012; 33(3):529–37. https://doi.org/10.1093/carcin/bgr309 PMID: 22201186.

81. Zhou W, Wang L, Gou SM, Wang TL, Zhang M, Liu T, et al. ShRNA silencing glycogen synthase kinase-3 beta inhibits tumor growth and angiogenesis in pancreatic cancer. Cancer Lett. 2012; 316 (2):178–86. https://doi.org/10.1016/j.canlet.2011.10.033 PMID: 22100174.

82. Zhu Q, Yang J, Han S, Liu J, Holzbeierlein J, Thrasher JB, et al. Suppression of glycogen synthase kinase 3 activity reduces tumor growth of prostate cancer in vivo. Prostate. 2011; 71(8):835–45. https://doi.org/10.1002/pros.21300 PMID: 21456066.

83. Shakoori A, Mai W, Miyashita K, Yasumoto K, Takahashi Y, Ooi A, et al. Inhibition of GSK-3 beta activity attenuates proliferation of human colon cancer cells in rodents. Cancer Sci. 2007; 98(9):1388–93. https://doi.org/10.1111/j.1349-7006.2007.00545.x PMID: 17640304.

84. Mirlashari MR, Randen I, Kjeldsen-Kragh J. Glycogen synthase kinase-3 (GSK-3) inhibition induces apoptosis in leukemic cells through mitochondria-dependent pathway. Leuk Res. 2012; 36(4):499–508. https://doi.org/10.1016/j.leukres.2011.11.013 PMID: 22177455.

85. Hsieh HY, Shen CH, Lin RI, Feng YM, Huang SY, Wang YH, et al. Cyproheptadine exhibits antitumor activity in urothelial carcinoma cells by targeting GSK3beta to suppress mTOR and beta-catenin signaling pathways. Cancer Lett. 2016; 370(1):56–65. https://doi.org/10.1016/j.canlet.2015.09.018 PMID: 26454215.

86. Dickey A, Schleicher S, Leahy K, Hu R, Hallahan D, Thotala DK. GSK-3beta inhibition promotes cell death, apoptosis, and in vivo tumor growth delay in neuroblastoma Neuro-2A cell line. J Neurooncol. 2011; 104(1):145–53. https://doi.org/10.1007/s11060-010-0491-3 PMID: 21161565.

87. Yoshino Y, Ishioka C. Inhibition of glycogen synthase kinase-3 beta induces apoptosis and mitotic catastrophe by disrupting centrosome regulation in cancer cells. Sci Rep. 2015; 5:13249. https://doi.org/10.1038/srep13249 PMID: 26292722.

88. Hoeflich KP, Luo J, Rubie EA, Tsao MS, Jin O, Woodgett JR. Requirement for glycogen synthase kinase-3beta in cell survival and NF-kappaB activation. Nature. 2000; 406(6791):86–90. https://doi.org/10.1038/35017574 PMID: 10894547.

89. Shah OJ, Wang Z, Hunter T. Inappropriate activation of the TSC/Rheb/mTOR/S6K cassette induces IRS1/2 depletion, insulin resistance, and cell survival deficiencies. Curr Biol. 2004; 14(18):1650–6. https://doi.org/10.1016/j.cub.2004.08.026 PMID: 15380067.

90. De Santi M, Annibalini G, Barbieri E, Villarini A, Vallorani L, Contarelli S, et al. Human IGF1 pro-forms induce breast cancer cell proliferation via the IGF1 receptor. Cell Oncol (Dordr). 2016; 39(2):149–59. https://doi.org/10.1007/s13402-015-0263-3 PMID: 26701791.

91. Ma Y, Han CC, Huang Q, Sun WY, Wei W. GRK2 overexpression inhibits IGF1-induced proliferation and migration of human hepatocellular carcinoma cells by downregulating EGR1. Oncol Rep. 2016; 35(5):3068–74. https://doi.org/10.3892/or.2016.4641 PMID: 26936374.

92. Nurwidya F, Andarini S, Takahashi F, Syahruddin E, Takahashi K. Implications of Insulin-like Growth Factor 1 Receptor Activation in Lung Cancer. Malays J Med Sci. 2016; 23(3):9–21. PMID: 27418865.

93. Svalina MN, Kikuchi K, Abraham J, Lal S, Davare MA, Settelmeyer TP, et al. IGF1R as a Key Target in High Risk, Metastatic Medulloblastoma. Sci Rep. 2016; 6:27012. https://doi.org/10.1038/srep27012 PMID: 27255663.

94. von Wichert G, Jehle PM, Hoeflich A, Koschnick S, Dralle H, Wolf E, et al. Insulin-like growth factor-I is an autocrine regulator of chromogranin A secretion and growth in human neuroendocrine tumor cells. Cancer Research. 2000; 60(16):4573–81. PMID: 10969809

95. Li J, Song J, Cassidy MG, Rychahou P, Starr ME, Liu J, et al. PI3K p110alpha/Akt signaling negatively regulates secretion of the intestinal peptide neurotensin through interference of granule transport. Mol Endocrinol. 2012; 26(8):1380–93. https://doi.org/10.1210/me.2012-1024 PMID: 22700584.

96. Aoyagi K, Ohara-Imaizumi M, Nishiwaki C, Nakamichi Y, Ueki K, Kadowaki T, et al. Acute inhibition of PI3K-PDK1-Akt pathway potentiates insulin secretion through upregulation of newcomer granule fusions in pancreatic beta-cells. PLoS One. 2012; 7(10):e47381. https://doi.org/10.1371/journal.pone.0047381 PMID: 23077605.

97. Korse CM, Taal BG, Vincent A, van Velthuysen ML, Baas P, Buning-Kager JC, et al. Choice of tumour markers in patients with neuroendocrine tumours is dependent on the histological grade. A marker study of Chromogranin A, Neuron specific enolase, Progastrin-releasing peptide and cytokeratin fragments. Eur J Cancer. 2012; 48(5):662–71. https://doi.org/10.1016/j.ejca.2011.08.012 PMID: 21945100.

98. Cakir M, Dworakowska D, Grossman A. Somatostatin receptor biology in neuroendocrine and pituitary tumours: part 2—clinical implications. J Cell Mol Med. 2010; 14(11):2585–91. https://doi.org/10.1111/j.1582-4934.2010.01125_1.x PMID: 20629988.

99. Brunner P, Jorg AC, Glatz K, Bubendorf L, Radojewski P, Umlauft M, et al. The prognostic and predictive value of sstr2-immunohistochemistry and sstr2-targeted imaging in neuroendocrine tumors. Eur J Nucl Med Mol Imaging. 2017; 44(3):468–75. https://doi.org/10.1007/s00259-016-3486-2 PMID: 27539020.

100. Qian ZR, Li T, Ter-Minassian M, Yang J, Chan JA, Brais LK, et al. Association Between Somatostatin Receptor Expression and Clinical Outcomes in Neuroendocrine Tumors. Pancreas. 2016; 45 (10):1386–93. https://doi.org/10.1097/MPA.0000000000000700 PMID: 27622342.

101. Gao L, Zhao M, Li P, Kong J, Liu Z, Chen Y, et al. Glycogen synthase kinase 3 (GSK3)-inhibitor SB216763 promotes the conversion of human umbilical cord mesenchymal stem cells into neural precursors in adherent culture. Hum Cell. 2016. https://doi.org/10.1007/s13577-016-0146-6 PMID: 27604750.

102. Ougolkov AV, Fernandez-Zapico ME, Bilim VN, Smyrk TC, Chari ST, Billadeau DD. Aberrant nuclear accumulation of glycogen synthase kinase-3beta in human pancreatic cancer: association with kinase activity and tumor dedifferentiation. Clin Cancer Res. 2006; 12(17):5074–81. https://doi.org/10.1158/1078-0432.CCR-06-0196 PMID: 16951223.

103. Jang S, Yu XM, Odorico S, Clark M, Jaskula-Sztul R, Schienebeck CM, et al. Novel analogs targeting histone deacetylase suppress aggressive thyroid cancer cell growth and induce re-differentiation. Cancer Gene Ther. 2015; 22(8):410–6. https://doi.org/10.1038/cgt.2015.37 PMID: 26251030.

104. Veenstra MJ, van Koetsveld PM, Dogan F, Farrell WE, Feelders RA, Lamberts SW, et al. Epidrug-induced upregulation of functional somatostatin type 2 receptors in human pancreatic neuroendocrine tumor cells. Oncotarget. 2016. https://doi.org/10.18632/oncotarget.9462 PMID: 27223067.

105. Giubellino A, Bullova P, Nolting S, Turkova H, Powers JF, Liu Q, et al. Combined inhibition of mTORC1 and mTORC2 signaling pathways is a promising therapeutic option in inhibiting pheochromocytoma tumor growth: in vitro and in vivo studies in female athymic nude mice. Endocrinology. 2013; 154(2):646–55. https://doi.org/10.1210/en.2012-1854 PMID: 23307788.

106. Tanthaisong P, Imsoonthornruksa S, Ngernsoungnern A, Ngernsoungnern P, Ketudat-Cairns M, Parnpai R. Enhanced Chondrogenic Differentiation of Human Umbilical Cord Wharton's Jelly Derived Mesenchymal Stem Cells by GSK-3 Inhibitors. PLoS One. 2017; 12(1):e0168059. https://doi.org/10.1371/journal.pone.0168059 PMID: 28060847.

107. McCubrey JA, Rakus D, Gizak A, Steelman LS, Abrams SL, Lertpiriyapong K, et al. Effects of mutations in Wnt/beta-catenin, hedgehog, Notch and PI3K pathways on GSK-3 activity-Diverse effects on cell growth, metabolism and cancer. Biochim Biophys Acta. 2016; 1863(12):2942–76. https://doi.org/10.1016/j.bbamcr.2016.09.004 PMID: 27612668.

FOXM1: A novel drug target in gastroenteropancreatic neuroendocrine tumors

Franziska Briest[1,3], Erika Berg[2], Irina Grass[1,3], Helma Freitag[1], Daniel Kaemmerer[5], Florentine Lewens[1], Friederike Christen[1,10], Ruza Arsenic[9], Annelore Altendorf-Hofmann[8], Almut Kunze[7], Jörg Sänger[7], Thomas Knösel[4], Britta Siegmund[1], Michael Hummel[2] and Patricia Grabowski[1,6]

[1] Department of Gastroenterology, Infectious Diseases, Rheumatology CC13, Medizinische Klinik 1, CBF, Germany

[2] Institute of Pathology, CBF, Charité - Universitätsmedizin Berlin, Germany

[3] Department of Chemistry and Biochemistry, Freie Universität (FU) Berlin, Germany

[4] Institute of Pathology, Ludwig-Maximilians-Universität (LMU), Munich, Germany

[5] Department of General and Visceral Surgery, Zentralklinik Bad Berka GmbH, Germany

[6] Department of Internal Oncology and Hematology, Zentralklinik Bad Berka GmbH, Germany

[7] Institute of Pathology, Bad Berka, Germany

[8] Department of General, Visceral and Vascular Surgery, Friedrich-Schiller-Universität (FSU) Jena, Germany

[9] Institute of Pathology, CCM, Charité-Universitätsmedizin Berlin, Germany

[10] Institute of Biology, Humboldt-Universität Berlin, Germany

***Correspondence to**: Patricia Grabowski, **email**: patricia.grabowski@charite.de*

Keywords: gastroenteropancreatic neuroendocrine neoplasms, FOXM1, siomycin A, differentiation, cancer signaling

***Received**: September 24, 2014 **Accepted**: January 20, 2015 **Published**: March 15, 2015*

ABSTRACT

Gastroenteropancreatic neuroendocrine neoplasms (GEP-NENs) are heterogeneous tumors that need to be molecularly defined to obtain novel therapeutic options. Forkheadbox protein M1 (FOXM1) is a crucial transcription factor in neoplastic cells and has been associated with differentiation and proliferation. We found that FOXM1 is strongly associated with tumor differentiation and occurrence of metastases in gastrointestinal NENs. *In vitro* inhibition by the FOXM1 inhibitor siomycin A led to down-regulation of mitotic proteins and resulted in a strong inhibitory effect. Siomycin A decreased mitosis rate, induced apoptosis in GEP-NEN cell lines and exerts synergistic effects with chemotherapy. FOXM1 is associated with clinical outcome and FOXM1 inhibition impairs survival *in vitro.* We therefore propose FOXM1 as novel therapeutic target in GEP-NENs.

INTRODUCTION

Gastroenteropancreatic neuroendocrine neoplasias (GEP-NENs) are heterogeneous tumors of the gastrointestinal system and the pancreas with limited therapeutic options, possibly due to crosstalks that re-activate mitogen signaling [1]. The search for novel "druggable" targets, therapeutic strategies and prognostic markers remains a considerable challenge.

Forkheadbox protein M1 (FOXM1) is regarded to be a crucial transcription factor in a plethora of solid cancers. As one of the early up-regulated proteins in cancerogenesis, FOXM1 has been demonstrated to contribute to all hallmarks of cancer [2-6]. It is considered a key regulator of the G2/M transition of the cell cycle and of the mitotic spindle integrity by regulation of cyclin A and B, cdc25B, aurora A and B kinases, survivin, PLK1, SKP2, CENPB and CENPF/A/B, and degradation of p21 and p27 [3, 4, 6-13]. FOXM1 also triggers cancer progression by promoting a VEGF-dependent angiogenic switch [14, 15] and by facilitating invasion via MMP-2 and MMP-9 secretion [16-18]. FOXM1 can be repressed by wild type p53 [19] and by FOXO3a [20-22]. It is then a further downstream effector of the PI3K-AKT-FOXO-

Table 1: Summary of the most relevant results of the immunohistochemical analyses: number of analyzed specimens is indicated in the table: 88 gastrointestinal NEN specimens were stained for FOXM1, 49 and 36 pancreatic and gastrointestinal cases were analyzed for survivin and STAT3, respectively. Lower numbers in the metastatic status analyses resulted from 3 cases with unknown status. All markers could be associated with metastatic status, and FOXM1 and nuclear survivin could be significantly linked to differentiation. FOXM1 further significantly correlated with survivin and STAT3 high nuclear staining.

Parameters	FOXM1 expression	Nuclear STAT3	Nuclear survivin	Differentiation	Metastatic status
FOXM1 expression		N=36 p=0.001*	N=49 p=0.030*	N=88 p=0.026*°	N=85 p=0.007*°
Nuclear STAT3	° assessed only in gastrointestinal NENs * univarite analysis **multivariate analysis		N.D.	N=36 not sig.*	N=36 p=0.007* p=0.011**
Nuclear survivin				N=49 p=0.000*	N=46 p=0.000*

axis, which is frequently deregulated in GEP-NENs [1, 23, 24]. It is also regulated by cell cycle proteins such as CDK4/6 [25]. The role of FOXM1 in neuroendocrine neoplasms has rarely been explored to date, but it has been recently described as marker for subtyping neuroendocrine lung cancer [26].

In this study we demonstrate that FOXM1 expression is associated with proliferation, differentiation and metastasis in gastrointestinal NEN and that inhibition of FOXM1 is a potential new therapeutic option.

RESULTS

FOXM1expression correlates with differentiation and metastasis in gastrointestinal NENs

First, we assessed the clinical relevancy of FOXM1 in GEP-NEN tumor specimens (summarized in table 1). High FOXM1 staining (Figure 1) was detected in 30/131 (22.9%) of the GEP-NENs tissues. As only 3 specimens of the pancreatic subgroup were poorly differentiated, we focused on the analysis of the 88 specimens of gastrointestinal primary localization.

In this group, FOXM1 expression correlated with tumor differentiation according to WHO 2010 classification (refer to table 2). In an univariate analysis, we found that 9/72 (12.5%) of the well-differentiated (G1 and G2) and 6/16 (37.5%) of the poorly-differentiated (G3) specimens had high FOXM1 expression (fisher's exact test: p=0.026). Interestingly, we found a strong difference of FOXM1 expression between G1 (5.5%) and G2 (35.3%) well-differentiated gastrointestinal NENs (fisher's exact test: p=0.004). The latter FOXM1 expression was similar to those tumors with G3 grading. Accordingly, gastrointestinal NENs can be subgrouped by a strong FOXM1 expression increase with the most significant cut off between 2% to 4% of the proliferation marker Ki-67 (p=0.000, Fig. 1 E and F).

In a subsequent univariate analysis, we could also demonstrate that FOXM1 expression is associated with the occurrence of metastasis in gastrointestinal NENs as 4/49 (8.2%) of the M0 subgroup and 11/36 (30.6%) of the M1 subgroup showed high FOXM1 expression (N=85; p=0.007).

FOXM1 is up-regulated jointly with STAT3 and survivin in GEP-NEN

In order to determine how FOXM1 is co-regulated with other oncogenes, we chose (potential) upstream and downstream mediator of FOXM1. Immunohistochemical analysis was used to determine the expression status of STAT3 in 36 and of survivin in 49 cases of pancreatic and gastrointestinal NENs, respectively. The high FOXM1 expression could be linked to a high survivin nuclear localization (fisher's test: p=0.030; for gastrointestinal NENs only: p=0,029) which was up-regulated in 16/49 (32.7%) cases [27] of the study and was associated with both, differentiation and metastatic status (both: p=0.000).

High FOXM1 expression could further be linked to STAT3 nuclear localization (Figure 1D) in a fisher's exact test (p=0.001; for gastrointestinal NENs only: p=0.005). Nuclear STAT3 furthermore correlated with metastatic status in NENs (p=0,007; for gastrointestinal NENs only: p=0.034). In a multivariate analysis we analyzed the dependency of metastatic status from STAT3 and FOXM1 expression. In a binary logistic regression, STAT3 was determined to be an independent parameter with an odds ratio of 6.72 (p=0.011) in forward and backward stepwise regression, indicating that FOXM1 may be under transcriptional control of STAT3.

A correlation between FOXM1 and cytoplasmic survivin (p=1.00) or cytoplasmic STAT3 (p>0.428) and with phospho STAT3 (p>0.072) expression were not significant in our analyses (data not shown).

The strong correlation of FOXM1 and STAT3

Table 2: Clinicopathological data of immunohistochemically analyzed gastrointestinal GEP-NENs: Distribution of localization, grading, differentiation and metastatic status. More detailed information about clinicopathological data of all 131 patients can be found in Supplement 3.

Grading (WHO 2010)		G1 Ki-67 ≤ 2	G2 Ki-67 = 3-20	G3 Ki-67 > 20	total
primary	Ileum	38	12	1	51
	Colon	9	2	8	19
	Rectum	4	1	6	11
	other	4	2	1	7
differentiation	well	55	17	0	72
	poorly	0	0	16	16
metastatic status	M0	38	6	5	49
	M1	14	11	11	36
	N/A	3	0	0	3
total		55	17	16	88

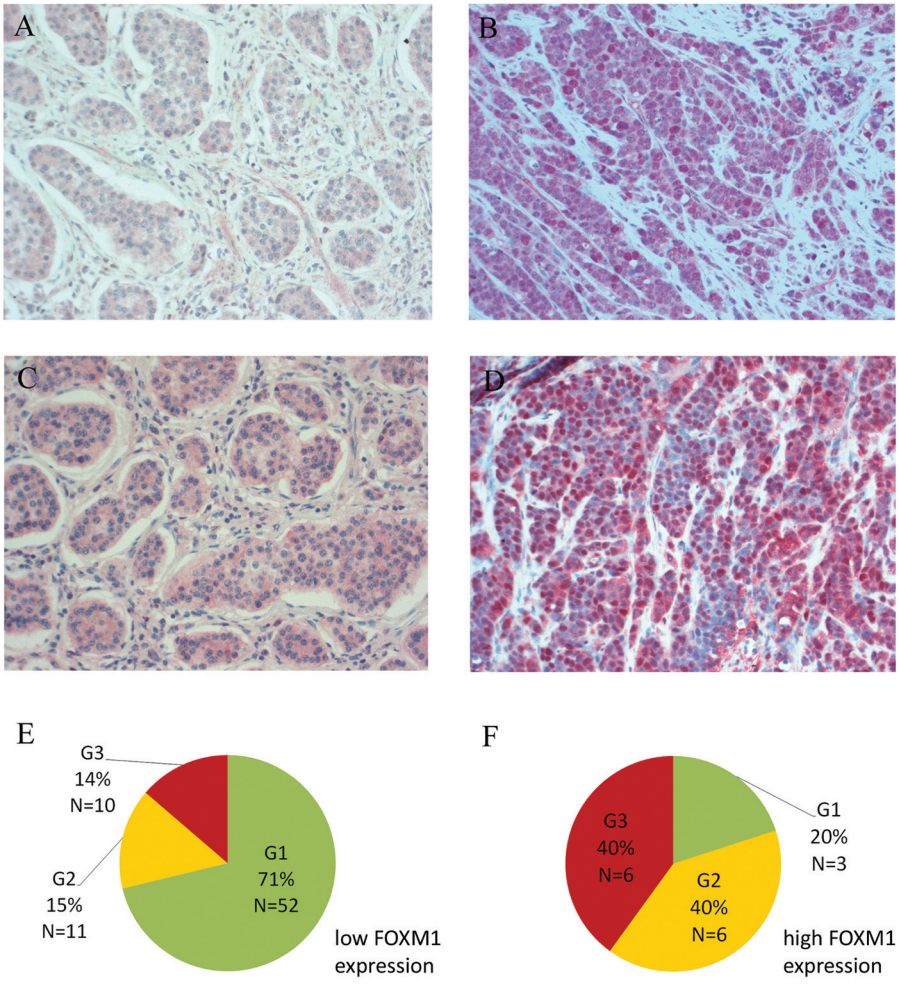

Figure 1: Immunohistochemical staining of FOXM1. A. Weak cytoplasmic and negative nuclear FoxM1 and **C.** negative nuclear STAT3 staining in a well differentiated ileal G1 NEN with liver metastasis. **B.** Strong FOXM1 (nuclear and cytoplasmic immunoreactivity) and **D.** nuclear STAT3 staining of a poorly differentiated gastric G3 NEC with liver metastasis. Nuclear localization of the oncogenic transcription factor STAT3 is associated with high FOXM1 expression (p=0.001). All pictures: light microscopy, 200x magnification. **E**+**F**. Distribution of WHO 2010 grading subgroups within the two FOXM1 expression groups of gastrointestinal NENs (N=88): in the FOXM1 low expression group, 71% of the tumors were graded G1, G2 tumors represented 15% and G3 tumors 14%. The FOXM1 high expression group is predominated by G2 and G3 tumors with 40% each. Only 20% of this group were G1 tumors.

expression could be confirmed in lysates obtained from frozen primary and metastasis tumor material of GEP-NEN patients. Here, FOXM1 was significantly associated with STAT3 expression (p=0.000; Figure 2A). We could further detect a tendency of FOXM1 and STAT3 to be higher expressed in the metastasis group of tumor tissue than in the primary tumor group (Figure 2). We therefore show that STAT3 and FOXM1 in GEP-NENs may have prognostic significance.

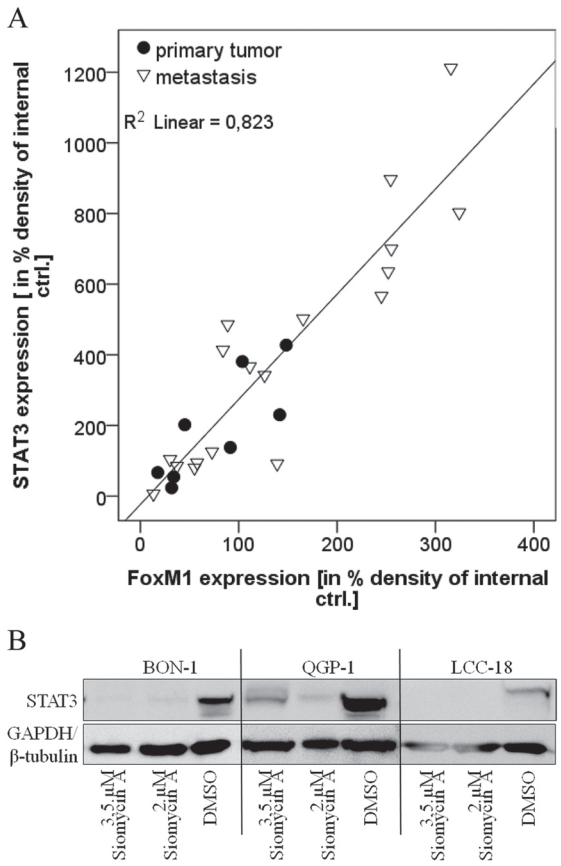

Figure 2: Role of STAT3 expression. A. Primary tumor samples were lysed, analyzed by western blot in three independent experiments and densitometrically assessed. Statistical evaluation was done by linear multivariable regression and by non-parametric Mann-Whitney U Test, respectively. On tissue level, FOXM1 expression strongly correlated with STAT3 expression (*R square*= 0.823, *adjusted R square*=0.816) by linear regression. STAT3 is therefore associated with FOXM1 expression. A tendency of both proteins to be expressed to a higher extent in metastasis, compared to primary tumor material can be assumed, but requires a larger number of tumor samples. **B.** BON, QGP-1 and LCC-18 cell lines were treated with 2 and 3.5µM siomycin A for 72h. Cells were lysed and lysates were prepared by western blot. Immunodetection of STAT3 showed a strong decrease of STAT3 expression after siomycin A treatment in all cell lines.

Siomycin A treatment induces regulation of proteins that are involved in GEP-NEN tumor biology

In our preliminary experiments, we have demonstrated that FOXM1 is expressed in GEP-NENs to a high extent and can be correlated to differentiation and the occurrence of metastasis in gastrointestinal NEN. Until now, effective therapy options for these tumors are not available. We therefore analyzed the effect of proteasome inhibitors, which target FOXM1 [28-31], *in vitro*. To initiate our studies, we assessed the basal expression of FOXM1 in the GEP NEN cell lines BON, QGP-1, KRJ-1, LCC-18 by western blot. All cell lines expressed detectable levels of FOXM1 (Figure 3A).

We chose the natural thiazole antibiotic, siomycin A and evaluated its effect on FOXM1 expression in treated GEP-NEN cell lines. We could demonstrate that FOXM1 was down-regulated time-dependently in all cell lines and that the cell cycle regulator p21 was up-regulated simultaneously (Figure 3B). Siomycin A is thus competent to inhibit FOXM1 in GEP-NEN cell lines and might influence the cell cycle regulation of GEP-NEN cells.

Chromogranin A is a common clinical neuroendocrine marker. Aurora kinases and survivin are mitosis associated proteins, the latter with a strong prognostic potential in GEP-NENs. Through western blot analyses, we found that chromogranin A, survivin, and aurora A were synchronously down-regulated after siomycin A treatment (Figure 3C). FOXM1 dependent down-regulation of aurora A and chromogranin A could be further confirmed by determining the expression after knockdown of FOXM1 by RNA interference (Figure 3D). Everolimus did not exert mentionable effects on FOXM1 expression (Figure 3E), as it affects the mTOR signaling and is not considered to be involved in FOXM1 regulation.

Interestingly, we found STAT3 also down-regulated under siomycin A treatment, which reveals some insight into the mode of action of this natural agent (Figure 2B).

Siomycin A treatment induces antiproliferative effects on GEP-NEN cell lines *in vitro*

To assess siomycin A not only as modulator of neuroendocrine markers and proliferation regulators, but also as effective treatment option for GEP-NENs, we calculated the dose of half maximal inhibitory effect (IC50) of siomycin A and everolimus for each GEP-NEN cell line (Suppl. 1). Everolimus was chosen because it is one of only 3 molecular therapy options that have been approved for GEP-NEN treatment. The IC50 of siomycin A was determined as ~1µM for BON and LCC-18 cells and ~2µM for QGP-1 cells and are consistent with the already published IC50 values for this natural agent in other cells lines *in vitro* [32]. We could not determine

an IC50 for KRJ-1 cells due to the interference of native cellular clustering of this non-adherent cell line. We hypothesize that the surface cell layer of the spherical cell clusters protected the inner cells from the treatment and gave an incalculable growth advantage increasing with the size of the clusters. For these cells we estimated an IC50 similar to those of the other GEP NEN cell lines.

We could demonstrate a significant antiproliferative effect of siomycin A on GEP-NEN cell lines p=0.000; Figure 4). Siomycin A is therefore superior even to equal doses of everolimus, which only showed significant impact on the cell lines BON (p=0.008) and LCC-18 (p=0.000), whereas QGP-1 (p=0.092) and KRJ-1 (p= 0.38) did not significantly respond to everolimus even in concentrations equal to siomycin A treatment (Figure 4).

Siomycin A reduces mitosis and induces apoptosis in GEP-NEN cell lines *in vitro*

As FOXM1 is strongly associated with mitotic regulation, we wanted to understand the impact of siomycin A on the cell cycle of GEP-NEN cells. After 96h of treatment, the majority of BON, and LCC-18 and a large population of KRJ-1 cells analyzed by mitotic index flow cytometry, have undergone apoptosis or necrosis (indicated as Sub-G1) and showed a significantly decreased mitotic population (p<0.001; Figure 5). QGP-1 cells only showed a moderate increase in apoptotic or necrotic cells and an average 6-fold decrease of the mitotic cell population could be detected (Figure 5 and Suppl. 2).

To distinguish whether cells undergo apoptosis or necrosis, we completed our analyses by an LDH-based cytotoxicity assay. Siomycin A in effective doses showed

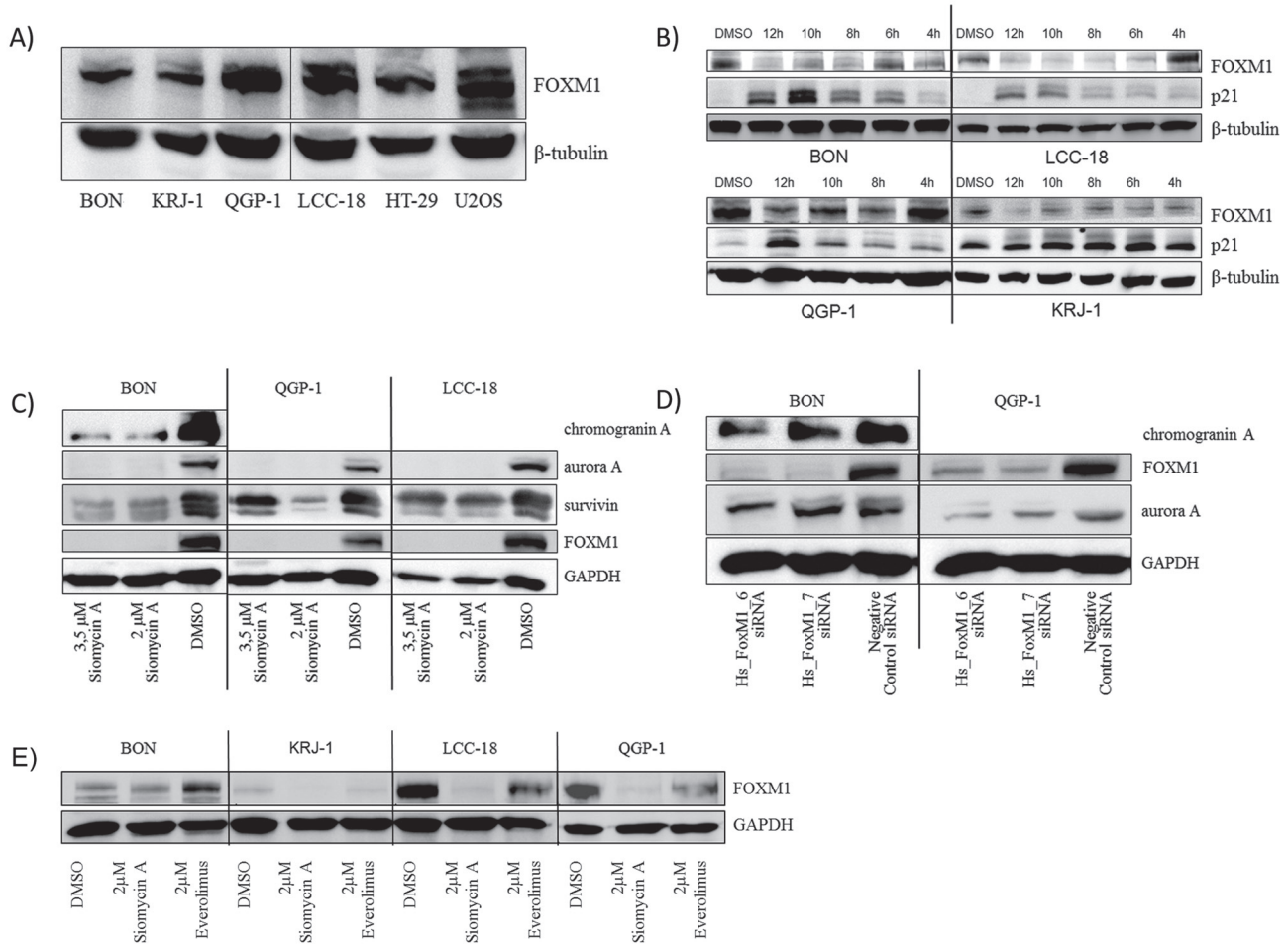

Figure 3: Western blot analysis of FOXM1 and potential target expression in GEP-NEN cell lines. All cell lines including the non-neuroendocrine HT-29 and the FOXM1 overexpressing U2OS control cell lines expressed FOXM1 **A.** KRJ-1 cells, which is the only wild type *TP53* GEP-NEN cell line in this study (unpublished data) expressed the lowest level of FOXM1. After short time (12h) treatment with 10µM siomycin A, an increase of p21 expression was detected in a time-dependent manner **B.** Treatment of synchronized GEP-NEN cell lines with 2 and 3.5µM siomycin A for 72 hours resulted in a decrease of FOXM1, chromogranin A, aurora A and survivin expression **C.** Dependency of chromogranin A and aurora A down-regulation from FOXM1 depletion could be verifed by RNA interference with two different siRNAs targeting FOXM1 mRNA **D.** in BON and QGP-1 cells. Treatment with 2µM everolimus for 72 hours did not remarkably reduce FOXM1 expression **E.**

a low cytotoxic effect on BON, QGP-1 and LCC-18 (Figure 6 A-C). Only in KRJ-1 there were strong cytotoxic effects, presumably due to the loss of intercellular contact. As resuspending the cell clusters was obligatory for equal cell numbers and the time of incubation was too short for a reattachment, induction of anoikis might be an explanation for an early and strong loss of membrane integrity (Figure 6D).

We conclude that siomycin A predominantly induces a decrease of mitotic activity and apoptosis in GEP-NEN cell lines and its *in vivo* tolerability should be further assessed in animal studies.

Siomycin A induces synergistic effects combined with chemotherapy

Siomycin A might not be used in monotherapy regimens, but inhibition of FOXM1 has been already assessed to have synergistic effects combined with genotoxic drugs [19, 33, 34]. We therefore examined the effect of siomycin A combined with cisplatin or temozolomide versus everolimus combined with chemotherapy. 10µM cisplatin induced moderate inhibitory effects in WST proliferation studies. 10µM Temozolomide did not inhibit cellular proliferation in BON, QGP-1 and LCC-18 cells and showed a moderate antiproliferative effect in KRJ-1 cells. Quantitated by the combination index method after Chou and Talalay [35, 36], we found *slight synergistic* to *synergistic* effects in all cell lines for 0.1µM everolimus combined with 10µM cisplatin after 72 hours of treatment (Figure 7). This favorable combination has been described before [37] and could be reproduced for GEP-NENs in this study. Nevertheless, even the combined everolimus treatment was less effective than the siomycin A monotherapy in all cell lines. Everolimus combined to temozolomide did not show enhanced effects.

2 or 3 µM Siomycin A combined to 10 or 5µM cisplatin, respectively, induced *nearly additive* to *very strong synergistic* inhibitory effects in GEP-NEN cell lines. Interestingly, the effect of siomycin A combined

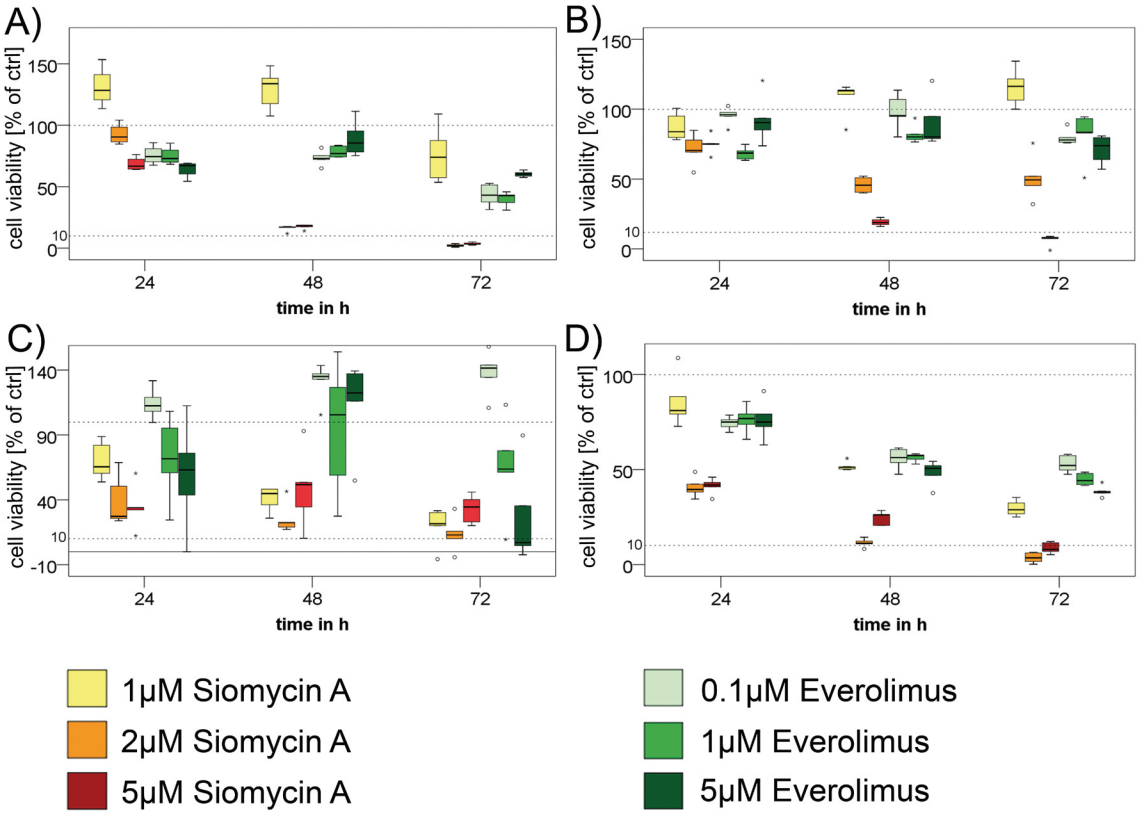

Figure 4: Treatment of GEP-NEN cell lines with siomycin A. In three independent experiments, BON **A.**, QGP-1 **B.**, KRJ-1 **C.** and LCC-18 **D.** cells were treated with increasing concentrations (1µM, 2µM, 5µM) of siomycin A and (0.1µM,1µM, 5µM) everolimus for 24, 48 and 72 hours and analyzed by colorimetric proliferation assays (graphs in percent of internal DMSO controls). Siomycin A significantly inhibits GEP-NEN cell proliferation (p=0.000) and was superior to everolimus treatment in all cell lines. Antiproliferative effects could be shown for concentration ≥1µM in BON, KRJ 1, LCC 18 and ≥2µM for QGP-1 cells in relation to DMSO internal controls and were verified in a linear regression analysis. KRJ-1 cells showed a strong variance in the response due to intercellular clustering effects. Nevertheless these changes were highly significant (p=0.000). Representative data of one experiment is shown. Dotted lines indicate 100% and 10% of control.

to temozolomide was *antagonistic* in pancreatic BON (Figure 7A) and QGP-1 cells (Figure 7B), whereas the gastrointestinal cell lines KRJ-1 (Figure 7C) and LCC-18 (Figure 7D) responded with *synergistically* reduced proliferation. Siomycin A combined to everolimus induced *antagonistic* effects and increased cellular proliferation in relation to DMSO controls (data not shown).

DISCUSSION

GEP-NENs, in particular tumors that originate in the gut, lack tailored molecular therapies and biomarkers. Interestingly, the expression of several proteins, such as survivin, aurora kinases, p16(INK4A) and IGF-1, have been found altered in GEP-NENs, and are associated with FOXM1 expression in other cancer entities [38-40]. *FOXM1* has further been described as a crucial proto-oncogene. There are currently few prognostic markers and

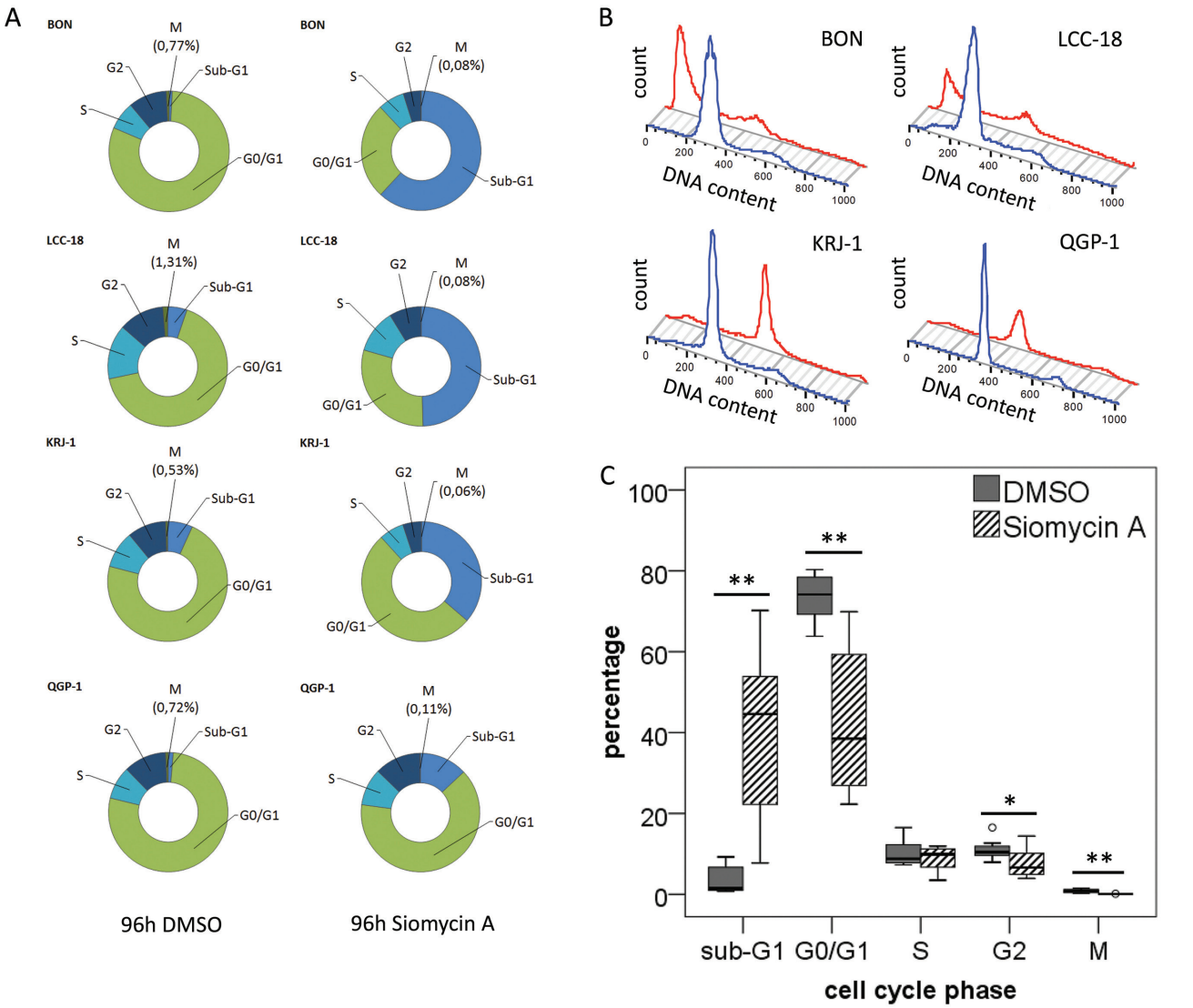

Figure 5: Cell cycle analysis of GEP-NEN cell lines treated with siomycin A. Unsynchronized BON, QGP-1, KRJ-1, LCC-18 cells were treated with 2μM siomycin A for 96h and analyzed by mitotic index flow cytometry. Cells were stained with an anti-phospho-H3 antibody and propidium iodide and analyzed versus 0.04% DMSO controls. All changes were calculated with respect to DMSO controls. **A.** Average of cell cycle changes in the distinct GEP-NEN cell lines after Siomycin A treatment. BON cells show a strong 72-fold increase in the sub-G1 cell death population; in KRJ-1, QGP-1 and LCC-18 cells a 5- to 9-fold increase could be detected. Most notably, the number of mitotic cells (indicated by phosphorylated histone H3) significantly decreases after siomycin. A treatment in the range of 6.5- to 16-fold. **B.** Representative histogram of one 96h incubation experiment, blue line indicates the DMSO control, red lines visualizes the cell cycle histogram after siomycin A treatment (more detailed flow cytometry data can be found in Suppl. 2). The average chances of all cell lines under siomycin A treatment are visualized in **C.**, all significant values are indicated by stars. Double starred bars indicate significance levels $P \leq 1\%$.

therapeutic options, especially in the NENs of the gut, and prognosis is only associated with the proliferation index indicated by Ki-67. We therefore assessed FOXM1 as a potential disease progression marker and therapy target.

We found FOXM1 significantly up-regulated in poorly differentiated tumors (p=0.026). FOXM1 could not be validated as a significant independent marker. This result may be due to its crucial role in mitosis and proliferation, which would influence the expression of proliferation markers, such as Ki-67.

Interestingly, the correlation of FOXM1 expression and Ki-67 staining reveals a low expression in the G1-graded tumors and FOXM1 expression significantly increases in the tumor subgroup with a Ki-67 value higher than 2-4% (p=0.000). There is currently an unclear Ki-67 cut-off value to distinguish G1 and G2 GEP-NENs, since former WHO classifications stated Ki-67 cut-off values from 2 to 5%, which were dependent from the localization of the primary tumor (WHO2000/2004). As Ki-67 is only a descriptive marker, these changes in the FOXM1 transcription factor expression might give a mechanistic explanation for the distinct clinical prognoses of both subgroups. Therefore, FOXM1 might serve as a secondary refining marker to discriminate between G1 and G2 gastrointestinal NENs.

FOXM1 expression could also be related to the occurrence of metastases (p=0.007) and showed a tendency to be up-regulated in primary metastases material. Therefore, we could show that FOXM1 is a progression associated protein in GEP-NENs. These data are consistent with already published results for FOXM1 as oncogene in many other cancer entities [41-43].

FOXM1 is described as a transcriptional target of STAT3 [44]. Here, we demonstrate that FOXM1 is up-regulated jointly with nuclear STAT3 in GEP-NENs. Although being localized in the nucleus, stained STAT-3 molecules were not consistently phosphorylated, as the parallel immunohistochemical staining with the phospho-STAT3 antibody was highly variable (data not shown). We hypothesize that STAT3 might transactivate

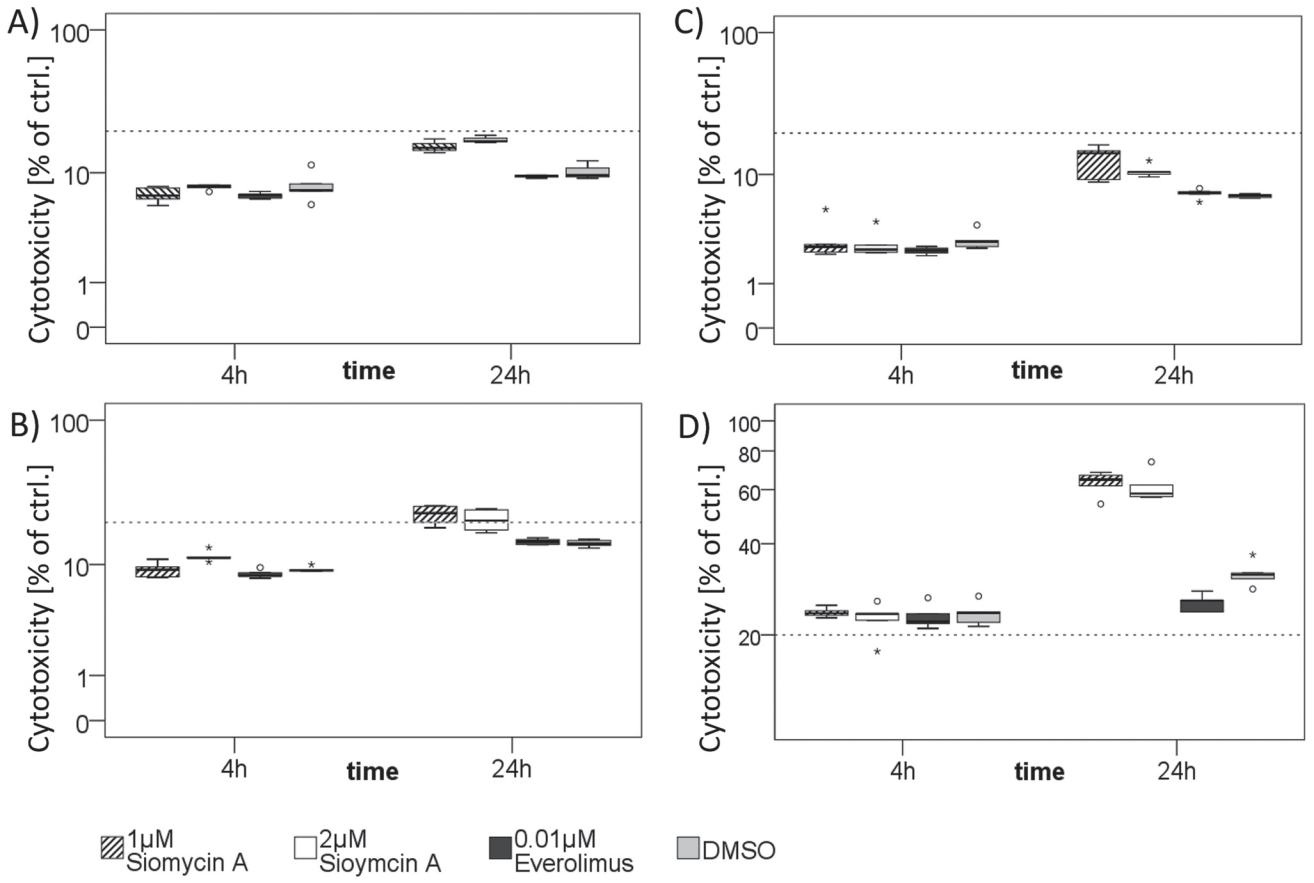

Figure 6: Cytotoxic effects of siomycin A treatment *in vitro*. BON **A.**, LCC-18 **B.**, QGP-1 **C.**, and KRJ-1 **D.** cells were treated with 1 and 2µM siomycin A versus 0.04% DMSO, 0.01µM Everolimus and 1% Triton X (total cell lysis control) for 4 and 24 hours. LDH release from necrotic cells was colorimetrically measured in % of Triton X lysed cell control by LDH cytotoxicity assay. Dotted line indicates 20%. BON and LCC-18 cells showed very low spontaneous cytotoxicity (lower than 20%). QGP-1 cells had cytotoxic effects in the range of 20%. Only KRJ-1 cells had higher cytotoxicity values up to 63%. Further studies should be performed to assess the *in vivo* tolerability of siomycin A.

FOXM1 expression in GEP-NENs. These results may be reflected in recent studies showing that unphosphorylated STAT3 (U-STAT3) can be shuttled into the nucleus by importin-alpha3 and -alpha6 and is crucially involved in cancer signal transduction [45]. It has been demonstrated to cooperate with other transcription factors such as unphosphorylated NF-kappaB to bind to DNA and transactivate target genes [46, 47]. Furthermore, U-STAT3 can mediate FOXO3a nuclear export and thus FOXO3a inactivation and FOXM1 activation, whereas phosphorylated STAT3 re-localizes FOXO3a into the nucleus and therefore promotes its FOXM1 antagonistic activity [48].

Thiazole compounds, such as siomycin A, have been assessed as promising FOXM1 inhibitors with little impact on untransformed cells [49]. In general, proteasome inhibitors might stabilize a hypothetical negative regulator of FOXM1 [29, 32, 50]. In this study, siomycin A treatment decreases the expression of both, STAT3 and FOXM1, although the mechanism of action is relatively unknown [4, 29, 30]. Therefore it is possible that the proteasome inhibitor sioymcin A targets FOXM1

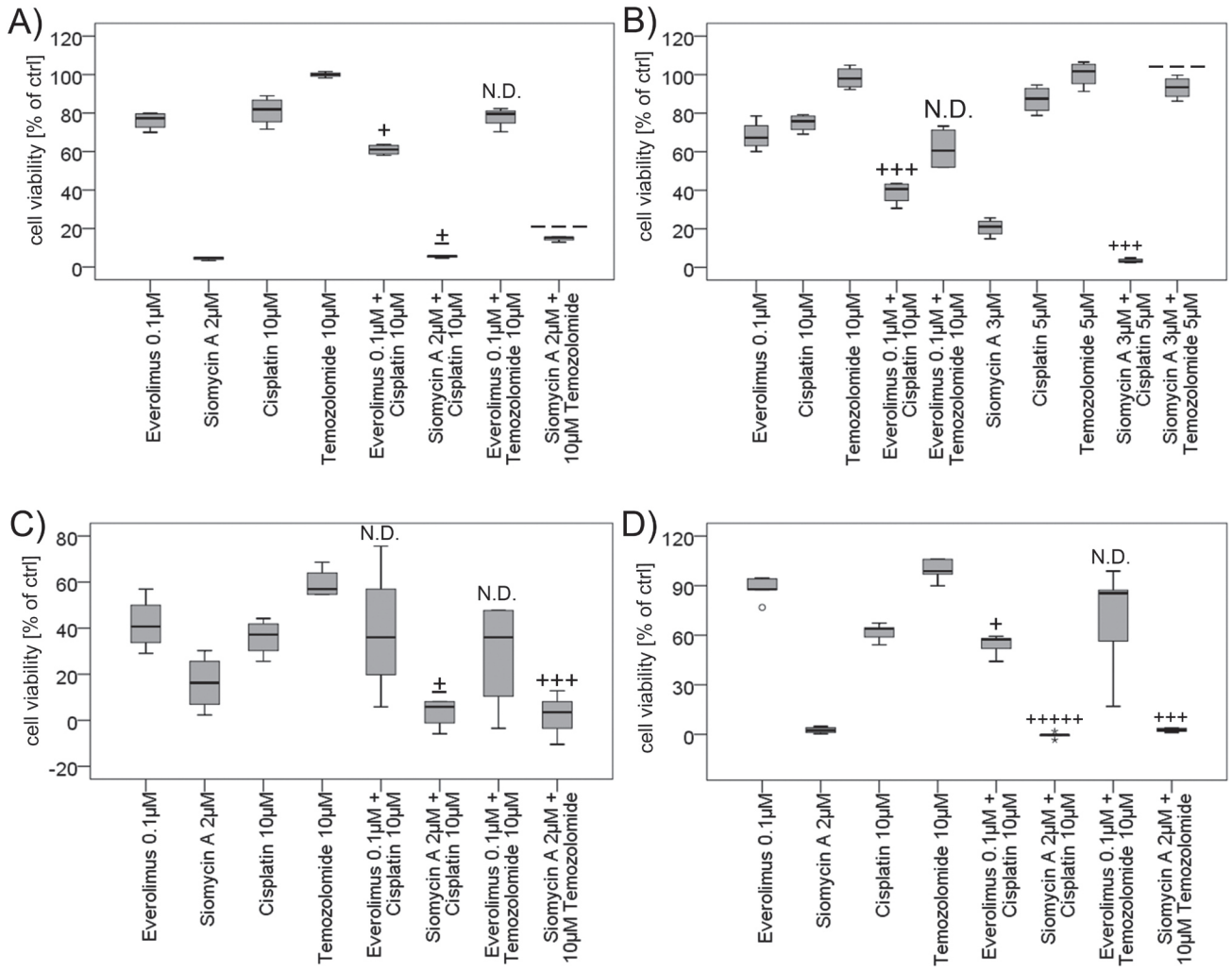

Figure 7:Combined treatment of GEP-NEN cell lines with siomycin or everolimus and genotoxic drugs. BON **A.** KRJ-1 **C.** and LCC-18 **D.** cells were treated with 2µM siomycin A or 0.1µM everolimus alone and combined with 10µM cisplatin or temozolomide for 72 h versus 0.1% DMSO. QGP-1 cells **B.** were treated with 3µM siomycin A combined to 5µM of cisplatin or temozolomide. Proliferation was analyzed by colorimetric WST proliferation assays (graphs in percent of internal DMSO controls) and mean combination index was calculated using the Chou and Talalay method by CompuSyn 1.0 software [35, 36]. Everolimus combined to cisplatin showed *slight synergism* to *synergism* (BON: CI=0.864; QGP-1: CI=0.457; KRJ-1: n.d.; LCC 18: CI=0.862) after 72 hours of treatment. Siomycin A combined to cisplatin induced *nearly additive effects to very strong synergisms* in GEP-NEN cell lines (BON: CI=0.996; QGP-1: CI=0.548; KRJ-1: CI=1.066; LCC-18: CI=0.062) and the combination with temozolomide was *antagonistic* in pancreatic BON (CI=1.538) and QGP-1 cells (CI=2.627), and *synergistic* in gastrointestinal KRJ-1 (CI=0.526) and LCC-18 (CI=0.645) cell lines. (Captions [35]: very *strong synergism*: +++++; *strong synergism*: ++++; *synergism*: +++; *moderate synergism*: ++; *slight synergism*: +; *nearly additive*: +/-; *slight antagonism*: -, *moderate antagonism*: --; *antagonism*: ---; *strong antagonism*: ----; *very strong antagonism*: -----)

indirectly by a JNK-STAT3-dependent mechanism [31, 51]. This may explain the effectiveness of siomycin A, as STAT3 has been shown to interfere with FOXO proteins [48]. Thus, siomycin A might interfere with STAT3, which contributes to FOXO3a nuclear localization and results in *FOXM1* repression and inhibition of mitosis.

In our study we have further confirmed that survivin and aurora kinases are FOXM1 targets. This is not a novel result, but as aurora kinases have previously been described as druggable targets in GEP-NENs [52, 53], novel combinatory treatments are conceivable. Furthermore, the fact that aurora A kinase and survivin are down-regulated under FOXM1 inhibition supports the notion that the mitotic instability, and not the (in-) activation of various kinases, may be the better approach for the treatment of GEP-NENs.

Independently from its impact on neuroendocrine tumor signaling, we could show the natural agent siomycin A as effective therapeutic option when applied in the range of 1-2µM. We hypothesize that the higher IC50 values in QGP-1 are related to a *TP53* frameshift mutation and thus loss of p53 expression (unpublished data) which impairs apoptosis induction. In all cell lines, siomycin A shows a strong maximum effect, but presumably due to its pharmacochemical characteristics, it must be applied in relatively high doses *in vitro* [32]. Notably, is has been described not to affect normal cells [29, 49, 54, 55]. We could demonstrate that siomycin A treatment reduces mitosis and induces low unspecific cell cytotoxicity in three cell lines. We further showed beneficial combinatory effects combined to cisplatin in all cell lines and combined with temozolomide in the gastrointestinal cells. As FOXM1 expression is critically linked to DNA damage signaling and p53 status [33, 56], subtype specific prediction markers for combined therapy approaches should be further evaluated.

Therefore, the inhibition of FOXM1 by proteasome inhibitors is a potential therapeutic option in GEP-NENs which should be further evaluated.

In conclusion, we could demonstrate an association of FOXM1 with the proliferation index indicated by Ki-67 and with mitotic proteins that have been assessed as crucial players in GEP-NEN biology [27, 52, 53]. This effect could be confirmed by an overall decreased mitotic activity in cells after siomycin A treatment. We have further linked FOXM1 to STAT3 expression and metastasis.

Finally, we have demonstrated that FOXM1 inhibition by siomycin A showed a stronger effect on the tested GEP-NEN cell lines than everolimus. Given the fact that everolimus is a well-established therapy in pancreatic NENs, but its efficacy is limited, we propose a potential for the assessment of a combination therapy with FOXM1 inhibitors. FOXM1 inhibition should be also considered as a (combinatory) therapeutic approach especially in gastrointestinal NENs, where effective therapeutic options are currently not available. In this context, our data further provide a strong rationale for assessing other proteasome inhibitors, such as casticin, thiostrepton and bortezomib [36, 37] as therapeutic strategies.

In conclusion, FOXM1 may serve as a clinical prognostic factor and a therapeutic target for GEP-NENs.

MATERIALS AND METHODS

Patients and samples

For immunohistochemical analysis, 131 paraffin embedded specimens of pancreatic (n=43), ileal (n=51), colorectal (n=30) and gastric (n=7) neuroendocrine neoplasms have been retrospectively analyzed for FOXM1 expression. Cases (age 17-87 years) were collected and prepared as tissue microarray (TMA) at Universitätsklinikum Jena (n=82) and as whole section (3-5µm) tissue slides at Charité-Universitätsmedizin Berlin (n=49), respectively, with permission of the local ethical committees. The TMA was assembled using 0.6 cm punch biopsies from all samples according to standard procedures [57]. Five-year follow-up was complete in all 131 cases. Inclusion criteria for this study were: positive staining for neuroendocrine markers and availability of clinicopathological information. Tumors were re-classified and Ki-67 re-stained according to the WHO 2010 classification: 85 patients had G1 neuroendocrine neoplasms, 27 patients suffered from G2 NEN. 19 patients were diagnosed to have a G3 neuroendocrine cancer. Further clinicopathological information can be found in table 2 and supplement 3.

In addition, 36 specimens of the whole section cohort were selected for further staining against STAT3 and phospho-STAT3. Nuclear survivin (N=49) has been stained in the same cohort before [27].

In a further prospective study, 44 tissue samples of fresh frozen material of GEP-NENs derived from 15 patients were collected at the Department of General and Visceral Surgery at the Zentralklinik Bad Berka GmbH between 2009 and 2013 with an institutional review board approval for guidelines and ethical procedures. The diagnosis of NEN was based on immunohistochemical characterization of chromogranin A and synaptophysin expression, on proliferation index (Ki-67) and on morphological criteria according to the WHO 2010 grading classification. On-site fresh frozen tissue specimens were H&E (hematoxylin and eosin) stained and analyzed for tumor cell ratio and morphological features such as high immune cell invasion or vascularization. Only samples with tumor cell content higher than 80 percent were included. The samples were mechanically homogenized and lysed in NP-40 buffer.

Data derived from different samples of the same

tumor were aggregated and mean values were calculated. Total number of analyzed tumors thus results in 26. Further clinicopathological data is provided in supplement 4.

Cell lines

The following GEP-NEN cell lines were used for *in vitro* experiments: pancreatic: BON [58] and QGP-1 [59]; obtained from *Japanese Collection of Research Bioresources*), ileal: KRJ-1 [60] and colonic: LCC-18 [61].

All cell lines were authenticated (if indicated as unique) by genetic STR typing by the DSMZ, Braunschweig, Germany in 2012 and 2013 and only cells passaged not longer than 15 passages after receipt were used. Cells were tested periodically for maintained cell line specific expression of neuroendocrine markers (chromogranin A, synaptophysin, cytokeratin, vimentin, syntaxin) by immunofluorescence microscopy. All cell lines were grown in Quantum 263 for tumor cells (GE Healthcare Munich, Germany) including 1% penicillin/streptomycin or in cell line specific medium (containing 10% FBS gold and 1% penicillin/streptomycin): BON and KRJ-1 in Dulbecco's Modified Eagle Medium: Nutrient Mixture 1:1 F-12 (DMEM/F12) with stable glutamine, QGP-1 were cultured in RPMI 1640 with stable glutamine and LCC-18 were grown in DMEM 4.5g/l glucose with stable glutamine. The non-neuroendocrine HT-29 and the FOXM1 overexpressing U2OS cell lines were used as controls, if indicated.

Western blot

SDS page and western blot of NP-40 lysed material was performed using a standard protocol and documented by ponceau S staining. Primary antibodies (obtained from Cell Signaling Technology Inc. Danvers, MA, USA: pan-actin (D18C11), phospho-Tyr705-STAT3; Santa Cruz Biotechnology Inc. Dallas, Texas, USA: FOXM1 (C-20), p21; GeneTex Inc. Irvine, CA, USA: GAPDH; Abcam plc Cambridge, UK: aurora A; PROGEN GmbH Heidelberg: chromogranin A (klon LK2H10)); BD Transduction Laboratories, Franklin Lakes, NJ, USA: STAT3; Sigma-Aldrich: beta-tubulin) and secondary antibodies (Dako Deutschland GmbH, Hamburg, Germany: swine anti rabbit IgG-HRP, goat anti-mouse IgG-HRP; Santa Cruz Biotechnology Inc: donkey anti-goat IgG-HRP) were applied. Antibody binding was detected with ECL™ *prime Western Blotting detection reagent* (Amersham™ GE healthcare) and documented by Fujifilm LAS-4000 luminescent image analyzer. For re-probing, membranes were incubated in acidic glycine buffer (0.2 M glycine, 1% SDS, 0.1% Tween 20, pH 2.2). Chemiluminescence signals were densitometrically detected with Multi Gauge V3.1. Values of three independent experiments were normalized to an internal control and statistical assessment was performed with IBM SPSS Statistics 20.

Immunohistochemistry of paraffin-embedded specimens

Immunohistochemistry was performed by APAAP method. Antibody (FOXM1 C-20) was obtained from Santa Cruz Inc. and diluted to a working concentration of 2µg/ml. The scoring of FOXM1 was assessed by 1.) administration of a nuclear (based on a previously described method for FOXM1 nuclear staining in neuroendocrine lung cancer [26] and a cytoplasmic score; 2.) integrating both in one overall score. The cytoplasmic FOXM1 immunoreactivity was assessed as 0 (no staining), 1 (weak staining), 2 (moderate staining) and 3 (strong staining). Only moderate and high staining was included in the FOXM1 cytoplasmic positive score. Due to the fact that FOXM1 cytoplasmic staining is described as important parameter [62] and FOXM1 nuclear staining was presumed to be the more critical marker overall, thus we created a dichotomized score with a proper weighting of both parameters. Here, nuclear and cytoplasmic scores were summated and a score of "2" was defined as high staining. Consequently, both nuclear and cytoplasmic staining had to be 2 or greater to be assessed as "high FOXM1" expression. Immunohistochemical evaluation was done by two independent experts (P.G. and R.A.).

STAT3 antibody was obtained from BD biosciences and diluted to 1:100; phospho-(Tyr705)-STAT3 antibody was purchased from Cell Signaling Technology and administered in a 1:50 dilution. Score was assessed separately for nuclear and cytoplasmic staining as 0 (no), 1 (weak), 2 (moderate), 3 (strong) immunoreactivity. To dichotomize this variable, only moderate and high staining were included as STAT3 high expression. Scores and utilized antibodies for survivin have been previously described [27].

Statistical analyses

Correlation analyses of continuous variables were analyzed by multivariate linear regression in forward and backward stepwise regression. For univariate analyses containing one or two dichotomized variables, the Mann-Whitney *U* test or the χ^2 test were applied, respectively. For results with low expected counts due to low sample numbers, we applied the exact fisher's test, if possible. Multivariate analysis with dichotomized dependent variables was performed by binary logistic regression in forward and backward regression. Overall survival was estimated by the Kaplan-Meier method, starting from the time of diagnosis. The survival was evaluated by the Mantel-Cox log-rank test and in a multivariate analysis

by Cox regression. Differences were considered to be significant for $p < 0.05$. All statistical analyzes were performed using IBM SPSS Statistics 20 software.

GEP-NEN cell lines treatment with siomycin A vs. everolimus

For cell cycle synchronization, cells were incubated in 10µM thymidine (Sigma-Aldrich, St. Louis, MO, USA; in culture media) for 72 hours or starved 24 hours in culture medium containing 0.01% FBS.

Siomycin A was obtained from Sigma-Aldrich and dissolved in DMSO. Everolimus as control therapy was obtained from Cell Signaling Technology. For proliferation and cytotoxicity assays, 10000-20000 cells per well were used in quintuplets in 96 well plates and treated 4 and 24h for LDH and 24, 48 and 72h for WST-assay with different concentrations and controls. *WST-1 proliferation reagent* and *LDH cytotoxicity detection reagent* (Roche; Basel, Switzerland) were applied according to the manufactures' instructions. In the LDH assay, 3% FBS was used instead of 1%, as recommended in the instructions. Cell density was colorimetrically quantified with a multi-well spectrophotometer (TECAN sunrise™).

In vitro RNAi knockdown of FOXM1

Cells were transfected with *Lipofectamine 2000* (Life technologies, Carlsbad, CA, USA) containing 40 pmol/ml siRNA (*FlexiTube siRNA* against human FOXM1 transcript NCBI Reference Sequence NM_001243088, NM_001243089, NM_021953, NM_202002, NM_202003; QIAGEN; Target Sequences: Hs_FOXM1_6: 5'-AACATCAGAGGAGGAACCTAA-3', Hs_FOXM1_7: 5'-TGGGATCAAGATTATT AACCA-3') or *AllStars Negative Control* siRNA; both QIAGEN) according to the manufacturer's instructions for 72 h.

Cell cycle analysis by mitotic index flow cytometry

Cells were seeded into 6-well plates and incubated unsynchronized with 2µM siomycin A for 96h. Cells fixed in 70% cold ethanol and washed in PBS containing 0,5% Tritin X and 1 % BSA. For intercellular antibody staining, cells were incubated for 1h in Phospho-(Serine-10)-Histone H3 antibody (Cell signaling #3377) diluted 1:6000 in PBS/Triton/BSA. Secondary antibody (Alexa Fluor goat anti-rabbit; Life technologies) was applied 1:500. Cells were incubated 30 min. in PBS containing 20µg/ml propidium iodide (Life technologies) and 10µg/ml RNase A. Flow cytometry was conducted with FACSCalibur (Becton Dickinson) by BD Cell Quest Pro software and analyzed with FlowJo 8.7 software.

Combination therapy of GEP-NEN cell lines

Cells were grown, synchronized by reduced serum supply and seeded in quintuplets in 96 well plates. Cells were synchronously treated with increasing concentrations of Siomycin A, everolimus, cisplatin (Charité Berlin dispensary) or temozolomide (Santa Cruz Biotechnology Inc.) and 0.1% DSMO, respectively, to obtain dose response curves as recommended by the Chou-Talalay method [35]. Additionally, several non-constant combinations of >IC50 concentrations of siomycin A or everolimus and cisplatin or temozolomide were assessed. WST-1 proliferation assay (Roche; Basel, Switzerland) was performed colorimetrically quantified. Data was analyzed by CompuSyn 1.0 at Fa=0.5 [63] and IBM SPSS Statistics 22 software.

ACKNOWLEDGEMENTS

The support of the German Wilhelm und Ingeburg Dinse Gedächtnis-Stiftung and of the Sonnenfeld Stiftung Berlin is gratefully acknowledged.

The authors would like to thank Liliana H. Mochmann (Charité Berlin) for critically reading the manuscript, Werner Hopfenmüller from the Institute of Biometry and clinical Epidemiology (Charité Berlin) for support in the context of statistical evaluation, the colleagues of the Theranostics Research Network, especially Prof. Dieter Hörsch (Zentralklinik Bad Berka) for providing specialist advice and support. We further would like to thank Dr. Katharina Detjen (Charité Berlin) for technical advice and support and Annika Lingnau and Sara Iwazkiewicz (FU Berlin) for technical support.

BON cells were a generous gift from CM Townsend (University of Texas, Galveston). KRJ-I midgut NET cells were generated by R. Pfragner (Medical University of Graz) and kindly provided by I. Modlin (Yale University, New Haven).

Disclosure

The group of Dr. Patricia Grabowski receives financial support from Ipsen Pharma, Novartis and Pfizer. The group of Dr. Knösel is supported by the YING (Young Investigator Neuroendocrine, Germany, Novartis).

REFERENCES

1. Briest F and Grabowski P. PI3K-AKT-mTOR-signaling and beyond: the complex network in gastroenteropancreatic neuroendocrine neoplasms. Theranostics. 2014; 4(4):336-365.
2. Hanahan D and Weinberg RA. Hallmarks of cancer: the next generation. Cell. 2011; 144(5):646-674.

3. Halasi M and Gartel AL. Targeting FOXM1 in cancer. Biochemical pharmacology. 2013; 85(5):644-652.
4. Halasi M and Gartel AL. FOX(M1) news--it is cancer. Molecular cancer therapeutics. 2013; 12(3):245-254.
5. Katoh M, Igarashi M, Fukuda H, Nakagama H and Katoh M. Cancer genetics and genomics of human FOX family genes. Cancer letters. 2013; 328(2):198-206.
6. Koo CY, Muir KW and Lam EW. FOXM1: From cancer initiation to progression and treatment. Biochimica et biophysica acta. 2012; 1819(1):28-37.
7. Wierstra I. FOXM1 (Forkhead box M1) in tumorigenesis: overexpression in human cancer, implication in tumorigenesis, oncogenic functions, tumor-suppressive properties, and target of anticancer therapy. Advances in cancer research. 2013; 119:191-419.
8. Wierstra I. The transcription factor FOXM1 (Forkhead box M1): proliferation-specific expression, transcription factor function, target genes, mouse models, and normal biological roles. Advances in cancer research. 2013; 118:97-398.
9. Myatt SS and Lam EW. Targeting FOXM1. Nature reviews Cancer. 2008; 8(3):242.
10. Wang Z, Ahmad A, Li Y, Banerjee S, Kong D and Sarkar FH. Forkhead box M1 transcription factor: a novel target for cancer therapy. Cancer treatment reviews. 2010; 36(2):151-156.
11. Wonsey DR and Follettie MT. Loss of the forkhead transcription factor FoxM1 causes centrosome amplification and mitotic catastrophe. Cancer research. 2005; 65(12):5181-5189.
12. Lam EW, Brosens JJ, Gomes AR and Koo CY. Forkhead box proteins: tuning forks for transcriptional harmony. Nature reviews Cancer. 2013; 13(7):482-495.
13. Wang M and Gartel AL. The suppression of FOXM1 and its targets in breast cancer xenograft tumors by siRNA. Oncotarget. 2011; 2(12):1218-1226.
14. Karadedou CT, Gomes AR, Chen J, Petkovic M, Ho KK, Zwolinska AK, Feltes A, Wong SY, Chan KY, Cheung YN, Tsang JW, Brosens JJ, Khoo US and Lam EW. FOXO3a represses VEGF expression through FOXM1-dependent and -independent mechanisms in breast cancer. Oncogene. 2012; 31(14):1845-1858.
15. Zhang Y, Zhang N, Dai B, Liu M, Sawaya R, Xie K and Huang S. FoxM1B transcriptionally regulates vascular endothelial growth factor expression and promotes the angiogenesis and growth of glioma cells. Cancer research. 2008; 68(21):8733-8742.
16. Uddin S, Ahmed M, Hussain A, Abubaker J, Al-Sanea N, AbdulJabbar A, Ashari LH, Alhomoud S, Al-Dayel F, Jehan Z, Bavi P, Siraj AK and Al-Kuraya KS. Genome-wide expression analysis of Middle Eastern colorectal cancer reveals FOXM1 as a novel target for cancer therapy. The American journal of pathology. 2011; 178(2):537-547.
17. Ahmad A, Wang Z, Kong D, Ali S, Li Y, Banerjee S, Ali R and Sarkar FH. FoxM1 down-regulation leads to inhibition of proliferation, migration and invasion of breast cancer cells through the modulation of extra-cellular matrix degrading factors. Breast cancer research and treatment. 2010; 122(2):337-346.
18. Dai B, Kang SH, Gong W, Liu M, Aldape KD, Sawaya R and Huang S. Aberrant FoxM1B expression increases matrix metalloproteinase-2 transcription and enhances the invasion of glioma cells. Oncogene. 2007; 26(42):6212-6219.
19. Zhang X, Cheng L, Minn K, Madan R, Godwin AK, Shridhar V and Chien J. Targeting of mutant p53-induced FoxM1 with thiostrepton induces cytotoxicity and enhances carboplatin sensitivity in cancer cells. Oncotarget. 2014.
20. Gomes AR, Zhao F and Lam EW. Role and regulation of the forkhead transcription factors FOXO3a and FOXM1 in carcinogenesis and drug resistance. Chinese journal of cancer. 2013; 32(7):365-370.
21. Wilson MS, Brosens JJ, Schwenen HD and Lam EW. FOXO and FOXM1 in cancer: the FOXO-FOXM1 axis shapes the outcome of cancer chemotherapy. Current drug targets. 2011; 12(9):1256-1266.
22. Katoh M and Katoh M. Human FOX gene family (Review). International journal of oncology. 2004; 25(5):1495-1500.
23. Mori S, Nada S, Kimura H, Tajima S, Takahashi Y, Kitamura A, Oneyama C and Okada M. The mTOR pathway controls cell proliferation by regulating the FoxO3a transcription factor via SGK1 kinase. PloS one. 2014; 9(2):e88891.
24. Zhao F and Lam EW. Role of the forkhead transcription factor FOXO-FOXM1 axis in cancer and drug resistance. Frontiers of medicine. 2012; 6(4):376-380.
25. Franco J, Witkiewicz AK and Knudsen ES. CDK4/6 inhibitors have potent activity in combination with pathway selective therapeutic agents in models of pancreatic cancer. Oncotarget. 2014; 5(15):6512-6525.
26. Ha SY, Lee CH, Chang HK, Chang S, Kwon KY, Lee EH, Roh MS and Seo B. Differential expression of forkhead box M1 and its downstream cyclin-dependent kinase inhibitors p27(kip1) and p21(waf1/cip1) in the diagnosis of pulmonary neuroendocrine tumours. Histopathology. 2012; 60(5):731-739.
27. Grabowski P, Griss S, Arnold CN, Hörsch D, Goke R, Arnold R, Heine B, Stein H, Zeitz M and Scherübl H. Nuclear survivin is a powerful novel prognostic marker in gastroenteropancreatic neuroendocrine tumor disease. Neuroendocrinology. 2005; 81(1):1-9.
28. Bhat UG, Halasi M and Gartel AL. FoxM1 is a general target for proteasome inhibitors. PloS one. 2009; 4(8):e6593.
29. Gartel AL. A new target for proteasome inhibitors: FoxM1. Expert opinion on investigational drugs. 2010; 19(2):235-242.
30. Gartel AL. Suppression of the Oncogenic Transcription Factor FOXM1 by Proteasome Inhibitors. Scientifica. 2014;

2014.

31. Saunders P, Cisterne A, Weiss J, Bradstock KF and Bendall LJ. The mammalian target of rapamycin inhibitor RAD001 (everolimus) synergizes with chemotherapeutic agents, ionizing radiation and proteasome inhibitors in pre-B acute lymphocytic leukemia. Haematologica. 2011; 96(1):69-77.
32. Bhat UG, Halasi M and Gartel AL. Thiazole antibiotics target FoxM1 and induce apoptosis in human cancer cells. PloS one. 2009; 4(5):e5592.
33. Nestal de Moraes G, Bella L, Zona S, Burton MJ and Lam EW. Insights into a Critical Role of the FOXO3a-FOXM1 Axis in DNA Damage Response and Genotoxic Drug Resistance. Current drug targets. 2014.
34. Zhang N, Wu X, Yang L, Xiao F, Zhang H, Zhou A, Huang Z and Huang S. FoxM1 inhibition sensitizes resistant glioblastoma cells to temozolomide by downregulating the expression of DNA-repair gene Rad51. Clinical cancer research : an official journal of the American Association for Cancer Research. 2012; 18(21):5961-5971.
35. Chou TC. Theoretical basis, experimental design, and computerized simulation of synergism and antagonism in drug combination studies. Pharmacological reviews. 2006; 58(3):621-681.
36. Chou TC and Talaly P. A simple generalized equation for the analysis of multiple inhibitions of Michaelis-Menten kinetic systems. The Journal of biological chemistry. 1977; 252(18):6438-6442.
37. Beuvink I, Boulay A, Fumagalli S, Zilbermann F, Ruetz S, O'Reilly T, Natt F, Hall J, Lane HA and Thomas G. The mTOR inhibitor RAD001 sensitizes tumor cells to DNA-damaged induced apoptosis through inhibition of p21 translation. Cell. 2005; 120(6):747-759.
38. Sengupta A, Kalinichenko VV and Yutzey KE. FoxO1 and FoxM1 transcription factors have antagonistic functions in neonatal cardiomyocyte cell-cycle withdrawal and IGF1 gene regulation. Circulation research. 2013; 112(2):267-277.
39. Teh MT, Gemenetzidis E, Patel D, Tariq R, Nadir A, Bahta AW, Waseem A and Hutchison IL. FOXM1 induces a global methylation signature that mimics the cancer epigenome in head and neck squamous cell carcinoma. PloS one. 2012; 7(3):e34329.
40. Wang IC, Chen YJ, Hughes D, Petrovic V, Major ML, Park HJ, Tan Y, Ackerson T and Costa RH. Forkhead box M1 regulates the transcriptional network of genes essential for mitotic progression and genes encoding the SCF (Skp2-Cks1) ubiquitin ligase. Molecular and cellular biology. 2005; 25(24):10875-10894.
41. Xu N, Jia D, Chen W, Wang H, Liu F, Ge H, Zhu X, Song Y, Zhang X, Zhang D, Ge D and Bai C. FoxM1 is associated with poor prognosis of non-small cell lung cancer patients through promoting tumor metastasis. PloS one. 2013; 8(3):e59412.
42. Liu D, Zhang Z and Kong CZ. High FOXM1 expression was associated with bladder carcinogenesis. Tumour biology : the journal of the International Society for Oncodevelopmental Biology and Medicine. 2013; 34(2):1131-1138.
43. Xu N, Wu SD, Wang H, Wang Q and Bai CX. Involvement of FoxM1 in non-small cell lung cancer recurrence. Asian Pacific journal of cancer prevention : APJCP. 2012; 13(9):4739-4743.
44. Mencalha AL, Binato R, Ferreira GM, Du Rocher B and Abdelhay E. Forkhead box M1 (FoxM1) gene is a new STAT3 transcriptional factor target and is essential for proliferation, survival and DNA repair of K562 cell line. PloS one. 2012; 7(10):e48160.
45. Liu L, McBride KM and Reich NC. STAT3 nuclear import is independent of tyrosine phosphorylation and mediated by importin-alpha3. Proceedings of the National Academy of Sciences of the United States of America. 2005; 102(23):8150-8155.
46. Yang J and Stark GR. Roles of unphosphorylated STATs in signaling. Cell research. 2008; 18(4):443-451.
47. Yang J, Liao X, Agarwal MK, Barnes L, Auron PE and Stark GR. Unphosphorylated STAT3 accumulates in response to IL-6 and activates transcription by binding to NFkappaB. Genes & development. 2007; 21(11):1396-1408.
48. Oh HM, Yu CR, Dambuza I, Marrero B and Egwuagu CE. STAT3 protein interacts with Class O Forkhead transcription factors in the cytoplasm and regulates nuclear/cytoplasmic localization of FoxO1 and FoxO3a proteins in CD4(+) T cells. The Journal of biological chemistry. 2012; 287(36):30436-30443.
49. Radhakrishnan SK, Bhat UG, Hughes DE, Wang IC, Costa RH and Gartel AL. Identification of a chemical inhibitor of the oncogenic transcription factor forkhead box M1. Cancer research. 2006; 66(19):9731-9735.
50. Gartel AL. Thiazole Antibiotics Siomycin a and Thiostrepton Inhibit the Transcriptional Activity of FOXM1. Frontiers in oncology. 2013; 3:150.
51. Lim CP and Cao X. Serine phosphorylation and negative regulation of Stat3 by JNK. The Journal of biological chemistry. 1999; 274(43):31055-31061.
52. Georgieva I, Koychev D, Wang Y, Holstein J, Hopfenmuller W, Zeitz M and Grabowski P. ZM447439, a novel promising aurora kinase inhibitor, provokes antiproliferative and proapoptotic effects alone and in combination with bio- and chemotherapeutic agents in gastroenteropancreatic neuroendocrine tumor cell lines. Neuroendocrinology. 2010; 91(2):121-130.
53. Fraedrich K, Schrader J, Ittrich H, Keller G, Gontarewicz A, Matzat V, Kromminga A, Pace A, Moll J, Blaker M, Lohse AW, Horsch D, Brummendorf TH and Benten D. Targeting aurora kinases with danusertib (PHA-739358) inhibits growth of liver metastases from gastroenteropancreatic neuroendocrine tumors in an orthotopic xenograft model.

Clinical cancer research : an official journal of the American Association for Cancer Research. 2012; 18(17):4621-4632.

54. Li Y, Zhang S and Huang S. FoxM1: a potential drug target for glioma. Future oncology (London, England). 2012; 8(3):223-226.

55. Li X, Qiu W, Liu B, Yao R, Liu S, Yao Y and Liang J. Forkhead box transcription factor 1 expression in gastric cancer: FOXM1 is a poor prognostic factor and mediates resistance to docetaxel. Journal of translational medicine. 2013; 11:204.

56. Halasi M, Pandit B and Gartel AL. Proteasome inhibitors suppress the protein expression of mutant p53. Cell cycle (Georgetown, Tex). 2014; 13(20):3202-3206.

57. Knosel T, Chen Y, Altendorf-Hofmann A, Danielczok C, Freesmeyer M, Settmacher U, Wurst C, Schulz S, Yang LL and Petersen I. High KIT and PDGFRA are associated with shorter patients survival in gastroenteropancreatic neuroendocrine tumors, but mutations are a rare event. Journal of cancer research and clinical oncology. 2012; 138(3):397-403.

58. Parekh D, Ishizuka J, Townsend CM, Jr., Haber B, Beauchamp RD, Karp G, Kim SW, Rajaraman S, Greeley G, Jr. and Thompson JC. Characterization of a human pancreatic carcinoid in vitro: morphology, amine and peptide storage, and secretion. Pancreas. 1994; 9(1):83-90.

59. Iguchi H, Hayashi I and Kono A. A somatostatin-secreting cell line established from a human pancreatic islet cell carcinoma (somatostatinoma): release experiment and immunohistochemical study. Cancer research. 1990; 50(12):3691-3693.

60. Modlin IM, Kidd M, Pfragner R, Eick GN and Champaneria MC. The functional characterization of normal and neoplastic human enterochromaffin cells. The Journal of clinical endocrinology and metabolism. 2006; 91(6):2340-2348.

61. Lundqvist M, Mark J, Funa K, Heldin NE, Morstyn G, Wedell B, Layton J and Oberg K. Characterisation of a cell line (LCC-18) from a cultured human neuroendocrine-differentiated colonic carcinoma. European journal of cancer (Oxford, England : 1990). 1991; 27(12):1663-1668.

62. Hui MK, Chan KW, Luk JM, Lee NP, Chung Y, Cheung LC, Srivastava G, Tsao SW, Tang JC and Law S. Cytoplasmic Forkhead box M1 (FoxM1) in esophageal squamous cell carcinoma significantly correlates with pathological disease stage. World journal of surgery. 2012; 36(1):90-97.

63. http://www.combosyn.com/. 02/01/2015.

LEBENSLAUF

Mein Lebenslauf wird aus datenschutzrechtlichen Gründen in der elektronischen Version meiner Arbeit nicht veröffentlicht.

PUBLIKATIONSLISTE

1. C. Scheibenbogen, M. Loebel, H. Freitag, A. Krueger, S. Bauer, M. Antelmann, W. Doehner, N. Scherbakov, H. Heidecke, P. Reinke, H. D. Volk and P. Grabowski: Immunoadsorption to remove ss2 adrenergic receptor antibodies in Chronic Fatigue Syndrome CFS/ME. *PLoS One*, 13(3), e0193672 (2018) doi:10.1371/journal.pone.0193672

2. J. F. Mieves, K. Wittke, H. Freitag, H. D. Volk, C. Scheibenbogen and L. G. Hanitsch: Influenza Vaccination in Patients with Common Variable Immunodeficiency (CVID). *Curr Allergy Asthma Rep*, 17(11), 78 (2017) doi:10.1007/s11882-017-0749-3

3. C. Scheibenbogen, H. Freitag, J. Blanco, E. Capelli, E. Lacerda, J. Authier, M. Meeus, J. Castro Marrero, Z. Nora-Krukle, E. Oltra, E. B. Strand, E. Shikova, S. Sekulic and M. Murovska: The European ME/CFS Biomarker Landscape project: an initiative of the European network EUROMENE. *J Transl Med*, 15(1), 162 (2017) doi:10.1186/s12967-017-1263-z

4. S. Taromi, F. Lewens, R. Arsenic, D. Sedding, J. Sanger, A. Kunze, M. Mobs, J. Benecke, H. Freitag, F. Christen, D. Kaemmerer, A. Lupp, M. Heilmann, H. Lammert, C. P. Schneider, K. Richter, M. Hummel, B. Siegmund, M. Burger, F. Briest and P. Grabowski: Proteasome inhibitor bortezomib enhances the effect of standard chemotherapy in small cell lung cancer. *Oncotarget*, 8(57), 97061-97078 (2017) doi:10.18632/oncotarget.21221

5. F. Briest, I. Grass, D. Sedding, M. Mobs, F. Christen, J. Benecke, K. Fuchs, D. Kaemmerer, S. Mende, J. Sanger, A. Kunze, C. Geisler, H. Freitag, F. Lewens, L. Worpenberg, S. Iwaszkiewicz, B. Siegmund, W. Walther, M. Hummel and P. Grabowski: Mechanisms of targeting the MDM2-p53-FOXM1 axis in well-differentiated intestinal neuroendocrine tumors. *Neuroendocrinology* (2017) doi:10.1159/000481506

6. S. Nolting, J. Rentsch, H. Freitag, K. Detjen, F. Briest, M. Mobs, V. Weissmann, B. Siegmund, C. J. Auernhammer, E. T. Aristizabal Prada, M. Lauseker, A. Grossman, S. Exner, C. Fischer, C. Grotzinger, J. Schrader and P. Grabowski: The selective PI3Kalpha inhibitor BYL719 as a novel therapeutic option for neuroendocrine tumors: Results from multiple cell line models. *PLoS One*, 12(8), e0182852 (2017) doi:10.1371/journal.pone.0182852

7. H. Freitag, F. Christen, F. Lewens, I. Grass, F. Briest, S. Iwaszkiewicz, B. Siegmund and P. Grabowski: Inhibition of mTORs Catalytic Site by PKI-587 is a Promising Therapeutic Option for Gastroenteropancreatic Neuroendocrine Tumor Disease. *Neuroendocrinology* (2016) doi:10.1159/000448843

8. F. Briest, E. Berg, I. Grass, H. Freitag, D. Kaemmerer, F. Lewens, F. Christen, R. Arsenic, A. Altendorf-Hofmann, A. Kunze, J. Sanger, T. Knosel, B. Siegmund, M. Hummel and P. Grabowski: FOXM1: A novel drug target in gastroenteropancreatic neuroendocrine tumors. *Oncotarget*, 6(10), 8185-99 (2015)

9. H. Freitag, F. Christen, I. Grass, F. Briest, F. Lewens, B. Siegmund and P. Grabowski: Dual Inhibition of PI3K and mTORC1/C2 by PKI-587 (PF-05212384) as a Promising Therapeutic Option for Gastroenteropancreatic Neuroendocrine Tumor Disease and Its Effect on AKT-Signaling. 12th Annual ENETS Conference for the Diagnosis and Treatment of Neuroendocrine Tumor Disease. March 11-13, 2015, Barcelona, Spain: Abstracts. *Neuroendocrinology*, 102(1-2), 77-168 (2015) doi:10.1159/000431385

10. H. Freitag, F. Briest, F. Lewens, B. Siegmund and P. Grabowski: Vom besseren Verständnis tumor-assoziierter Signalwege und der „Übersetzung“ in innovative Therapeutika: präklinische Ergebnisse zur dualen PI3K/mTOR-Inhibition bei gastroenteropankreatischen neuroendokrinen Neoplasien. *Z Gastroenterol*, 52(08), KG192 (2014) doi:10.1055/s-0034-1386214

11. H. Freitag, G. Gress, K. Messer, G. Sivaz, O. Weinbender, I. Zundorf and T. Dingermann: [Please a BiTE!]. *Pharm Unserer Zeit*, 38(5), 396-8 (2009) doi:10.1002/pauz.200990069

DANKSAGUNG

Mein besonderer Dank gilt meiner betreuenden Hochschullehrerin PD Dr. Patricia Grabowski, die jederzeit bei der Planung und Durchführung dieser Arbeit mit Rat und Tat unterstützend zur Seite stand. Mit ihrer wissenschaftlichen Kompetenz und herzlichen Art schuf sie ein sehr angenehmes und produktives Arbeitsklima, die vielen fachlichen Diskussionen und ihre Einfälle waren immer wieder motivierend und haben großen Anteil am Zustandekommen dieser Arbeit. Die Entwicklung eigener Vorstellungen und Ideen hat sie stets unterstützt, womit sie nicht nur diese Arbeit voranbrachte sondern auch meine berufliche Qualifikation förderte.

Außerdem danke ich sehr herzlich meinen Labor-Kolleginnen Florentine Lewens und Franziska Briest, für die immer tatkräftige Hilfe, die bereichernden, nicht ausschließlich wissenschaftlichen Diskurse und die angenehme Zeit im Labor.

Sehr dankbar bin ich weiterhin der gesamten AG Baldus, Dr. Rita Rosenthal, Hedwig Lammert, Prof. Dr. Michael Hummel, Ines Eichhorn, Sandra Bauer, Dr. Andrea Dörner, Julia Winter und ganz besonders Sabine Knüppel für ihre Hilfe bei der praktischen Durchführung verschiedener Methoden und die Bereitstellung von Gerätschaften.

Der Sonnenfeld-Stiftung danke ich sehr herzlich für die Unterstützung durch ein Promotionsstipendium, ohne das diese Arbeit unmöglich gewesen wäre. Des Weiteren danke ich der Firma Pfizer für das zur Verfügung stellen des Wirkstoffs Gedatolisib.

Nicht zuletzt danke ich besonders meinen Freunden, die mich während der gesamten Zeit begleitet und mental unterstützt haben.